

The Quark-Gluon Plasma in Equilibrium

Dirk H. Rischke

Institut für Theoretische Physik
Johann Wolfgang Goethe-Universität Frankfurt am Main
Germany

April 25, 2019

Abstract

Our current knowledge of the quark-gluon plasma in thermodynamical equilibrium is reviewed. The phase diagram of strongly interacting matter is discussed, with emphasis on the quark-hadron phase transition and the color-superconducting phases of quark matter. Lattice QCD results on the order of the phase transition, the thermodynamical functions, the heavy quark free energy, mesonic spectral functions, and recent results for nonzero quark chemical potential are presented. Analytic attempts to compute the thermodynamical properties of strongly interacting matter, such as perturbation theory, quasiparticle models, “hard-thermal-loop” (HTL)-resummed perturbation theory, the Polyakov-loop model, as well as linear sigma models are discussed. Finally, color-superconducting quark matter is considered in the limit of weak coupling. The gap equation and the excitation spectrum are derived. The solution of the gap equation, gap parameters in various color-superconducting phases, and critical temperatures for the transition to normal-conducting quark matter are presented. A summary of gluon and photon properties in color superconductors is given.

1 Introduction and Summary

Quantum chromodynamics (QCD) is the fundamental theory of the strong interaction. QCD is an asymptotically free theory [1], i.e., interactions between quarks and gluons become weaker as the mutual distance decreases or as the exchanged momentum increases. Consequently, at very large temperatures and/or densities, the interactions which confine quarks and gluons inside hadrons should become sufficiently weak to release them [2]. The phase where quarks and gluons are deconfined is termed the *quark-gluon plasma* (QGP). Lattice QCD calculations have established the existence of such a phase of strongly interacting matter at temperatures larger than ~ 150 MeV and zero net-baryon density. Depending on the number of quark flavors and the masses of the quarks, the transition between ordinary hadronic matter and the QGP could be a thermodynamic phase transition of first order, of second order, or simply a crossover transition.

The QGP was certainly present in the evolution of the early universe. The early universe was very hot, but close to net-baryon free. In the opposite limit of small temperature and large baryon

density, the QGP may exist even nowadays in the interior of compact stellar objects such as neutron stars. The main effort in present-day nuclear physics is to create the QGP under controlled conditions in the laboratory via collisions of heavy nuclei at ultrarelativistic energies [3]. The temperatures and net-baryon densities reached in nuclear collisions depend on the bombarding energy. They interpolate between the extreme conditions of the early universe on one side and compact stellar objects on the other.

If at all, the QGP is only transiently created in a nuclear collision; free quarks and gluons will not be released. Therefore, deciding whether a QGP was formed or not is not easy. Detectors in the laboratory can only measure hadrons, leptons, or photons. The bulk of the particles emerging from a nuclear collision are hadrons with transverse momenta of order ~ 1 GeV. They carry information about the final stage of the collision after hadronization of the QGP. The formation of the latter can only indirectly influence this final stage, for instance by modifying the collective dynamics of the system through a softening of the equation of state in the hadronization transition [4]. Very few hadrons are emitted with transverse momenta of the order of several GeV. They arise from the fragmentation of jets and may carry information also about the earlier stages of the collision. Of particular interest is the situation where the jet has to traverse hot and dense matter possibly formed in the collision and is quenched by multiple rescattering in the medium [5]. From this “jet-quenching” process one may indirectly learn about the properties of the hot and dense environment. Finally, leptons and photons only interact electromagnetically. Once formed in the early stage of the collision, they leave the system unimpededly and carry information about this stage to the detector [6]. The difficulty is to disentangle the thermal radiation from a hot, equilibrated QGP [7] from the initial production of leptons and photons in the very first, highly energetic partonic collisions and from the thermal radiation of hot hadronic matter [8].

In order to decide whether a QGP was formed, one has to have detailed knowledge about its properties. Otherwise it is impossible to find an unambiguous signature for QGP formation in nuclear collisions. In this review, I present an overview of the *thermodynamical properties* of the QGP. Section 2 contains a detailed discussion of the phase diagram of strongly interacting matter. The present status of knowledge is shown schematically in Fig. 1. Depending on the temperature, T , and the quark chemical potential, μ , strongly interacting matter may occur in three distinct phases: the hadronic phase, the QGP, and color-superconducting quark matter. The ground state of (infinite) nuclear matter is at $(T, \mu)_0 = (0, 308)$ MeV. There is a line of first-order phase transitions emerging from this point and terminating in a critical endpoint at a temperature of order ~ 10 MeV. At this point, the transition is of second order. This phase transition is the nuclear liquid-gas transition [9]. To the left of the line nuclear matter is in the gaseous phase, and to the right in the liquid phase. Above the critical endpoint, there is no distinction between these two phases.

For temperatures below ~ 160 MeV and quark chemical potentials below ~ 350 MeV (corresponding to net-baryon densities which are a few times the ground state density of nuclear matter), strongly interacting matter is in the hadronic phase. Quite similar to the liquid-gas transition, there is a line of first-order phase transitions which separates the hadronic phase from the QGP and terminates in a critical endpoint where the transition is of second order. This endpoint is approximately at $(T, \mu) \simeq (160, 240)$ MeV, cf. Sec. 3.6. For smaller quark chemical potentials (smaller net-baryon densities), the transition becomes crossover, and there is no real distinction between hadronic matter and the QGP. As will be discussed in detail in Sec. 2, the position of the critical endpoint depends on the value of the quark masses. Finally, at large quark chemical potential (large baryon density) and small temperature, quark matter becomes a color superconductor. There can be multitude of color-superconducting phases, depending on the symmetries of the order parameter for condensation of quark Cooper pairs. The discussion in Sec. 2 is qualitative and is meant to give an overview of the phase structure of strongly

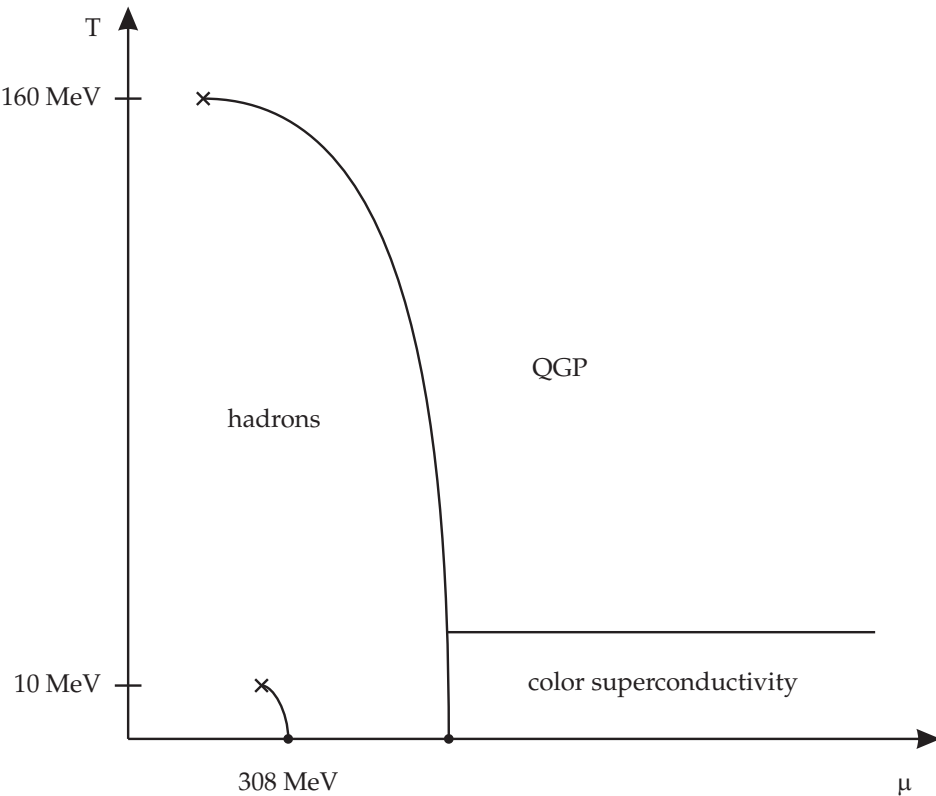


Figure 1: The phase diagram of strongly interacting matter (schematic).

interacting matter at nonzero temperature and quark chemical potential. The discussion in the following sections is both more quantitative as well as technical and focusses on the properties of the QGP and color-superconducting quark matter.

The early universe evolved close to the temperature axis in the phase diagram of strongly interacting matter. Matter in the core of compact stellar objects, like neutron stars, is close to the quark chemical potential axis, at values of μ around 400 – 500 MeV. Nuclear collisions at bombarding energies around $E_{\text{Lab}} \sim 1$ AGeV explore a region of temperatures and quark chemical potentials around $(T, \mu) \sim (70, 250)$ MeV. Collisions at current RHIC energies of $\sqrt{s} = 200$ AGeV are expected to excite matter in a region around and above $(T, \mu) \sim (170, 10)$ MeV. Collision energies in between these two extremes cover the intermediate region and, in particular, may probe the critical endpoint.

Section 3 presents a review of lattice QCD. After a brief introduction to the basic principles, results on the order of the QCD phase transition, the equation of state of strongly interacting matter, the heavy quark free energy, and mesonic spectral functions are collected. For technical reasons, most lattice QCD calculations have been done at zero quark chemical potential. An extension to nonzero values of μ is difficult and has only fairly recent begun. First results will also be discussed.

Lattice QCD is in principle an exact method to solve QCD. If one had sufficiently large computer power, one could not only decrease the lattice spacing and increase the size of the system to come sufficiently close to the continuum and thermodynamic limit, one could also sample over a sufficiently large number of configurations to make the statistical errors arbitrarily small. However, one still has to interpret the results in physical terms. In this respect, analytic approaches to solve QCD have a certain advantage over lattice QCD. In an analytic approach, one has complete control over the physical

assumptions entering the calculation. Section 4 gives an overview of what is known about the QGP from analytic calculations.

The most simple approach from a conceptual (albeit not technical) point of view is to determine the thermodynamical properties of the QGP by a perturbative computation of the QCD partition function in terms of a power series in the strong coupling constant, g . This can be done up to terms of order $O(g^6 \ln g)$. At order $O(g^6)$, the perturbative series breaks down [10, 11], and the remaining nonperturbative contribution has to be determined, for instance, from a lattice QCD calculation. The perturbative series converges rapidly at high temperatures where the strong coupling constant is small, $g \ll 1$. For temperatures of order ~ 150 MeV, however, $g \sim 1$ and the perturbative series does not converge very well. Therefore, one has tried other ways to compute the partition function, either by expanding around a nonperturbative ground state or by resumming certain classes of diagrams to improve the convergence properties of the perturbative series. In both approaches, quarks and gluons are considered as quasiparticles with a dispersion relation which is modified as compared to the one in the vacuum. Still another approach is to construct an effective theory for QCD which can be solved exactly or at least within a many-body approximation scheme. All these approaches will be reviewed in Sec. 4.

Section 5 contains an introduction to color superconductivity at large quark chemical potentials. In this case, analytic calculations are well under control, because corrections can be systematically computed in terms of powers of g . After a derivation of the gap equation for the color-superconducting gap function, the excitation spectrum in a color superconductor is presented. The solution of the gap equation is discussed and the magnitude of the gap parameter is determined. As in ordinary superconductors, quark Cooper pairs break up, if the thermal motion becomes too large. The critical temperature for the transition between the normal- and the superconducting phase is computed. Finally, the properties of gluons and photons in color superconductors are discussed. Section 6 concludes this review with a brief summary of the material and an outlook towards future directions of research in this area.

A lot of the material in this review can also be found in other places. The standard review for properties of hot and dense, strongly interacting matter is the seminal work of Gross, Pisarski, and Yaffe [12]. The contents as well as more recent developments have found their way into textbooks [10, 13]. For early reviews focussing on the properties of the QGP, see Ref. [14]. An introduction to lattice QCD and recent results can be found in Ref. [15]. The present status of lattice QCD is also reviewed in Ref. [16]. Resummation techniques which attempt to compute the QCD partition function analytically are discussed in great detail in Ref. [17].

The present review tries to give a balanced overview of all subfields concerned with the equilibrium properties of the QGP. Therefore, the presentation is not as detailed as in a more specialized review. On the other hand, I tried to explain the basics in somewhat greater detail than usually found in the literature. My hope is that in this way, this review will become useful for early-stage researchers working in both theory as well as experiment, and for all researchers who would like to get an overview of the theoretical activity related to equilibrium properties of the QGP.

The only somewhat more specialized and thus more technical part is the section on color superconductivity. This field has seen a lot of activity only fairly recently, but there are already a couple of excellent reviews [18]. These, however, focus mainly on the basics of the phenomenon of color superconductivity and its phenomenological implications. In contrast, Sec. 5 contains a very detailed discussion of how to compute properties of the quasiparticle excitations in a color superconductor in the weak-coupling limit. By clarifying some of the technical details, I hope to remove the obstacles that may prevent other researchers to enter this rapidly evolving and rather exciting new field of strongly interacting matter physics.

Due to space restrictions this review is forced to omit many things that could (and possibly, should) also have been said about strongly interacting matter at high temperature and/or density. In particular, non-equilibrium properties of the QGP will not be discussed at all. I am also not aware of a review which the interested reader could be referred to. Other subjects not discussed here have already been covered in review articles. These are, for instance, the physics of instantons in non-Abelian gauge theories [19]. Another important topic which is not mentioned in this work, but for which excellent reviews exist [20], are the experimental signatures for the QGP. Recent developments in the field of color superconductivity are mainly focussed on deriving effective theories for quarks around the Fermi surface. These greatly simplify calculations and allow to systematically study effects of nonzero quark masses, for details, see Ref. [21]. Finally, the list of references is, necessarily, far from complete. I would like to apologize to all authors whose work should have been (but was not) mentioned.

The units are $\hbar = c = k_B = 1$. I work in Euclidean space-time at nonzero temperature T , i.e., space-time integrals are $\int_X \equiv \int_0^{1/T} d\tau \int_V d^3\mathbf{x}$, where V is the 3-volume of the system. Energy-momentum integrals are $\int_K \equiv T \sum_n \int d^3\mathbf{k} / (2\pi)^3$; n labels the Matsubara frequencies $\omega_n^b = 2n\pi T$ for bosons and $\omega_n^f = (2n+1)\pi T$ for fermions, $n = 0, \pm 1, \pm 2, \dots$. I denote 4-vectors with capital letters, but unless mentioned otherwise, retain a notation familiar from Minkowski space: $X^\mu \equiv (t, \mathbf{x})$, where $t \equiv i\tau$, and $K^\mu \equiv (k_0, \mathbf{k})$, where $k_0 = i\omega_n$, with the metric tensor $g^{\mu\nu} = \text{diag}(+, -, -, -)$. 3-vectors \mathbf{k} have length $k \equiv |\mathbf{k}|$ and direction $\hat{\mathbf{k}} \equiv \mathbf{k}/k$.

2 The QCD Phase Diagram

2.1 Basics

In order to understand the phase structure of strongly interacting matter, one has to know its equation of state. In the grand canonical ensemble, the equation of state is determined by the grand partition function [10, 13]

$$\mathcal{Z}(T, V, \mu) = \int \mathcal{D}\bar{\psi} \mathcal{D}\psi \mathcal{D}A_a^\mu \exp \left[\int_X (\mathcal{L} + \mu \mathcal{N}) \right], \quad (1)$$

where μ is the quark chemical potential associated with (net) quark number conservation. The QCD Lagrangian is given by

$$\mathcal{L} = \bar{\psi} (i\gamma^\mu D_\mu - m) \psi - \frac{1}{4} F_a^{\mu\nu} F_{\mu\nu}^a + \mathcal{L}_{\text{gauge}}. \quad (2)$$

For N_c colors and N_f flavors, ψ is the $4N_c N_f$ -dimensional spinor of quark fields, $\bar{\psi} \equiv \psi^\dagger \gamma_0$ is the adjoint quark spinor, γ^μ are the Dirac matrices and m is the quark mass matrix. The covariant derivative is defined as $D_\mu = \partial_\mu - ig A_\mu^a T_a$, with the strong coupling constant g , the gluon fields A_a^μ , and the generators T_a of the local $[SU(N_c)_c]$ symmetry. (Throughout this paper, I indicate local, i.e. gauged, symmetries by square brackets.) The latter are usually taken as $T_a \equiv \lambda_a/2$, where λ_a are the Gell-Mann matrices. The gluonic field strength tensor is defined as

$$F_a^{\mu\nu} = \partial^\mu A_a^\nu - \partial^\nu A_a^\mu + g f_{abc} A_b^\mu A_c^\nu, \quad (3)$$

where f_{abc} are the structure constants of $[SU(N_c)_c]$. The term $\mathcal{L}_{\text{gauge}}$ in Eq. (2) will not be specified further. It comprises gauge fixing terms and the contribution from Faddev-Popov ghosts. The number density operator associated with the conserved (net) quark number is $\mathcal{N} \equiv \bar{\psi} \gamma_0 \psi$.

For any finite volume V and nonzero temperature T , the partition function is defined for a compact Euclidean space-time volume $V \times 1/T$. For the sake of simplicity (but without loss of generality), assume that the spatial volume V is a box, $V = L^3$, with L being the length of the box in one spatial dimension.

All fields are then usually taken to be periodic in spatial directions, $\phi(\tau, 0, y, z) = \phi(\tau, L, y, z)$, where ϕ stands generically for ψ , $\bar{\psi}$, and A_a^μ . Bosonic fields, such as gluons, are periodic also in temporal direction, $A_a^\mu(0, \mathbf{x}) = A_a^\mu(1/T, \mathbf{x})$, while fermionic fields, such as quarks, are antiperiodic in temporal direction, $\psi(0, \mathbf{x}) = -\psi(1/T, \mathbf{x})$.

From the grand partition function, one can derive other thermodynamic quantities, for instance the pressure,

$$p(T, \mu) = T \frac{\partial \ln \mathcal{Z}}{\partial V} \rightarrow \frac{T}{V} \ln \mathcal{Z} \quad (V \rightarrow \infty). \quad (4)$$

In the thermodynamic limit, $\ln \mathcal{Z}$ is an extensive quantity ($\sim V$) and the dependence of the pressure on V drops out.

Phase transitions are determined by studying the derivatives of the pressure with respect to T and μ for a given point (T, μ) in the phase diagram of the independent thermodynamic variables temperature and chemical potential. For a phase transition of first order, the first derivatives

$$s = \left. \frac{\partial p}{\partial T} \right|_\mu, \quad n = \left. \frac{\partial p}{\partial \mu} \right|_T, \quad (5)$$

are discontinuous while the pressure p is continuous at the point (T, μ) . Here, s is the entropy density and n the (net) quark number density. For a phase transition of second order, the second derivatives are discontinuous, while p and its first derivatives are continuous. In this way, phase transitions of arbitrarily high order can be defined. One speaks of a crossover transition, if thermodynamic properties change rapidly within a narrow range of values T and μ , but the pressure and all its derivatives remain continuously differentiable. Usually, the points (T, μ) where a phase transition occurs are continuously connected and thus determine a *line* of phase transitions in the phase diagram. These lines usually start on either the T or the μ axis. They may terminate for nonzero values of T and μ . Two examples for this behavior, the liquid-gas transition in nuclear matter and the quark-hadron transition, have already been seen in the phase diagram of strongly interacting matter, Fig. 1, and will be discussed in more detail in the following.

2.2 The Liquid-Gas Phase Transition

The liquid-gas transition in nuclear matter is a consequence of the fact that nuclear matter assumes its ground state at a nonvanishing baryon density $n_{B,0} \simeq 0.17 \text{ fm}^{-3}$ at zero temperature $T = 0$. The underlying microscopic mechanism for this phenomenon is a competition between attractive and repulsive forces among nucleons, with the attraction winning at this particular value of the baryon density. (This is good, because otherwise there would be no stable atomic nuclei, precluding the existence of our universe as we know it.) In infinite nuclear matter, nucleons in the ground state are bound by -16 MeV, i.e., the energy per baryon is $(E/N_B)_0 \equiv (\epsilon/n_B)_0 = m_N - 16 \text{ MeV} \simeq 924 \text{ MeV}$, where ϵ is the energy density, n_B the baryon density, and $m_N \simeq 939 \text{ MeV}$ is the rest mass of the nucleon. Nuclear matter is mechanically stable in the ground state, such that the pressure vanishes, $p = 0$. From the fundamental relation of thermodynamics, $\epsilon = Ts + \mu n - p$, one then concludes that the baryon chemical potential in the ground state is identical to the energy per baryon, $\mu_{B,0} \equiv (\epsilon/n_B)_0 \simeq 924 \text{ MeV}$. Since a baryon consists of three quarks, $n_B = n/3$ and $\mu_B = 3\mu$. Hence, the ground state of nuclear matter is the point $(T, \mu)_0 \simeq (0, 308) \text{ MeV}$ in the nuclear matter phase diagram.

Obviously, it costs energy to compress nuclear matter to baryon densities $n_B > n_{B,0}$. Such an increase in energy leads to an increase in pressure. At zero temperature, this can be immediately seen from the identity $p = n_B^2 d(E/N_B)/dn_B$. Since the pressure is a continuous function of the thermodynamic

variables, and since it vanishes in the ground state, there are only two possibilities for the behavior of p for densities $n_B < n_{B,0}$: either the pressure remains zero as the density decreases, $p = 0$, or the pressure further decreases such that $p < 0$. The latter possibility implies that the system becomes mechanically unstable. This can be prevented by fragmenting nuclear matter into droplets. These droplets are mechanically stable, i.e., the density inside each droplet is equal to $n_{B,0}$ and the pressure vanishes. The total baryon density in the system can be further reduced by simply decreasing the droplet density. The pressure in such a system remains zero down to arbitrarily small densities, because compression just results in a decrease of the space between droplets. Thus, $p = 0$ from $n_B = 0$ to $n_B = n_{B,0}$, and then $p > 0$ for $n_B > n_{B,0}$.

At small, but nonzero temperatures, this picture remains valid, with the additional possibility to thermally evaporate single nucleons from the surface of the droplets. At small temperatures and densities below the ground state density, one thus has a mixed phase of nucleons and droplets of nuclear matter. This is reminiscent of water which, at room temperature and normal pressure, consists of a mixed phase of water molecules and water droplets. Changing the density one can alter the relative fraction of molecules and droplets. Beyond the density where droplets fill the entire volume one enters the liquid phase, while below the density where the last droplet fragments into molecules one enters the gas phase. This behavior is typical for a first-order phase transition. In this case, this is the so-called liquid-gas transition in water.

Nuclear matter shows a similar behavior, featuring a “gaseous” phase of nucleons at small chemical potentials (densities) and a “liquid” phase of nuclear matter at large chemical potentials (densities), cf. Fig. 1. At small temperatures the transition between the two phases is of first order. Thus, in the (T, μ) phase diagram there is a line of first-order phase transitions extending from the nuclear ground state $(0, 308)$ MeV up towards larger values of T and smaller values of μ . As for water, this line terminates at a critical point where the transition becomes of second order. The critical temperature is of the order of 10 MeV. As for water, one cannot distinguish between the gaseous and the liquid phase for temperatures above this critical temperature. The existence of the liquid-gas phase transition has been confirmed in heavy-ion collision experiments at BEVALAC and GSI energies ($E_{\text{Lab}} \sim 1$ AGeV), although the precise value for the critical temperature and the critical exponents remain a matter of debate [9].

The liquid-gas transition is also a feature of phenomenological models for the nuclear interaction, for instance, the Walecka model [22]. In the following section another phase transition in strongly interacting matter is discussed, which very much resembles the liquid-gas transition in that it (most likely) is of first order for small temperatures and terminates in a critical point where the transition becomes of second order. This transition is the so-called quark-hadron transition.

2.3 The Quark-Hadron Phase Transition

2.3.1 Qualitative arguments

For a non-interacting, translationally invariant system a convenient basis of states are the single-particle momentum eigenstates. Due to the Pauli principle, the density in a fermionic system can only be increased by successively filling states with higher momentum. The highest filled state defines the Fermi surface of the system, and the corresponding momentum is the Fermi momentum, k_F . For non-interacting systems at zero temperature, the single-particle density n is given in terms of the Fermi momentum as

$$n = \frac{d}{6\pi^2} k_F^3 , \quad (6)$$

where d counts the internal degrees of freedom of the fermion (like spin, color, flavor, etc.). Thus, at large densities the Fermi momentum becomes large.

In a cold, dense fermionic system particles can only scatter elastically if their momenta lie on the Fermi surface, as states below the Fermi surface are not accessible due to the Pauli principle (the so called “Pauli-blocking” phenomenon), and states above the Fermi surface are not accessible due to energy conservation. If the Fermi momentum exceeds the QCD scale parameter $\Lambda_{\text{QCD}} \sim 200$ MeV, scattering events between nucleons start to probe distances of the order 1 fm or less, i.e., the nucleonic substructure of quarks and gluons becomes visible. The Fermi momentum in the ground state of nuclear matter can be inferred from Eq. (6) to be $k_{F,0} \simeq 250$ MeV. This is already of the order of Λ_{QCD} . Nevertheless, a description of nuclear matter in terms of nucleonic degrees of freedom is certainly feasible around the ground state. At which densities does a description in terms of quark and gluon degrees of freedom become more appropriate? The “volume” occupied by a single nucleon can be estimated from its charge radius to be ~ 2 fm³. On the other hand, the specific volume of the system in the ground state is $n_{B,0}^{-1} \sim 6$ fm³. In this sense, nuclear matter in the ground state is dilute. However, increasing the density to about $3 n_{B,0}$, the system becomes densely packed with nucleons. At larger densities, they will even start to overlap. Therefore, around densities of a few times nuclear matter ground state density, one expects that a description of the system in terms of quarks and gluons is more appropriate.

Similar arguments also apply to a system at nonzero temperature, even when the net-baryon number density is small. At nonzero temperature, nuclear matter consists not only of nucleons but also of other, thermally excited hadrons. For a non-interacting system in thermodynamical equilibrium and neglecting quantum statistics, the hadron number densities are proportional to $n_i \sim m_i^2 T K_2(m_i/T) e^{\mu_i/T}$, where i labels the hadron species, m_i is their mass, μ_i is their chemical potential, and $K_2(x)$ is a modified Bessel function of the second kind. For nonzero temperature and small net-baryon number density, the lightest hadrons, the pions, are most abundant. At nonzero temperature and small baryon chemical potential, the typical momentum scale for scattering events between hadrons is set by the temperature T . If the temperature is on the order of or larger than Λ_{QCD} , scattering between hadrons starts to probe their quark-gluon substructure. Moreover, since the particle density increases with the temperature, the hadronic wave functions will start to overlap for large temperatures. Consequently, above a certain temperature one expects a description of nuclear matter in terms of quark and gluon degrees of freedom to be more appropriate.

The picture which emerges from these considerations is the following: for quark chemical potentials μ which are on the order of 350 MeV or smaller, and for temperatures $T < \Lambda_{\text{QCD}} \sim 200$ MeV, nuclear matter is a gas of hadrons. (At very small temperatures $T < 10$ MeV, there is a gaseous and a liquid nucleonic phase, cf. Sec. 2.2.) On the other hand, for $T, \mu \gg \Lambda_{\text{QCD}}$, nuclear matter consists of quarks and gluons. The natural question which emerges is, whether the “hadron phase” and the “quark-gluon phase”, the so-called *quark-gluon plasma* (QGP), are separated by a phase transition in the thermodynamic sense. The rigorous way to decide this question is by identifying an order parameter which is nonzero in one phase and zero in the other. This will be discussed in more detail in the following.

2.3.2 Pure gauge theory

Let us first study the pure $[SU(N_c)]$ gauge theory, i.e., QCD without dynamical quarks (sometimes also termed the $N_f = 0$ case). In this theory, there is a phase transition between a low-temperature and a high-temperature phase, cf. Sec. 3.2. The order parameter for this transition is the expectation value

$\langle L(\mathbf{x}) \rangle$ of the Polyakov loop (or Wilson line)

$$L(\mathbf{x}) = \frac{1}{N_c} \text{Tr} \left\{ \text{P} \exp \left[ig \int_0^{1/T} d\tau A_a^0(\tau, \mathbf{x}) T_a \right] \right\} , \quad (7)$$

where P stands for path-ordering. The expectation value of an operator \mathcal{O} in the grand canonical ensemble is defined as

$$\langle \mathcal{O} \rangle \equiv \frac{1}{\mathcal{Z}} \int \mathcal{D}\bar{\psi} \mathcal{D}\psi \mathcal{D}A_a^\mu \mathcal{O} \exp \left[\int_X (\mathcal{L} + \mu \mathcal{N}) \right] . \quad (8)$$

The expectation value $\langle L(\mathbf{x}) \rangle$ vanishes in the low-temperature phase. If one interprets this expectation value as $\sim \exp(-F_Q/T)$, where F_Q is the free energy of an infinitely heavy quark [23], then $\langle L(\mathbf{x}) \rangle = 0$ implies that the free energy is infinite, corresponding to confinement of color charges. In the high-temperature phase, $\langle L(\mathbf{x}) \rangle \neq 0$, which implies that the free energy of an infinitely heavy quark is finite. This indicates the liberation of colored degrees of freedom, i.e., deconfinement. The expectation value of the Polyakov loop is therefore the order parameter for the deconfinement transition.

For an $[SU(N_c)]$ gauge theory the action has a global $Z(N_c)$ symmetry. In the high-temperature phase, the nonzero expectation value of the Polyakov loop breaks this symmetry spontaneously. In the low-temperature phase, $\langle L(\mathbf{x}) \rangle = 0$, and this symmetry is restored. For two colors, $N_c = 2$, the effective theory in the critical region around the phase transition is given by a $Z(2)$ spin model, i.e., it is in the same universality class as the Ising model [23]. This model has a second-order phase transition. For $N_c = 3$, the effective theory is that of a $Z(3)$ spin model [24], i.e., it is in the universality class of the 3-state Potts model which has a first-order phase transition [25]. The transition temperature was computed to be $T_c \simeq 270$ MeV [15, 16], see also Sec. 3.2.

2.3.3 Dynamical quarks

In the presence of dynamical quarks, $N_f > 0$, the picture becomes somewhat more complicated. The fermionic term in the QCD Lagrangian (2) breaks the $Z(N_c)$ symmetry explicitly, and thus there is strictly speaking no order parameter for deconfinement. Nevertheless, the QCD transition in the presence of dynamical quarks has an order parameter, which is related to the chiral symmetry of QCD. While the QCD Lagrangian (2) is chirally symmetric, the ground state of QCD is not, i.e., chiral symmetry is spontaneously broken. It is instructive to review these arguments in more detail.

In the chiral limit, where the quark mass matrix is zero, $m = 0$, the QCD Lagrangian (2) is invariant under global chiral $U(N_f)_r \times U(N_f)_\ell$ rotations of the quark fields. To see this, decompose the quark spinors into right- and left-handed spinors,

$$\psi \equiv \psi_r + \psi_\ell , \quad \psi_{r,\ell} \equiv \mathcal{P}_{r,\ell} \psi , \quad \mathcal{P}_{r,\ell} \equiv \frac{1 \pm \gamma_5}{2} , \quad (9)$$

where $\mathcal{P}_{r,\ell}$ are chirality projectors. Then perform a $U(N_f)_{r,\ell}$ transformation on the right/left-handed quark spinors,

$$\psi_{r,\ell} \rightarrow U_{r,\ell} \psi_{r,\ell} , \quad U_{r,\ell} \equiv \exp \left(i \sum_{a=0}^{N_f^2-1} \alpha_{r,\ell}^a T_a \right) \in U(N_f)_{r,\ell} , \quad (10)$$

where $\alpha_{r,\ell}^a$ are the parameters and T_a the generators of $U(N_f)_{r,\ell}$. The Lagrangian (2) remains invariant under this transformation, $\mathcal{L}(\psi_r, \psi_\ell) \equiv \mathcal{L}(U_r \psi_r, U_\ell \psi_\ell)$. The chiral group $U(N_f)_r \times U(N_f)_\ell$ is isomorphic to the group $U(N_f)_V \times U(N_f)_A$ of unitary vector and axial transformations, where $V \equiv r + \ell$, $A \equiv r - \ell$, i.e., $\alpha_V \equiv (\alpha_r + \alpha_\ell)/2$, $\alpha_A \equiv (\alpha_r - \alpha_\ell)/2$. Any unitary group is the direct product of a special unitary group and a complex phase, $U(N_f) \cong SU(N_f) \times U(1)$. Thus, $U(N_f)_r \times U(N_f)_\ell \cong$

$SU(N_f)_r \times SU(N_f)_\ell \times U(1)_r \times U(1)_\ell \cong SU(N_f)_r \times SU(N_f)_\ell \times U(1)_V \times U(1)_A$. The vector subgroup $U(1)_V$ of this symmetry group corresponds to quark number conservation. As physical states trivially conserve quark number, this subgroup does not affect the chiral dynamics and can be omitted from the further symmetry consideration. This leaves an $SU(N_f)_r \times SU(N_f)_\ell \times U(1)_A$ symmetry. The axial subgroup $U(1)_A$ is broken explicitly by instantons (the so-called $U(1)_A$ anomaly of QCD) [26], leaving an $SU(N_f)_r \times SU(N_f)_\ell$ symmetry which determines the chiral dynamics. Since instantons are screened in a hot and/or dense medium [12], the $U(1)_A$ symmetry may become effectively restored in matter. Then, the chiral symmetry is again enlarged to $SU(N_f)_r \times SU(N_f)_\ell \times U(1)_A$.

Nonzero quark masses break the chiral symmetry of the QCD Lagrangian explicitly. The quark mass term in Eq. (2) is

$$\bar{\psi}^i m_{ij} \psi^j \equiv \bar{\psi}_r^i m_{ij} \psi_\ell^j + \bar{\psi}_\ell^i m_{ij} \psi_r^j, \quad (11)$$

where flavor indices $i, j = 1, \dots, N_f$ are explicitly written, a sum over repeated indices is implied, and the properties $\mathcal{P}_{r,\ell}\gamma_0 = \gamma_0\mathcal{P}_{\ell,r}$, $\mathcal{P}_r \mathcal{P}_\ell = \mathcal{P}_\ell \mathcal{P}_r = 0$ of the chirality projectors were used. Now suppose all quark masses were equal, $m_{ij} \equiv m \delta_{ij}$. Performing chiral $SU(N_f)_r \times SU(N_f)_\ell \times U(1)_A$ rotations of the quark fields, one observes that the mass term (11) preserves an $SU(N_f)_V$ symmetry. All axial symmetries are explicitly broken. If less than N_f quark masses are equal, say $M < N_f$, the preserved vector symmetry is $SU(M)_V$. In nature, where $m_u \simeq m_d \ll m_s \ll m_c \ll m_b \ll m_t$, one only has the well-known (approximate) $SU(2)_V$ isospin symmetry. Consequently, exotic hadrons with strange, charm, bottom, or top degrees of freedom are not degenerate in mass with their non-strange counterparts.

The mass term $\bar{\psi}^i m_{ij} \psi^j$ in the QCD Lagrangian is of the same form as the term $\mathbf{H} \cdot \mathbf{S}$ in spin models, which couples the spin \mathbf{S} to an external magnetic field \mathbf{H} . Obviously, the operator $\bar{\psi}^i \psi^j$ corresponds to the spin \mathbf{S} , while the quark mass matrix m_{ij} assumes the role of the external magnetic field \mathbf{H} . Thus, the expectation value $\langle \bar{\psi}^i \psi^j \rangle$ is the analogue of the expectation value of the spin, the magnetization $\mathbf{M} \equiv \langle \mathbf{S} \rangle$. While the mass term explicitly breaks the chiral symmetry $SU(N_f)_r \times SU(N_f)_\ell \times U(1)_A$ of the QCD Lagrangian to an (approximate) $SU(2)_V$ symmetry, the external magnetic field in spin models explicitly breaks the rotational symmetry $O(3)$ to $O(2)$.

The analogy between QCD and spin models, however, extends further than this. Even in the absence of external magnetic fields, in spin models with ferromagnetic interactions rotational symmetry is spontaneously broken due to a nonvanishing magnetization $\mathbf{M} \neq 0$ in the ferromagnetic phase. Analogously, in the QCD vacuum, chiral symmetry is spontaneously broken by a nonvanishing expectation value $\langle \bar{\psi}^i \psi^j \rangle_{\text{vac.}} \neq 0$. Let us introduce the so-called chiral condensate Φ^{ij} and its complex conjugate, $\Phi^{ij\dagger}$, via

$$\Phi^{ij} \sim \langle \bar{\psi}_\ell^i \psi_r^j \rangle, \quad \Phi^{ij\dagger} \sim \langle \bar{\psi}_r^i \psi_\ell^j \rangle. \quad (12)$$

A nonvanishing expectation value $\langle \bar{\psi}^i \psi^j \rangle \neq 0$ is then equivalent to $\Phi^{ij} + \Phi^{ij\dagger} \neq 0$. Just like the mass term in the QCD Lagrangian, a nonvanishing chiral condensate breaks the chiral symmetry. In the chiral limit, $m_{ij} \equiv 0$, nothing distinguishes one quark flavor from another and, consequently, $\Phi_{\text{vac.}}^{ij} = \phi_0 \delta^{ij}$. (In principle, there is another possibility how a chiral condensate could break the chiral symmetry, for a more detailed discussion see below and Ref. [27].) This chiral condensate breaks the chiral $U(N_f)_r \times U(N_f)_\ell$ symmetry spontaneously to $U(N_f)_V$. To see this, note that the chiral condensate is still invariant under vector transformations, $\Phi \rightarrow U_r \Phi U_\ell^\dagger \equiv \Phi$, if $U_r = U_\ell \equiv U_V$, but not under axial transformations, $\Phi \rightarrow U_r \Phi U_\ell^\dagger \neq \Phi$, if $U_r = U_\ell^\dagger \equiv U_A$.

According to Goldstone's theorem, the breaking of the global chiral symmetry leads to the occurrence of massless modes, the so-called Goldstone bosons. The number of Goldstone bosons is identical to the number of broken generators. In the QCD vacuum, where the $U(1)_A$ anomaly is present, the breaking pattern is $SU(N_f)_r \times SU(N_f)_\ell \rightarrow SU(N_f)_V$, i.e., in this case there are $N_f^2 - 1$ broken generators,

corresponding to the generators of the broken axial group $SU(N_f)_A$. For $N_f = 1$, there is no global chiral symmetry that could be broken, and thus no Goldstone boson. For $N_f = 2$, the Goldstone bosons are the three pions, the lightest hadronic species. In nature, the pions are not completely massless, because the chiral symmetry is explicitly broken by the small, but nonzero quark mass term in the QCD Lagrangian. This turns the Goldstone bosons into so-called pseudo-Goldstone bosons. For $N_f = 3$, the pseudo-Goldstone bosons correspond to the pseudoscalar meson octet, comprising pions, kaons, and the eta meson. Since chiral symmetry is more strongly broken by the larger strange quark mass, the pseudo-Goldstone bosons carrying strangeness are heavier than the pions. For $N_f \geq 4$, the explicit symmetry breaking by the heavy exotic quark flavors is so strong that the would-be Goldstone bosons are actually heavier than the ordinary (i.e. non-Goldstone) non-strange bosons.

In spin models, rotational symmetry is restored above some critical temperature and the magnetization vanishes. The magnetization is the order parameter for this so-called ferromagnet-diamagnet phase transition. By analogy, one expects a similar mechanism to occur in QCD, i.e., Φ^{ij} to vanish above some critical temperature. The symmetry of the ground state is then restored to the original chiral symmetry, i.e., $SU(N_f)_r \times SU(N_f)_\ell$, if the $U(1)_A$ anomaly is still present, or $SU(N_f)_r \times SU(N_f)_\ell \times U(1)_A$, if instantons are sufficiently screened at the transition in order to effectively restore the $U(1)_A$ symmetry. Lattice QCD calculations show that this expectation is indeed fulfilled: there is a phase transition between the low-temperature phase where chiral symmetry is broken and the high-temperature phase where it is restored, for details see Sec. 3. Just like the magnetization in spin models, the chiral condensate Φ^{ij} is the order parameter for this so-called chiral phase transition.

In the case of massless quarks, $m_{ij} \equiv 0$, based on universality arguments one can analyse the order of the chiral transition in the framework of a linear sigma model for the order parameter field Φ^{ij} [28]. This linear sigma model is an effective theory, i.e, all terms allowed by the original chiral symmetry must in principle appear,

$$\mathcal{L}_{\text{eff}} = \text{Tr} \left(\partial_0 \Phi^\dagger \partial^0 \Phi \right) - v^2 \text{Tr} \left(\nabla \Phi^\dagger \cdot \nabla \Phi \right) - V_{\text{eff}}(\Phi) , \quad (13)$$

where the effective potential

$$V_{\text{eff}}(\Phi) = m^2 \text{Tr} \left(\Phi^\dagger \Phi \right) + \lambda_1 \left[\text{Tr} \left(\Phi^\dagger \Phi \right) \right]^2 + \lambda_2 \text{Tr} \left(\Phi^\dagger \Phi \right)^2 - c \left(\det \Phi + \det \Phi^\dagger \right) + \dots \quad (14)$$

determines the ground state of the theory. In Eq. (13) it was assumed that the first term is canonically normalized. However, since Lorentz symmetry is explicitly broken in a medium at nonzero temperature, the coefficient v^2 in Eq. (13) may in general be different from one. In Eq. (14), \dots denote higher-dimensional operators which are irrelevant for the discussion of the order of the phase transition. For $c \neq 0$, the chiral symmetry of \mathcal{L}_{eff} is $SU(N_f)_r \times SU(N_f)_\ell$, while for $c = 0$, it is $SU(N_f)_r \times SU(N_f)_\ell \times U(1)_A$. Thus, the $U(1)_A$ anomaly is present for $c \neq 0$, and absent for $c = 0$. While these chiral symmetries are manifest in the Lagrangian (13), the ground state of the theory respects them only for $c = 0$ and $m^2 > 0$. For $c = 0$ and $m^2 < 0$ the chiral symmetry is spontaneously broken by a nonvanishing vacuum expectation value for the order parameter. Consequently, if the linear sigma model is to describe the chiral transition in QCD, one has to ensure that $m^2 < 0$ for $c = 0$. There are still two possibilities how the order parameter can break the symmetry. As shown in Ref. [27], if $\lambda_2 > 0$ the ground state is given by $\Phi_{\text{vac.}}^{ij} = \phi_0 \delta^{ij}$, while for $\lambda_2 < 0$ the ground state is given by $\Phi_{\text{vac.}}^{ij} = \phi_0 \delta^{i1} \delta^{j1}$. (The choice of the 1-direction in right- and left-handed flavor space is arbitrary.) Nature realizes the first possibility. For the case $c \neq 0$, no general arguments can be made; whether the ground state of the theory breaks chiral symmetry spontaneously depends on the particular values for the coupling constants c, λ_1, λ_2 and the number of flavors N_f . Note that nonvanishing quark masses can also be accounted for by adding a term

$$\mathcal{L}_H \equiv \text{Tr} \left[H \left(\Phi + \Phi^\dagger \right) \right] \quad (15)$$

to the right-hand side of Eq. (13). As discussed above, this term is the analogue of the term $\mathbf{H} \cdot \mathbf{S}$ in spin models. Consequently, the external “magnetic field” H_{ij} is proportional to the quark mass matrix m_{ij} .

For $N_f = 1$, there is no difference between the two quartic invariants in Eq. (14), and one may set $\lambda_1 + \lambda_2 \equiv \lambda$. In the presence of the $U(1)_A$ anomaly, $c \neq 0$, there is also no chiral symmetry, and the transition is crossover, due to the linear term $\sim c$, which tilts the effective potential such that the (thermal) ground state $\langle \Phi \rangle_T \neq 0$. If the $U(1)_A$ anomaly is absent, $c = 0$, the effective theory for the order parameter falls in the same universality class as that of the $O(2)$ Heisenberg magnet, and thus the transition is of second order.

For $N_f = 2$ and in the presence of the $U(1)_A$ anomaly, the chiral symmetry is $SU(2)_r \times SU(2)_\ell$, which is isomorphic to $O(4)$. The effective theory for the order parameter is in the universality class of the $O(4)$ Heisenberg magnet. Consequently, the transition is of second order [28]. If the $U(1)_A$ symmetry is effectively restored at the phase transition temperature, the symmetry group is larger, $SU(2)_r \times SU(2)_\ell \times U(1)_A$, which is isomorphic to $O(4) \times O(2)$, and the transition is of first order. Lattice QCD calculations determine the transition temperature to be $T_c \simeq 172$ MeV [15, 16].

For $N_f = 3$, the chiral transition is of first order, both when the $U(1)_A$ symmetry is explicitly broken by instantons or when it is effectively restored at the transition. In the first case, the effective theory features a cubic invariant in the order parameter field (the term $\sim \det \Phi + \det \Phi^\dagger$), which drives the chiral transition first order [28]. In the second case, the transition is fluctuation-induced of first order [28]. This also holds for $N_f \geq 4$, irrespective of whether the $U(1)_A$ symmetry is explicitly broken or not. For $N_f = 3$, lattice QCD calculations find the transition temperature to be $T_c \simeq 155$ MeV [16], cf. Sec. 3.2.

2.3.4 The quark-mass diagram

Nonvanishing quark masses lead to the term (15) in the effective theory for the order parameter field. This term is linear in Φ , such that the effective potential is tilted. This may render a first or second order phase transition a crossover transition (similar to the case $N_f = 1$ with $U(1)_A$ anomaly discussed in Sec. 2.3.3, where a tilt in the potential is induced by the linear term $\sim c$). For instance, the second-order transition for QCD with $N_f = 2$ massless flavors is rendered crossover by a nonvanishing quark mass. The first-order phase transition for QCD with $N_f = 3$ massless flavors can also become crossover, if the quark masses are sufficiently large. In the real world, the up and down quark are approximately of the same mass, while the strange quark is much heavier. It is customary to put $m_q \equiv m_u \simeq m_d$ and identify first-order regions, second-order lines, and crossover regions in an (m_q, m_s) diagram, see Fig. 2. To simplify the following discussion, only the case where the $U(1)_A$ anomaly is present will be considered.

The origin in Fig. 2 corresponds to the massless 3-flavor case, and the transition is of first order. The upper left corner corresponds to the massless 2-flavor case, since the strange quark is infinitely heavy. Here, the transition is of second order. The lower right corner is the case of one massless flavor. The transition is crossover. The upper right corner, where all quark flavors are infinitely heavy, corresponds to the pure gauge theory. At this point the transition is of first order.

The first-order regions around the origin and the upper right corner extend somewhat into the (m_q, m_s) plane and are bounded by critical lines where the transition is of second order. Along these critical lines, the second-order phase transitions are in the universality class of the Ising model, $Z(2)$. In between the critical lines, the transition is crossover. There is also a second-order phase transition line (with a phase transition in the $O(4)$ universality class) extending downwards from the upper left corner along the m_s axis. There is a tricritical point where this line meets the second-order phase transition

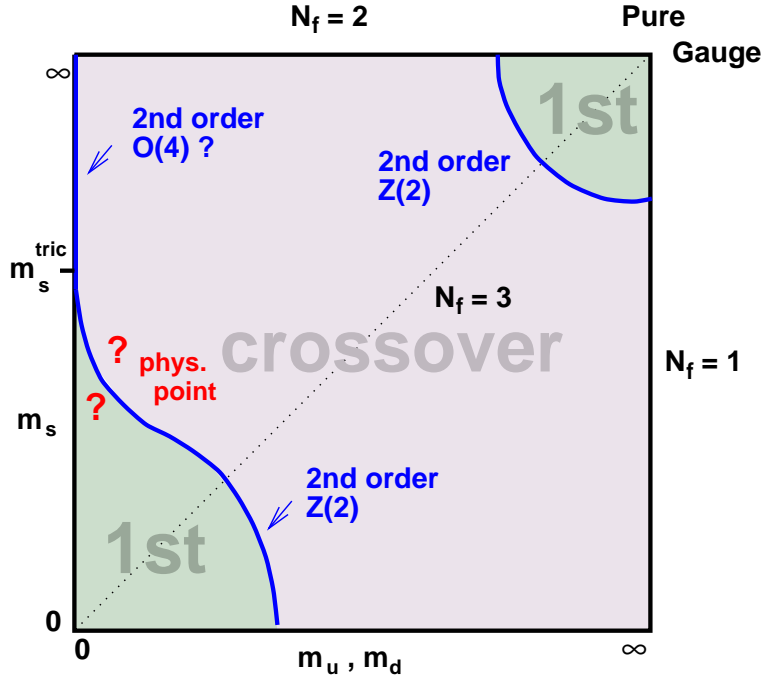


Figure 2: The quark-mass diagram (from Ref. [16]).

line bordering the first-order region around the origin [29]. It is an interesting question whether the real world, where $m_q \sim 5 \text{ MeV} \ll m_s \sim 100 \text{ MeV}$, is still inside the first-order phase transition region or already in the crossover region. There are ongoing lattice QCD studies to decide this question, which at present favor the latter possibility [16], see also Sec. 3.2 for more details.

2.3.5 Nonzero quark chemical potential

So far, the quark-hadron phase transition was studied at $\mu = 0$. Let us finally discuss the case of nonzero quark chemical potential. For many years, lattice QCD studies at nonzero chemical potential were hampered by numerical problems related to the so-called sign problem of the fermion determinant. Only recently there have been attempts to compute the order of the phase transition at nonzero quark chemical potential; for details, see Sec. 3.6. So far, these calculations have been done on fairly small lattices with rather heavy quarks. Consequently, they show a crossover transition at $\mu = 0$. This crossover transition extends to the point $(T, \mu)_{\text{cr}} = (160 \pm 3.5, 242 \pm 12) \text{ MeV}$, see also Fig. 10.

This point is a critical point where the transition is of second order. It is in the universality class of the Ising model, i.e., $Z(2)$. For smaller temperatures and larger chemical potentials, the transition becomes of first order. The critical point will move towards the T axis when the quark masses are decreased. From the discussion in Sec. 2.3.4 one cannot exclude the possibility that, for realistic quark masses, the first-order phase transition line emerges directly from the T axis.

Finally, the question arises whether the line of first-order phase transitions extends all the way down to $T = 0$, and if so, at which point it hits the μ axis. Renormalization group arguments [30] suggest that the behavior at zero temperature is very similar to the one at nonzero temperature: the transition is of first order for $N_f \geq 3$ as well as for $N_f = 2$ in the absence of the $U(1)_A$ anomaly, while it could be of second order for $N_f = 2$ in the presence of the $U(1)_A$ anomaly. In the latter case, however, it would remain of second order along the whole phase transition line, and only the universality class

would change from $O(4)$ critical behavior at nonzero temperature to Gaussian critical behavior at zero temperature. Since lattice QCD calculations [31] indicate that the transition becomes of first order for temperatures below the critical point, and since it is hard to imagine that the transition switches back to second order as the temperature decreases further, this possibility can most probably be ruled out. Note, however, that if quark-gluon matter is in a color-superconducting phase to the right of the QCD phase transition line, other possibilities emerge, for details, see Sec. 2.4.

In any case, model calculations [32] within a Nambu–Jona-Lasinio (NJL) model [33] support the picture that the transition remains of first order below the critical point all the way down to the μ axis. The value of μ , where the first-order phase transition line meets the μ axis, depends sensitively on the parameters used in these model calculations. In any case, its actual value should not be taken too seriously, because the NJL model with quark degrees of freedom does not have a phase where matter consists of nucleons. Instead, the transition to quark matter happens at a quark chemical potential which is of the order of the ground state quark chemical potential, $\mu_0 \simeq 308$ MeV. Since we know that nucleonic matter exists, this behavior is clearly unphysical.

The critical point has recently received a fair amount of attention [34]. For a second-order phase transition in the $Z(2)$ universality class, there must be one massless degree of freedom. The fact that this degree of freedom is massless causes critical fluctuations. These fluctuations were suggested to be an experimental signature for the critical point in heavy-ion collisions. Which physical particle does the massless degree of freedom correspond to? For realistic quark masses, the pions are not massless in the vacuum, and it is unlikely that they become massless at the critical point (the pions usually get more massive when temperature is increased). Moreover, since isospin is still a good symmetry at the critical point, all pions would simultaneously become massless. Then, one would have three massless modes instead of just one. Consequently, the pions cannot assume the role of the massless mode. Since the critical point exists even when considering only $N_f = 2$ quark flavors and since, for $N_f = 2$, there is only one other degree of freedom in the effective theory besides the pions, it must be this degree of freedom that becomes massless: the scalar σ meson [32, 34]. In the vacuum, this meson has a mass of about 400 – 1200 MeV [35], and consequently a large decay width into two pions. If it becomes massless, this decay channel closes, and its width should become small. Moreover, it should be abundantly produced. When these σ mesons decouple from the collision region, they assume their vacuum masses and rapidly decay into pions. Besides critical fluctuations, another signature for the critical point would thus be the late emission of a large amount of pions in a heavy-ion collision.

2.4 The Color-Superconducting Phases of QCD

2.4.1 Proof of existence of color superconductivity

There are other phases in the phase diagram of nuclear matter, which have recently received much attention in the literature, the so-called color-superconducting phases in sufficiently cold and dense quark matter [18]. Color superconductivity occurs, because there is an attractive interaction between two quarks at the Fermi surface [36, 37]. Then, by Cooper’s theorem, these quarks form Cooper pairs which condense in the new ground state of the system.

At least at asymptotically large quark chemical potentials, the existence of an attractive interaction between quarks at the Fermi surface, and thus the existence of color superconductivity, can be rigorously proven. Due to asymptotic freedom [1], when $\mu \gg \Lambda_{\text{QCD}}$, the strong coupling constant of QCD, evaluated at the scale μ , becomes small, $g(\mu) \ll 1$, such that the dominant interaction between quarks is given by single-gluon exchange. The scattering amplitude for single-gluon exchange in an $[SU(N_c)]$

gauge theory is proportional to

$$(T_a)_{ki} (T_a)_{lj} = -\frac{N_c + 1}{4N_c} (\delta_{jk} \delta_{il} - \delta_{ik} \delta_{jl}) + \frac{N_c - 1}{4N_c} (\delta_{jk} \delta_{il} + \delta_{ik} \delta_{jl}) , \quad (16)$$

where i, j are the fundamental colors of the two quarks in the incoming channel, and k, l their respective colors in the outgoing channel. Under the exchange of the color indices of either the incoming or the outgoing quarks the first term is antisymmetric, while the second term is symmetric. In group theoretical language, for $[SU(3)_c]$ Eq. (16) represents the coupling of two fundamental color triplets to an (antisymmetric) color antitriplet and a (symmetric) color sextet,

$$[\mathbf{3}]^c \times [\mathbf{3}]^c = [\bar{\mathbf{3}}]^c_a + [\mathbf{6}]^c_s . \quad (17)$$

The minus sign in front of the antitriplet contribution in Eq. (16) signifies the fact that this channel is attractive, while the sextet channel is repulsive. Therefore, one expects that quark Cooper pairs condense in the color-antitriplet channel.

This argument holds rigorously at asymptotically large densities. The highest densities of nuclear matter that can be achieved in the laboratory through heavy-ion collisions, or that occur in nature in the interior of neutron stars, are of the order of ten times nuclear matter ground state density. At these densities, the quark chemical potential is still fairly small, $\mu \sim 0.5$ GeV. For phenomenology it is therefore important to answer the question whether color superconductivity also exists at the (comparatively moderate) densities occurring in nature. There is no rigorous way to answer this question, as an extrapolation of the above asymptotic argument becomes unreliable when $g(\mu/\Lambda_{\text{QCD}}) \sim 1$. Nevertheless, calculations in the framework of the NJL model [38] show that color superconductivity does seem to occur also at moderate densities. In this case, the attractive interaction could be mediated by instanton (instead of single-gluon) exchange.

Color superconductivity is a much more complicated phenomenon than ordinary superconductivity. From a very qualitative point of view, in comparison to electrons, quarks carry additional quantum numbers such as color and flavor. The wave function of a Cooper pair has to be antisymmetric under the exchange of the two fermions forming the pair. Consequently, the possible color and flavor representations of the two-fermion state have to be chosen in a way which respects this antisymmetry. This requirement helps to classify all possible color-superconducting condensates [39, 40]. This classification will be presented in the following.

2.4.2 Classification of color-superconducting phases

The baryon density in heavy-ion collisions or in neutron stars is at most of the order of ten times the nuclear ground state density. Therefore, the quark chemical potential is unlikely to assume values beyond $\mu \sim 1$ GeV. At zero temperature, one can only have fermions if the Fermi energy μ exceeds their mass. Thus, only the three lightest quark flavors, up, down, and strange, play any role; charm, bottom, and top quarks are too heavy. For small temperatures, these heavy flavors can be thermally excited, but their abundance is exponentially suppressed $\sim \exp(-m_f/T)$, cf. Sec. 2.3.1. Therefore, they will be excluded from the following consideration. For $\mu \sim 1$ GeV, up and down quarks can be treated as truly ultrarelativistic particles, as $m_q/\mu \sim 10^{-3}$. To first approximation, also the strange quark will be considered to be massless. Corrections due to the strange quark mass can be treated perturbatively, the correction factor being of order $m_s/\mu \sim 10^{-1}$ [21].

For ultrarelativistic particles, spin S and angular momentum L are not separately good quantum numbers, only the total spin $J = L + S$ is. Therefore, possible Cooper pair wave functions should be classified according to their total spin J . Let us first focus on the spin-zero channel, $J = 0$. The $J = 0$

representation of the $SU(2)_J$ spin group is totally antisymmetric. Therefore, the remaining color and flavor part of the Cooper pair wave function has to be symmetric under the simultaneous exchange of color and flavor indices in order to fulfill the requirement of overall antisymmetry. If one assumes that quarks pair in the antisymmetric color-antitriplet channel, one has no choice but to also chose an antisymmetric flavor representation. For $N_f = 1$ flavor, this is impossible, as there is no flavor symmetry group with an antisymmetric representation.

One therefore has to consider at least $N_f = 2$ quark flavors (for instance, up and down), where the most simple representation is the antisymmetric flavor singlet $[1]_a^f$ representation of the $SU(2)_V$ flavor group. Therefore, the most simple $J = 0$ quark Cooper pair condensate has the form

$$\Phi_{ij}^{fg} = \epsilon_{ijk} \epsilon^{fg} \Phi_k . \quad (18)$$

Here, $i, j = 1, \dots, N_c$ are the color indices of the quarks forming the Cooper pair, while $f, g = 1, \dots, N_f$ are the corresponding flavor indices. The two totally antisymmetric tensors on the right-hand side ensure that the condensate belongs to the $[\bar{\mathbf{3}}]_a^c$ in color, as well as the $[1]_a^f$ representation in flavor space. The color-superconducting phase represented by the condensate (18) is commonly called the “2SC” phase (for “2-flavor color SuperConductor”).

Condensation of quark Cooper pairs occurs if the quantity Φ_k on the right-hand side of Eq. (18) is nonzero, $\Phi_k \neq 0$. Thus, the quark Cooper pair condensate carries a fundamental color index k . This indicates that the local $[SU(3)_c]$ color symmetry is spontaneously broken by the quark Cooper pair condensate, similarly to the spontaneous breaking of the global chiral symmetry $SU(N_f)_r \times SU(N_f)_\ell$ by the chiral condensate (12) in the QCD vacuum discussed in Sec. 2.3.3. In this sense, Φ_k is the order parameter for color superconductivity. It is zero in the phase of unbroken $[SU(3)_c]$ symmetry, and nonzero in broken phase where condensation of quark Cooper pairs occurs.

Of course, a local symmetry can never be truly broken spontaneously [41]. However, after fixing the gauge, spontaneous breaking does occur, just like in ordinary superconductivity or in the standard model of electroweak interactions. In ordinary superconductivity, the condensation of electron Cooper pairs breaks the $[U(1)_{\text{em}}]$ gauge symmetry of electromagnetism, while in the standard model, the Higgs field breaks $[SU(2)_\ell] \times [U(1)_Y]$ to $[U(1)_{\text{em}}]$. Analogously, the quark Cooper pair condensate (18) breaks the $[SU(3)_c]$ color gauge symmetry.

Since quarks carry baryon and electric charge, the Cooper pair condensate (18) in principle also breaks the global $U(1)_V$ of baryon number conservation and the local $[U(1)_{\text{em}}]$ of electromagnetism. In the discussion of chiral symmetry breaking, these symmetries were never broken because the chiral condensate consists of a quark and an antiquark which carry opposite baryon and electric charge. The chiral condensate is thus a singlet under $U(1)_V$ and $[U(1)_{\text{em}}]$ and consequently preserves these symmetries. This is different for a color-superconducting condensate which consists of two quarks. It turns out, however, that there exists a “rotated” baryon number $\tilde{U}(1)$ symmetry and a “rotated” electromagnetic $[\tilde{U}(1)]$ symmetry, which are formed from the original baryon number and electromagnetic symmetries and the eighth generator of $[SU(3)_c]$ [42]. This is similar to electroweak symmetry breaking, where the $[U(1)_{\text{em}}]$ symmetry of electromagnetism is a combination of the $[U(1)_Y]$ hypercharge symmetry and the third generator of $[SU(2)_\ell]$. Thus, the $U(1)_V$ and $[U(1)_{\text{em}}]$ symmetries are not really broken in the 2SC phase, but “rotated”. The rotation angle is the analogue of the Weinberg angle in the standard model of electroweak interactions; for more details, see Sec. 5.4.

Spontaneous symmetry breaking in gauge theories does not lead to Goldstone bosons. Rather, what would have been a Goldstone mode will be “eaten” by a gauge boson which in turn becomes massive and thus acquires an additional longitudinal degree of freedom. There are as many massive gauge bosons as there would have been Goldstone modes due to spontaneous symmetry breaking. In ordinary superconductors, the electromagnetic $[U(1)_{\text{em}}]$ symmetry is broken, which has only one

generator. Consequently, there is a single Goldstone mode which is “eaten” by the single gauge boson present in this case, the photon. The photon acquires a so-called Meissner mass. What happens physically is that magnetic fields are damped on length scales of the order of the inverse Meissner mass, which in turn leads to the Meissner effect, the expulsion of magnetic flux from the superconductor. In the standard model of electroweak interactions, $[SU(2)_\ell] \times [U(1)_Y]$ is broken to $[U(1)_{\text{em}}]$, i.e., there are three Goldstone modes which in turn lead to the massive gauge bosons of the weak interaction, W^\pm and Z . The photon is massless. This is required, since it is the gauge boson of the residual $[U(1)_{\text{em}}]$ symmetry of electromagnetism. Analogously, in a color superconductor one expects some of the gluons to become massive. Exactly how many gluons acquire a mass depends on the pattern of symmetry breaking. For the condensate (18), one can clarify this via the following argument.

By a global color rotation, one can always orient the order parameter Φ_k to point in the 3-direction in color space (more precisely, the *anti*-3-direction, as condensation occurs in the color *anti*-triplet channel),

$$\Phi_k \equiv \delta_{k3} \Phi . \quad (19)$$

Physically, this means that if we call color 1 red, color 2 green, and color 3 blue, red up (or down) quarks and green down (or up) quarks condense to form an anti-blue Cooper pair condensate. Blue up and down quarks do not participate in condensation. The condensate (19) does not break the color $[SU(3)_c]$ gauge symmetry completely. The residual symmetry is a local $[SU(2)_c]$ symmetry in the space of the first two colors (in our conventions, red and green). Including electromagnetism, the symmetry breaking pattern for the condensate (19) is therefore $[SU(3)_c] \times [U(1)_{\text{em}}] \rightarrow [SU(2)_c] \times [\tilde{U}(1)]$. Consequently, there are $8 - 3 = 5$ broken generators, which lead to five massive gluons. The remaining three gluons must remain massless as they correspond to the gauge bosons of the residual local $[SU(2)_c]$ symmetry. This is also borne out by an explicit calculation of the gluon Meissner masses in the 2SC phase [43, 44]. The gauge boson of the local $[\tilde{U}(1)]$ symmetry (the “rotated” photon) is also massless. For more details, see Sec. 5.4.

For $N_f = 3$ flavors, condensation of quark Cooper pairs becomes considerably more interesting. First, to preserve the antisymmetry of the Cooper pair wave function the two quarks have to be in the $[\bar{\mathbf{3}}]_a^f$ representation of the global $SU(3)_V$ flavor symmetry. Consequently, the quark Cooper pair condensate has the form

$$\Phi_{ij}^{fg} = \epsilon_{ijk} \epsilon^{fgh} \Phi_k^h . \quad (20)$$

The difference to Eq. (18) is that, to ensure antisymmetry in flavor space, one is required to use the totally antisymmetric tensor of rank 3, ϵ^{fgh} , rather than its rank-2 counterpart. Consequently, an additional flavor index h appears in the order parameter, Φ_k^h . A nonvanishing order parameter automatically implies that not only the local $[SU(3)_c]$ color, but also the global $SU(3)_V$ flavor symmetry is broken. The situation is not unlike the one encountered in superfluid helium-3 [45]. Superfluid helium-3 forms Cooper pairs with spin $S = 1$ and angular momentum $L = 1$. (Both spin and angular momentum are good quantum numbers, as helium-3 is a non-relativistic system.) Consequently, the order parameter breaks the global $SO(3)_S$ of spin as well as the global $SO(3)_L$ of angular momentum. This breaking can occur in many possible ways, giving rise to a plethora of phases in superfluid helium-3.

Similarly, one would expect many different phases to occur in a 3-flavor color superconductor. However, in fact there are only two possibilities, one of which is likely to be realized in nature [40]. To see this, note the formal similarity between the order parameter Φ_k^h and the one encountered in chiral symmetry breaking, Φ^{ij} , in Sec. 2.3.3. While Φ^{ij} transforms under $SU(N_f)_r \times SU(N_f)_\ell$ (in the presence of the $U(1)_A$ anomaly), Φ_k^h transforms under $[SU(3)_c] \times SU(3)_V$. Consequently, the effective Lagrangian for Φ_k^h is of the same form (13) as for Φ^{ij} . The two possible patterns of symmetry breaking occurring in such an effective theory were already mentioned above.

If the coupling constant $\lambda_2 > 0$, the order parameter assumes the form

$$\Phi_k^h = \delta_k^h \Phi . \quad (21)$$

In contrast to the 2SC case, where blue quarks remained unpaired, now all quark colors and flavors participate in the pairing process. The order parameter (21) is similar to the one for chiral symmetry breaking, where $\Phi^{ij} = \delta^{ij} \Phi$. (In the ground state, $\Phi_{\text{vac.}} \equiv \phi_0$.) Similar to the chiral symmetry breaking pattern $SU(N_f)_r \times SU(N_f)_\ell \rightarrow SU(N_f)_V$, $V = r + \ell$, the condensate (21) breaks $[SU(3)_c] \times SU(3)_V$ to the vectorial subgroup $SU(3)_{c+V}$. The condensate is still invariant under vector transformations in color and flavor space, or in other words, a transformation in color requires a simultaneous transformation in flavor to preserve the invariance of the condensate. Therefore, the discoverers [46] of this 3-flavor color-superconducting state termed it the “**Color-Flavor-Locked**”, or short, “CFL” state. The residual $SU(3)_{c+V}$ symmetry is no longer a local symmetry, so that there are no massless gluons. The complete pattern of symmetry breaking, including the $U(1)_V$ symmetry of baryon number and the $[U(1)_{\text{em}}]$ symmetry of electromagnetism is $[SU(3)_c] \times SU(3)_V \times U(1)_V \times [U(1)_{\text{em}}] \rightarrow SU(3)_{c+V} \times [\tilde{U}(1)]$. In the CFL case, unlike the 2SC case, baryon number is broken, but a rotated electromagnetic $[\tilde{U}(1)]$ is again preserved. The symmetry breaking pattern leads to nine Goldstone bosons, eight of which are “eaten” by the gluons, i.e., all gluons acquire a Meissner mass. There is one Goldstone boson from the breaking of the $U(1)_V$ symmetry.

In the chiral limit, the flavor symmetry of QCD is actually not just $SU(3)_V$ but $SU(3)_r \times SU(3)_\ell$. Assuming that also the $U(1)_A$ symmetry of QCD is effectively restored at large quark densities, quark Cooper pair condensation of the form (21) breaks $[SU(3)_c] \times SU(3)_r \times SU(3)_\ell \times U(1)_V \times U(1)_A \times [U(1)_{\text{em}}]$ to $SU(3)_{c+V} \times [\tilde{U}(1)]$, i.e., not only the local color, but also the global chiral symmetry is broken. In addition to the eight massive gluons, there are also ten real Goldstone bosons, eight from the breaking of the $SU(3)_A$ chiral symmetry, and one each from the breaking of $U(1)_V$ and $U(1)_A$.

Closer inspection [47] shows that the excitation spectrum in the CFL state bears a striking resemblance to the one in the hadronic phase. Let us first focus on the fermionic sector. In the CFL phase, there are nine gapped fermionic quasiparticles (cf. also Sec. 5.2), eight of which are degenerate in mass. These correspond to the baryon octet in the QCD vacuum. The ninth quasiparticle is twice as heavy and does not have a counterpart in hadronic matter, but this is not a reason to worry, as such a particle would have a large decay width into lighter particles. In the bosonic sector, there are nine Goldstone bosons from the breaking of the axial $SU(3)_A \times U(1)_A$ symmetry, which correspond to the pseudoscalar nonet in the hadronic phase. Only the tenth Goldstone boson from the breaking of $U(1)_V$ does not have a counterpart in the QCD vacuum. Such a boson exists, however, in dense nuclear matter, where a superfluid $\Lambda\Lambda$ condensate may form, which also breaks the $U(1)_V$ baryon number symmetry. The preceding arguments have led to the conjecture of “continuity” between hadron and quark matter [47]. This conjecture states that, since there is no difference in symmetry between quark matter in the CFL state and hadronic matter, there need not be any phase boundary between these two phases at all. Of course, this requires that there is no other color-superconducting phase, for instance the 2SC state, which separates CFL matter from hadronic matter.

For $\lambda_2 < 0$, the order parameter is given by

$$\Phi_k^h = \delta_k^{h3} \delta_{k3} \Phi , \quad (22)$$

where the 3-direction is arbitrary. This condensate breaks $[SU(3)_c] \times SU(3)_V$ to $[SU(2)_c] \times SU(2)_V$. In this case, $[SU(2)_c]$ is still a local symmetry. Consequently, like in the 2SC case only five gluons become massive, and blue up, down, and strange quarks do not participate in the formation of Cooper pairs. Additionally, there are also five Goldstone bosons from the breaking of the flavor symmetry. There is

a more technical and a more physical argument, why the CFL state is most likely realized in nature. From the more technical point of view, one can show [40] that, to one-loop order, in QCD $\lambda_1 = 0$ and $\lambda_2 > 0$. From the more physical point of view, the CFL state is energetically favored because *all* quark colors and flavors (instead of just a few) acquire a gap at the Fermi surface. The gain in condensation energy is thus expected to be larger than for a state with a condensate of the form (22).

Although a single quark flavor cannot form Cooper pairs with total spin $J = 0$, it can pair in the $J = 1$ channel. This channel corresponds to the symmetric $[3]_s^J$ representation of the $SU(2)_J$ spin group. If one still assumes pairing to occur in the color $[\bar{3}]_a^c$ channel, the Cooper pair wave function is, as required, overall antisymmetric. The condensate is a 3-vector in space which points in the direction of the spin of the Cooper pair. It has the form [37, 39, 48, 49]

$$\Phi_{ij}^a = \epsilon_{ijk} \Phi_k^a , \quad (23)$$

where $a = x, y, z$ denotes the spatial component of the spin vector. Condensation breaks the local color $[SU(3)_c]$ symmetry and the global $SO(3)_J$ spin symmetry. This is similar to superfluid helium-3 where condensation breaks $SO(3)_S \times SO(3)_L$ (see discussion above). While many different phases arise, let us just mention two which are quite similar to the ones discussed in the context of three quark flavors, the so-called “Color-Spin-Locked” or CSL phase, where the order parameter assumes the form

$$\Phi_k^a = \delta_k^a \Phi , \quad (24)$$

and the so-called polar phase, where

$$\Phi_k^a = \delta_{k3} \delta^{az} \Phi . \quad (25)$$

In the CSL phase, the order parameter (24) is strikingly similar to the one in the CFL phase, cf. Eq. (21). All quark colors participate in the formation of Cooper pairs. Also the symmetry breaking pattern is similar, $[SU(3)_c] \times SO(3)_J \times U(1)_V \times [U(1)_{\text{em}}] \rightarrow SO(3)_{c+J}$. The main difference is that now there is no rotated electromagnetism $[\tilde{U}(1)]$, cf. Sec. 5.4. Consequently, all eight gluons *and* the photon become massive [50]. In the polar phase, the order parameter resembles that of Eq. (22). Neglecting electromagnetic interactions for the moment, the symmetry breaking pattern is $[SU(3)_c] \times SO(3)_J \times U(1)_V \rightarrow [SU(2)_c] \times SO(2)_J \times \tilde{U}(1)$. Like in the 2SC phase, the residual $[SU(2)_c]$ color symmetry is a local symmetry, and there are three massless and five massive gluons. The breaking of the rotational $SO(3)_J$ symmetry to $SO(2)_J$ also leads to two real Goldstone bosons. Baryon number is not broken, but merely rotated. Including the $[U(1)_{\text{em}}]$ of electromagnetism there is a small subtlety which is explained in more detail in Sec. 5.4: If there is only a single flavor present, or if all flavors carry the same electric charge, a rotated electromagnetic $[\tilde{U}(1)]$ symmetry exists. If there are at least two flavors which differ in charge, the $[U(1)_{\text{em}}]$ symmetry is broken. Table 1 summarizes the results of this section for the 2SC, the CFL, the CSL, and the polar phase of color-superconducting quark matter.

2.4.3 Color-superconducting phases in the nuclear matter phase diagram

How does color-superconductivity affect the phase diagram of nuclear matter? Let us first assume that the temperature is sufficiently small to favor a color-superconducting over the normal-conducting state. As long as $\mu \gg m_s$, the CFL state is likely to be the ground state of quark matter. Since one has (approximately) equal numbers of up, down, and strange quarks of colors red, green, and blue, the system is (approximately) neutral with respect to color and electric charge. However, when one extrapolates down to smaller quark chemical potentials, say of the order of $\mu \sim 500$ MeV, the strange quark mass is no longer negligibly small and causes, for a given μ , a mismatch in the Fermi surfaces between non-strange and strange quarks [51]. In general, a nonzero strange quark mass reduces the

Table 1: Color-superconducting phases in dense quark matter. For the polar phase, there is an additional $[\tilde{U}(1)]$ symmetry, if all flavors in the system carry the same electric charge.

phase	condensate	order parameter	residual symmetry
2SC	$\Phi_{ij}^{fg} = \epsilon_{ijk} \epsilon^{fg} \Phi_k$	$\Phi_k = \delta_{k3} \Phi$	$[SU(2)_c] \times \tilde{U}(1) \times [\tilde{U}(1)]$
CFL	$\Phi_{ij}^{fg} = \epsilon_{ijk} \epsilon^{fgh} \Phi_k^h$	$\Phi_k^h = \delta_k^h \Phi$	$SU(3)_{c+V} \times [\tilde{U}(1)]$
CSL	$\Phi_{ij}^a = \epsilon_{ijk} \Phi_k^a$	$\Phi_k^a = \delta_k^a \Phi$	$SO(3)_{c+J}$
polar	$\Phi_{ij}^a = \epsilon_{ijk} \Phi_k^a$	$\Phi_k^a = \delta_{k3} \delta^{az} \Phi$	$[SU(2)_c] \times \tilde{U}(1)$

number of strange quarks as compared to the massless species. This, in turn, leads to nonzero electric and color charge in the system. Consequently, one is forced to introduce chemical potentials for electric and color charge, which have to be tuned to again ensure overall electric and color neutrality. The chemical potential for a quark species of color i and flavor f thus reads

$$\mu_i^f = \mu - q^f \mu_e + t_i^3 \mu_3 + t_i^8 \mu_8 , \quad (26)$$

where q^f is the electric charge of flavor f ($q^u = 2/3$, $q^{d,s} = -1/3$), μ_e is the electron chemical potential, t_i^3 and t_i^8 are the color charges associated with the third and eighth generator of $[SU(3)_c]$, respectively ($t_r^3 = 1/2$, $t_g^3 = -1/2$, $t_b^3 = 0$, $t_{r,g}^8 = 1/(2\sqrt{3})$, $t_b^8 = -1/\sqrt{3}$), and μ_3 , μ_8 are the associated color chemical potentials. (One could also introduce individual chemical potentials for red, green, and blue quarks, but these can be written as linear combinations of μ , μ_3 , and μ_8 .) The mismatch in the Fermi surfaces of different quark species forming Cooper pairs is then

$$\delta k_{Fij}^{fg} \equiv k_{Fi}^f - k_{Fj}^g \simeq -(q^f - q^g) \mu_e + (t_i^3 - t_j^3) \mu_3 + (t_i^8 - t_j^8) \mu_8 - \frac{m_f^2}{2\mu_i^f} + \frac{m_g^2}{2\mu_j^g} , \quad (27)$$

where only the first correction in $m_f/\mu_i^f \ll 1$ was taken into account. Equation (27) shows that the mismatch in the Fermi surface between different quark species is proportional to the electric and color chemical potentials, as well as their mass difference.

The formation of Cooper pairs occurs at the Fermi surface. Typically, a Cooper pair consists of fermions with momenta which are in magnitude close to the Fermi momentum, but which have opposite directions, such that the total momentum of the Cooper pair is zero. However, when the mismatch δk_{Fij}^{fg} increases, it becomes increasingly more difficult to form such pairs with zero total momentum. For the species with the smaller Fermi surface one may take a fermion right at its Fermi surfaces, but in order to match the momentum, one has to go deeper into the Fermi sea of the other species. Pictorially speaking, forming a Cooper pair becomes energetically disfavored once the cost of “diving” into the Fermi sea to find such a matching fermion is higher than the gain in condensation energy by forming a Cooper pair. Whether this condition is fulfilled depends on the magnitude of the color-superconducting gap at the Fermi surface, ϕ_0 , compared to the mismatch in the Fermi surfaces, δk_{Fij}^{fg} . As long as $\phi_0 \gg \delta k_{Fij}^{fg}$, the Cooper-paired state remains the ground state of the system. However, when δk_{Fij}^{fg} becomes of the

order of ϕ_0 , or even considerably exceeds it, the Cooper-paired state becomes energetically disfavored as compared to normal-conducting state [52].

It was recently realized, however, that instead of a transition to the normal-conducting state many other possibilities can be envisioned. For instance, imagine being in the CFL state and for the moment neglect μ_e , μ_3 , and μ_8 in Eq. (27). Then, the CFL state will become energetically disfavored when $m_s^2/2\mu$ exceeds ϕ_0 [51]. Nevertheless, quark matter will not simply become normal-conducting, because there is nothing to prevent the up and down quarks to form a 2SC state. Of course, one cannot simply discard μ_e , μ_3 , and μ_8 from the consideration. Taking these chemical potentials into account to ensure overall neutrality with respect to color and electric charges, the 2SC state may become unstable with respect to the formation of a gapless superconductor [53], a crystalline color superconductor [54], or some other state with an even more exotic pairing scenario [55, 56].

However, also a more conventional pairing scenario is conceivable [50]: the dominant terms in the mismatch (27) are the ones $\sim \mu_e$ and the mass difference (the color chemical potentials μ_3 and μ_8 are parametrically smaller than the gap ϕ_0). Consequently, instead of realizing one of the more exotic pairing scenarios, it could be energetically favorable to simply pair quarks with the same charge and the same mass, i.e., of the same flavor. As discussed above, these Cooper pairs must have spin one. Although spin-one gaps are orders of magnitude smaller than spin-zero gaps [48, 49, 57], the gain in condensation energy $\Delta E_{\text{cond.}}$ is parametrically larger than for some of the aforementioned exotic pairing scenarios, for instance $\Delta E_{\text{cond.}} \sim \mu^2 \phi_0^2$ for spin-one pairing vs. $\Delta E_{\text{cond.}} \sim \phi_0^4$ for gapless superconductivity [53]. Whether, and if yes, which of these pairing scenarios are realized in nature, can only be decided by a quantitative comparison of the pressure in the various cases. This has not been done so far and to draw definite conclusions about the structure of the phase diagram of nuclear matter at small temperatures and chemical potentials of the order of $\mu \sim 500$ MeV appears to be premature at this point.

On the other hand, it is far simpler to decide what happens to a particular color-superconducting phase when one increases the temperature at a given chemical potential. Like in any other superconducting system, thermal motion will break up quark Cooper pairs. In BCS theory, the transition between superconducting and normal-conducting phases is usually of second order and occurs at a temperature T_c^{BCS} proportional to the size of the superconducting gap parameter ϕ_0 ,

$$T_c^{\text{BCS}} = \frac{e^\gamma}{\pi} \phi_0 \simeq 0.567 \phi_0 , \quad (28)$$

where $\gamma \simeq 0.577$ is the Euler-Mascheroni constant. In all color-superconducting systems, T_c either rigorously obeys this relation or differs only by a factor of order one from it, for details see Sec. 5.3 and Ref. [49]. The value of the color-superconducting gap parameter ϕ_0 is therefore of great importance in order to locate the transition line between the normal and the color-superconducting quark matter phases in the nuclear matter phase diagram. In Sec. 5 it will be discussed how to compute this gap parameter. Here it suffices to know that an extrapolation of the result of solving a gap equation in weak coupling QCD down to moderate densities suggests gap parameters of the order of 10 MeV for pairing in the spin-zero channel. NJL model calculations suggest somewhat larger values around 100 MeV. With Eq. (28), this would lead to transition temperatures of the order of 6 to 60 MeV. In the spin-one channel, the gaps and critical temperatures are typically two to three orders of magnitude smaller [48, 49, 57].

3 Lattice QCD

3.1 Basic Concepts

The most fundamental approach to compute thermodynamic properties of strongly interacting matter and, in particular, its equation of state, are lattice QCD calculations [58]. In these calculations, one directly computes the grand partition function (1) on a discretized space-time lattice, $V \times 1/T = (a_\sigma N_\sigma)^3 a_\tau N_\tau$, where $a_\sigma \equiv L/N_\sigma$ is the lattice spacing in spatial direction, $a_\tau \equiv 1/(N_\tau T)$ is the lattice spacing in Euclidean time (i.e. temperature) direction, and N_σ and N_τ are the number of lattice points in spatial and temporal direction, respectively. Any space-time point in $V \times 1/T$ is then parametrized as $x^\mu \equiv (\tau, \mathbf{x}) = (a_\tau l, a_\sigma i, a_\sigma j, a_\sigma k)$, with $0 \leq l \leq N_\tau$, and $0 \leq i, j, k \leq N_\sigma$. Commonly, one uses symmetric lattices, where $a_\sigma = a_\tau \equiv a$. A space-time point on the lattice, a lattice *site*, is then uniquely determined by the 4-vector $n^\mu = (l, \mathbf{n})$, $\mathbf{n} = (i, j, k)$. Quantities with the dimension of energy are measured in units of the inverse lattice spacing a^{-1} , and different lattices are simply characterized by their extension $N_\sigma^3 \times N_\tau$. The smallest length scale on a lattice is the lattice spacing a , corresponding to a maximum momentum scale $\Lambda_{\text{UV}} \sim a^{-1}$. This scale serves as ultraviolet cut-off which regulates the ultraviolet divergences commonly appearing in quantum field theories. The largest length scale on the lattice is the lattice extension aN_σ . It determines the minimum momentum scale $\Lambda_{\text{IR}} \sim (aN_\sigma)^{-1}$.

The next step is to define the QCD action $S \equiv \int_X \mathcal{L}$, with \mathcal{L} given by Eq. (2), on the discretized space-time lattice. As a first guess, one could replace all derivatives with finite differences between lattice points. For reasons explained below, this naive prescription is, however, not particularly suitable, neither for the gauge field (gluon) nor the matter (quark) part of the action. To find an alternative, note that the only condition a discretized version of the QCD action has to fulfill is to reproduce the continuum action in the limit $a \rightarrow 0$. The choice of a discretized QCD action is therefore not unique. This apparent shortcoming can, however, be turned into an advantage by choosing a form of the action which reduces or even completely eliminates discretization errors (so-called *improved* or *perfect* actions, respectively).

To find a suitable discretized version of the gauge field part of the action, one first observes [59] that, on a finite-size lattice, the gauge fixing term $\mathcal{L}_{\text{gauge}}$ in Eq. (2) is no longer necessary, as the integration over gauge fields becomes convergent. Nevertheless, a naive discretization of the gauge field part of the action is still not gauge-invariant, and will remain so even when taking the continuum limit $a \rightarrow 0$. It is therefore advantageous to formulate the gauge field part of the action in a gauge-invariant form. A suitable choice was proposed by Wilson [59],

$$S_A = \sum_n \sum_{0 \leq \mu < \nu \leq 3} \left(1 - \frac{1}{N_c} \text{ReTr} \left(U_{n,\mu} U_{n+\hat{\mu},\nu} U_{n+\hat{\nu},\mu}^\dagger U_{n,\nu}^\dagger \right) \right) . \quad (29)$$

The sum over n runs over all lattice sites n^μ and the *link* variable $U_{n,\mu}$ is defined as

$$U_{n,\mu} = \text{P exp} \left[ig \int_x^{x+\hat{\mu}a} dy^\sigma A_\sigma^a(y) T^a \right] , \quad x^\mu \equiv a n^\mu . \quad (30)$$

The link variable describes the parallel transport of the gauge field between two neighbouring lattice sites n^λ and $n^\lambda + \hat{\mu}^\lambda$, where $\hat{\mu}^\lambda \equiv \delta^{\mu\lambda}$ is the 4-dimensional lattice unit vector pointing in μ -direction.

Visualizing the product of the four link variables on the right-hand side of Eq. (29), one realizes that this product transports the gauge field around an elementary lattice plaquette; it is therefore also called the *plaquette* operator. The trace of the plaquette operator, and thus also the Wilson action (29),

is gauge-invariant. The Polyakov loop (7) is related to the link variables via

$$L(\mathbf{x}) \equiv \frac{1}{N_c} \text{Tr} \prod_{l=1}^{N_\tau} U_{n,0} , \quad n^\mu = (l, \mathbf{n}) , \quad \mathbf{x} \equiv a \mathbf{n} . \quad (31)$$

Expanding the Wilson action (29) for small lattice spacing a , one obtains the continuum limit

$$-\beta S_A \simeq \int_X \left(-\frac{1}{4} F_{\mu\nu}^a F_a^{\mu\nu} \right) + O(a^2) , \quad (32)$$

where $\beta \equiv 2N_c/g^2 \equiv 6/g^2$ is the so-called *bare coupling*. The correction terms to the continuum result are of order $O(a^2)$. The construction principle behind an improved action [60] is to add further terms to S_A in Eq. (29) in order to eliminate corrections of order $O(a^2)$. The improved action then reproduces the continuum limit up to corrections of order $O(a^4)$. Repeating this procedure, one can systematically eliminate discretization errors up to a given power of a^2 . Extending this procedure in order to eliminate *all* corrections leads to so-called *perfect* actions [61].

The naive discretization of the fermionic part of the QCD action is not particularly suitable because of the so-called *doubling problem* for massless fermions on the lattice [58]. Fermion doubler states originate from the periodicity of the fermion dispersion relation within the Brillouin zone. One obtains one extra doubler state per space-time dimension, such that there are in total $2^4 = 16$ instead of a single fermion species. One way out is to break chiral symmetry explicitly by introducing a mass term. This leads to the so-called *Wilson* fermion prescription [59]. Wilson fermions eliminate the doubler states completely, but they have the disadvantage that one can in principle no longer study the restoration of chiral symmetry at the QCD transition. Another possibility is to distribute components of the fermion Dirac spinor over several lattice site. These so-called *staggered* or *Kogut-Susskind* fermions [62] do not completely solve the fermion-doubling problem: the number of doubler states is merely reduced to four. However, the solution to this problem is to interpret the doubler fermions as different flavor states. Hence, the standard staggered fermion action is interpreted as describing QCD with $N_f = 4$ flavors. The advantage of the staggered fermion prescription is that it preserves a subgroup of the original chiral symmetry. The chiral condensate is thus an order parameter for chiral symmetry restoration at the QCD transition. Other attempts have been made to solve the fermion-doubling problem, while at the same time improving (or even preserving) the chiral symmetry of the lattice action. To name a few, there are the so-called overlap [63], domain-wall [64], fixed-point [65] or chirally improved [66] fermions.

Let us take a closer look into the staggered fermion prescription, where the fermionic part of the QCD action reads

$$S_F^{KS} = \sum_{n,m} \bar{\psi}_n M_{n,m}^{KS} \psi_m , \quad (33)$$

with the inverse staggered fermion propagator

$$\begin{aligned} M_{n,m}^{KS}(\tilde{m}, \tilde{\mu}, U) &= \frac{1}{2} \sum_{\mu=1}^3 (-1)^{n^0 + \dots + n^{\mu-1}} \left(\delta_{n+\hat{\mu},m} U_{n,\mu} - \delta_{n,m+\hat{\mu}} U_{m,\mu}^\dagger \right) \\ &+ \frac{1}{2} \left(\delta_{n+\hat{0},m} U_{n,0} e^{\tilde{\mu}} - \delta_{n,m+\hat{0}} U_{m,0}^\dagger e^{-\tilde{\mu}} \right) + \delta_{n,m} \tilde{m} . \end{aligned} \quad (34)$$

Here, the fermion mass (in units of the inverse lattice spacing) is denoted as $\tilde{m} \equiv am$. This notation prevents confusion of the fermion mass with the lattice site vector $m \equiv m^\mu$. The chemical potential (in units of the inverse lattice spacing) is $\tilde{\mu} \equiv a\mu$. As shown in Ref. [67], the correct prescription to introduce the chemical potential in the discretized fermion action is as indicated in Eq. (34), i.e., in exponential form on a temporal link.

The fermionic part of the QCD action is bilinear in the Grassmann fields $\bar{\psi}$ and ψ . The fermion fields can thus be integrated out exactly. The result for the QCD partition function (1) on a discretized, 4-dimensional $N_\sigma^3 \times N_\tau$ lattice is

$$\mathcal{Z}(N_\sigma, N_\tau, \beta, \tilde{m}, \tilde{\mu}) = \int \prod_{n,\mu} dU_{n,\mu} \left[\det M^{KS}(\tilde{m}, \tilde{\mu}, U) \right]^{N_f/4} e^{-\beta S_A}. \quad (35)$$

The integration is over all link variables $U_{n,\mu}$. The power $N_f/4$ of the fermion determinant takes into account that, in the continuum limit, the standard staggered fermion prescription leads to $N_f = 4$ fermion species. In order to obtain results with less than $N_f = 4$ flavors, one has to take the appropriate root in Eq. (35). In this way, one can also obtain results for fermions with different masses. For instance, in order to compute the partition function for two light (say, up and down) and one heavy (say, strange) quark flavor (also called the “2 + 1” flavor scenario) one replaces the fermion determinant in Eq. (35) by the product $[\det M^{KS}(\tilde{m}_q, \tilde{\mu}_q, U)]^{1/2} [\det M^{KS}(\tilde{m}_s, \tilde{\mu}_s, U)]^{1/4}$.

For vanishing quark chemical potential, $\tilde{\mu} = 0$, the fermion determinant in Eq. (35) is real and positive, and standard Monte Carlo methods [58] can be applied to evaluate the integral over the link variables $U_{n,\mu}$. However, for nonzero quark chemical potential, the fermion determinant becomes complex. It is clear that the partition function itself cannot have an imaginary part, thus the imaginary part of the fermion determinant has to cancel when integrating over $U_{n,m}$. However, for a particular configuration of the gauge field, or equivalently, the link variables $U_{n,\mu}$ on the space-time lattice, the real part of the fermion determinant is no longer strictly positive. This so-called *sign problem* prevents the application of standard Monte Carlo techniques to evaluate the partition function. For this reason, most lattice QCD calculations have been performed at zero quark chemical potential, with data reaching an impressive level of quality. Results for the QCD phase transition and the equation of state, i.e., pressure as a function of temperature, are presented in Secs. 3.2 and 3.3, respectively. Only recently, attempts have been made to compute the partition function also for nonzero values of the quark chemical potential. This will be discussed in Sec. 3.6.

Finally, let us note that, in order to extract continuum physics from lattice calculations, one has to extrapolate the results to the case of vanishing lattice spacing, $a \rightarrow 0$. In order to change the value of a , one has to change the value of bare coupling $\beta = 6/g^2$. Since QCD is an asymptotic theory, the strong coupling constant at the momentum scale a^{-1} vanishes as a goes to zero, $g(a) \rightarrow 0$ for $a \rightarrow 0$. This, in turn, implies that $\beta(a) \rightarrow \infty$ as $a \rightarrow 0$. Asymptotically, the relation between a and β is given by the leading-order renormalization group result

$$a \Lambda_L \simeq \left(\frac{6b_0}{\beta} \right)^{-b_1/(2b_0^2)} \exp \left(-\frac{\beta}{12b_0} \right), \quad b_0 = \frac{11 - 2N_f/3}{16\pi^2}, \quad b_1 = \frac{102 - 38N_f/3}{(16\pi^2)^2}, \quad (36)$$

where Λ_L is the lattice scale parameter that can be unambiguously related to the scale parameter in other regularization schemes, for instance $\Lambda_{\overline{MS}}$ in the \overline{MS} scheme.

In principle, this allows one to convert the value of a physical quantity, say the pressure, which on the lattice is computed in units of a^{-4} , i.e., as $\tilde{p} \equiv a^4 p$, into physical units, i.e., MeV⁴. However, as Eq. (36) is strictly valid only for asymptotically small values of a , in practice one uses a different prescription. Consider a physical quantity, for instance a hadronic mass m_H , which is well-known in the continuum. Compute this quantity on the lattice, where its value is given in units of the inverse lattice spacing, $\tilde{m}_H = am_H$. Then, any other quantity with the dimension of energy can be determined in units of m_H , say the temperature, which is $T/m_H = (aN_\tau)^{-1}/(\tilde{m}_H/a) \equiv 1/(\tilde{m}_H N_\tau)$.

When decreasing the lattice spacing a (by increasing the value of the bare coupling β), the temperature $T = 1/(aN_\tau)$ increases, if one keeps the number of lattice points in temporal direction N_τ fixed.

(Simultaneously, for a fixed number of lattice points in spatial direction N_σ , the volume $V = (aN_\sigma)^3$ decreases.) Therefore, in order to determine the temperature dependence of a quantity, one simply has to compute it on a lattice with a fixed number of temporal points N_τ , but for different values of a , resp. β . Thus, one often finds lattice data presented as a function of β rather than as a function of T . Both presentations are equivalent, but note that the temperature *increases* with the bare coupling β . One should therefore never confuse the bare coupling β with the quantity $\beta \equiv (k_B T)^{-1}$ from thermodynamics and statistical mechanics, which *decreases* with temperature. (The way β appears in Eq. (35) certainly does not help to avoid this mistake.)

When extrapolating lattice results to the continuum limit $a \rightarrow 0$, one does not simultaneously want to increase the temperature T or decrease the volume V of the system. Rather, one has to ensure that these quantities are kept fixed. In other words, the continuum limit $a \rightarrow 0$ is obtained by simultaneously *increasing* the number of lattice points in space and time direction, $N_\sigma, N_\tau \rightarrow \infty$, such that $aN_\sigma = V^{1/3}$ and $aN_\tau = 1/T$ are constant. This is obviously quite costly numerically. There is, however, also another problem of numerical nature with this limit. Consider, for instance, a lattice computation of the pressure, which yields values for the quantity $\tilde{p} \equiv a^4 p \equiv (p/T^4)N_\tau^{-4}$. A given value for the physical temperature corresponds to some value for the physical pressure, such that p/T^4 assumes a certain value. Consequently, as $N_\tau \rightarrow \infty$ the *numerical* value for \tilde{p} on the lattice rapidly decreases as N_τ^{-4} when $a \rightarrow 0$. Since lattice QCD calculations are subject to statistical errors, it therefore becomes increasingly more difficult to extract the physically relevant quantity from the statistical noise. It is thus important to use improved actions (see discussion above), which reduce the discretization errors and allow one to perform calculations for moderate values of N_τ where \tilde{p} is still significantly larger than the statistical noise.

Finally, not only is one interested in the continuum limit for a *finite* volume V , but one would like to extrapolate to the thermodynamic limit $V = (aN_\sigma)^3 \rightarrow \infty$ as well. At a given nonzero temperature, however, $1/T = aN_\tau$ remains finite (in fact, it decreases as T increases). Therefore, simulations at nonzero temperature, which aim towards the thermodynamic limit, require $N_\sigma \gg N_\tau$, which represents another numerically expensive condition. Nowadays, typical “hot” lattices have space-like extensions $N_\sigma \sim 16 - 32$ while the time-like extension is $N_\tau \sim 4 - 8$. The only situation where one also has to have a large extension of the lattice in the time direction is the zero-temperature case, $T = 0$. “Cold” lattices typically have $N_\sigma = N_\tau \sim 16 - 32$.

How close to the thermodynamic limit are present-day lattice QCD calculations? Suppose one is doing a simulation at the critical bare coupling, i.e., where the QCD transition occurs (see Sec. 3.2). Physical values for the transition temperature are of the order of $T_c \sim 150$ MeV, cf. Sec. 2.3.3. Consequently, the lattice spacing at the critical bare coupling β_c is $a_c = 1/(T_c N_\tau)$. For temporal lattice extensions of the order of $N_\tau \sim 4 - 8$, this corresponds to values $a_c \sim 0.15 - 0.3$ fm. For typical spatial lattice extensions $N_\sigma \sim 16 - 32$ on a “hot” lattice, the physical volume is then $V \sim (2.5 - 10)^3 \text{ fm}^3 \sim (15 - 1000) \text{ fm}^3$. Is such a system sufficiently close to the thermodynamic limit? The answer is not necessarily no, as this depends on how large the system is in comparison to the size of its constituents. The latter can be estimated via their Compton wavelength $\lambda_C = m^{-1}$. For nucleons, the Compton wavelength is $\lambda_C \sim 0.2$ fm, so that many nucleons would comfortably fit into the system. (Of course, this is an optimistic estimate: taking the nuclear charge radius $r \sim 0.8$ fm instead of the Compton wavelength drastically worsens the situation.) For a pion, $\lambda_C \sim 1.4$ fm, such that the lattice volume for these light particles appears to be on the verge of being too small (unless the pion becomes much heavier at the phase transition, cf. Sec. 4.6). In any case, not more than a few pions would fit into the physical volume, which certainly casts doubts on whether one is able to reach the thermodynamic limit with present-day lattice sizes.

In the following, results from lattice calculations at zero and nonzero quark chemical potential will

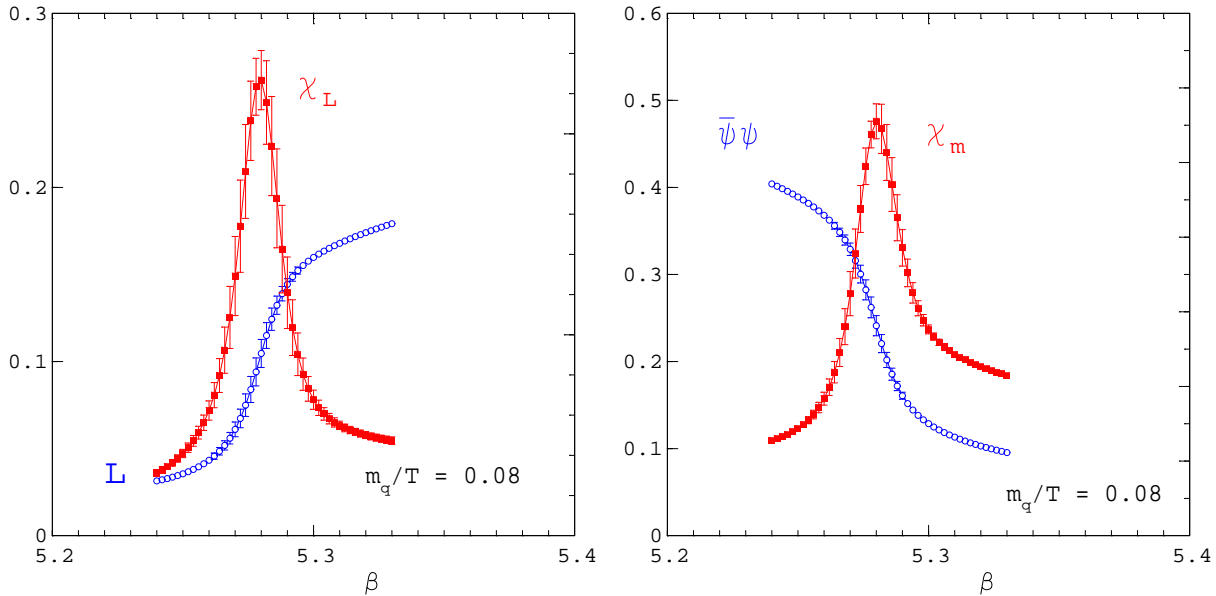


Figure 3: Deconfinement and chiral symmetry restoration in QCD with $N_f = 2$ dynamical quark flavors. (a) The expectation value of the Polyakov loop and the corresponding susceptibility as functions of the bare coupling. (b) The chiral condensate and the corresponding susceptibility as functions of the bare coupling. From Ref. [15].

be reviewed. For $\mu = 0$, a wealth of data is available; for the purpose of this introductory review, I only focus on the QCD phase transition, the equation of state, the heavy quark free energy, and mesonic spectral functions. The case $\mu \neq 0$ has only recently received a fair amount of attention. The main activity is still to find solutions of (or ways around) the sign problem of the fermion determinant. For more details, see Refs. [15, 16].

3.2 The QCD phase transition

As already discussed in Sec. 2.3, lattice QCD calculations have numerically established the existence of the quark-hadron transition. Figure 3 (a) shows the expectation value of the Polyakov loop, $\langle L(\mathbf{x}) \rangle$, with $L(\mathbf{x})$ as defined in Eq. (31), as a function of the bare coupling β (i.e., as explained in Sec. 3.1, as a function of temperature) for $N_f = 2$ quark flavors. For the pure gauge theory, i.e., for quark masses $\tilde{m} \rightarrow \infty$, the Polyakov loop is an order parameter for the deconfinement transition: it changes its value from zero in the confined phase below T_c to a nonzero value in the deconfined phase above T_c , cf. discussion in Sec. 2.3.2. However, the presence of dynamical quarks in the calculation of Fig. 3 breaks the $Z(3)$ symmetry of the pure gauge theory explicitly. Thus, the transition is no longer of first order, but crossover. This is also observed in the data.

In Fig. 3 (b) the chiral condensate $\langle \bar{\psi}\psi \rangle$ is shown as a function of the bare coupling β . For vanishing quark masses, the chiral condensate serves as an order parameter for chiral symmetry breaking: it is nonzero below and vanishes above T_c , cf. discussion in Sec. 2.3.3. Since the calculations of Fig. 3 have been done for a nonzero quark mass, chiral symmetry is explicitly broken. Consequently, the chiral transition is not of second order, as expected for $N_f = 2$ flavors, but crossover, which is also seen in Fig. 3 (b).

Table 2: The critical temperature T_c for QCD with different quark flavors (extrapolated to the chiral limit) and the pure $[SU(3)_c]$ gauge theory ($N_f = 0$). For the “2+1” case, T_c is close to the 2-flavor case. From Refs. [15, 16].

N_f	T_c	Remarks
2	(171 ± 4) MeV	Wilson fermions
2	(173 ± 8) MeV	Kogut-Susskind fermions
3	(154 ± 8) MeV	Kogut-Susskind fermions
0	(271 ± 2) MeV	pure gauge theory

Also shown in Figs. 3 (a) and (b) are the susceptibilities corresponding to the Polyakov loop and the chiral condensate. These are defined as

$$\chi_L \equiv N_\sigma^3 \left(\langle L^2 \rangle - \langle L \rangle^2 \right) , \quad \chi_m \equiv \frac{\partial}{\partial \tilde{m}} \langle \bar{\psi} \psi \rangle . \quad (37)$$

These quantities have a maximum at the value of β where the Polyakov loop and the chiral condensate change most rapidly. This value is the critical bare coupling β_c , which corresponds to the critical temperature T_c for the QCD transition. In this way, one can define a critical temperature, even if the transition is not of first or second order, but only crossover. The interesting observation one can make from Fig. 3 is that β_c assumes the *same* value for the deconfinement transition as for the chiral symmetry restoration transition. A possible explanation for this strong correlation between deconfinement and chiral transition is provided by the Polyakov-loop model of Ref. [68], see also Sec. 4.5. Current results for the phase transition temperature in the pure $[SU(3)]_c$ gauge theory, as well as in QCD with different flavors, extrapolated to vanishing quark mass (for details, see Ref. [70]) are summarized in Table 2.

Lattice QCD calculations have also begun to explore the quark-mass diagram discussed in Sec. 2.3.4 in order to decide the question about the order of the QCD transition. The present knowledge is summarized in Fig. 4. The open triangles are results from Ref. [69] and correspond to the line of second-order transitions separating the first-order from the crossover region in Fig. 2. The other data points confirm that the transition is of first order below the second-order line and crossover above. It is somewhat difficult to locate the physical point on this diagram. Naively, one would think that it suffices to determine the lattice spacing a in physical units, after which one finds the physical point in lattice units via multiplying the physical quark masses by this value of a , $\tilde{m}_{q,s}^{\text{phys.}} \equiv a m_{q,s}^{\text{phys.}}$. This deceptively simple method does not work in practice, because the physical mass in lattice units $\tilde{m}_{q,s}^{\text{phys.}}$ also receives contributions from renormalization, which violate this simple relationship. Present estimates seem to indicate, however, that the physical point is deep in the crossover region [74].

3.3 Equation of state

The equation of state is determined by the pressure $p(T, \mu)$ as a function of temperature T and chemical potential μ . Hence, according to Eq. (4) one has to compute $(T/V) \ln \mathcal{Z}$. From the pressure, other

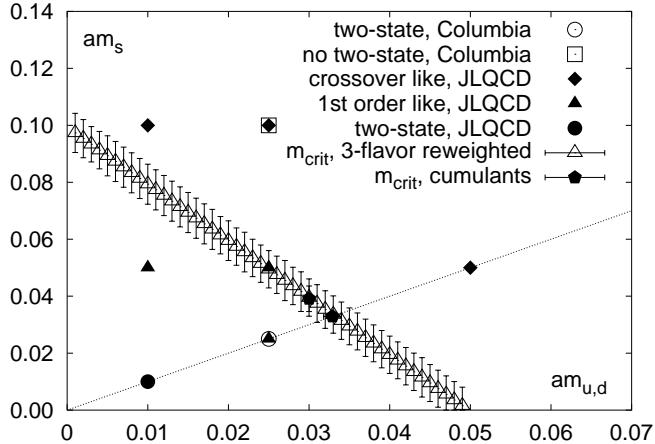


Figure 4: The quark-mass diagram as computed in lattice QCD. Below the line of open triangles, the transition is of first order, above it is crossover. The data points labelled ‘‘Columbia’’ are from Ref. [71], the ones labelled ‘‘JLQCD’’ are from Ref. [72]. The other points are from Refs. [69, 73].

thermodynamic quantities can be derived via differentiation, cf. Eq. (5), and the fundamental relation of thermodynamics, $\epsilon = Ts + \mu n - p$. For any quantum field theory in the continuum as well as on the lattice, the calculation of the absolute value of $(T/V) \ln \mathcal{Z}$ is plagued by ultraviolet divergences [10]. These arise from vacuum fluctuations and have to be subtracted in order to obtain a finite value for $p(T, \mu)$. The simplest way to achieve this is to subtract the value of $(T/V) \ln \mathcal{Z}$ in the vacuum, i.e., at $T = \mu = 0$,

$$p(T, \mu) = \frac{T}{V} \ln \mathcal{Z} - \left(\frac{T}{V} \ln \mathcal{Z} \right)_{T=\mu=0} . \quad (38)$$

In this way, the value of the pressure in the vacuum is normalized to zero, $p(0, 0) \equiv 0$.

A direct computation of the pressure using this formula is still cumbersome, because it requires the calculation of the absolute values of $\ln \mathcal{Z}(T, V, \mu)$ and $\ln \mathcal{Z}(0, V, 0)$, which then have to be subtracted from each other. On the lattice, it is much simpler to compute average values of quantities. Therefore, one uses the following method to determine the pressure. First, note that

$$\frac{p}{T^4} \equiv \frac{1}{T^4} \left[\frac{T}{V} \ln \mathcal{Z} - \left(\frac{T}{V} \ln \mathcal{Z} \right)_{T=\mu=0} \right] \equiv N_\tau^4 \left(\frac{\ln \mathcal{Z}(N_\sigma, N_\tau, \beta, \tilde{m}, \tilde{\mu})}{N_\sigma^3 N_\tau} - \frac{\ln \mathcal{Z}(N_\sigma, N_\sigma, \beta, \tilde{m}, \tilde{\mu})}{N_\sigma^4} \right) . \quad (39)$$

The assumption underlying this identity is that one can approximate the vacuum subtraction by the value of $(T/V) \ln \mathcal{Z}$ computed on a ‘‘cold’’ lattice with $N_\tau \equiv N_\sigma$, but at the same value of the bare coupling β (i.e., with the same lattice spacing a) as for the ‘‘hot’’ lattice (where $N_\tau \ll N_\sigma$), $(T/V) \ln \mathcal{Z}|_{T=\mu=0} \equiv (aN_\sigma)^{-4} \ln \mathcal{Z}(N_\sigma, N_\sigma, \beta, \tilde{m}, \tilde{\mu})$. Now introduce the expectation value of the (dimensionless) Wilson action *density* $\langle \tilde{s}_A \rangle \equiv a^4 \frac{T}{V} \langle S_A \rangle \equiv (N_\sigma^3 N_\tau)^{-1} \langle S_A \rangle$,

$$\langle \tilde{s}_A \rangle \equiv -\frac{1}{N_\sigma^3 N_\tau} \frac{\partial}{\partial \beta} \ln \mathcal{Z}(N_\sigma, N_\tau, \beta, \tilde{m}, \tilde{\mu}) , \quad (40)$$

and its zero-temperature value $\langle \tilde{s}_A \rangle_0$, which is computed on a ‘‘cold’’ lattice, i.e., by setting $N_\tau \equiv N_\sigma$ on the right-hand side of Eq. (40). The quantity p/T^4 in Eq. (39) can now be obtained through an

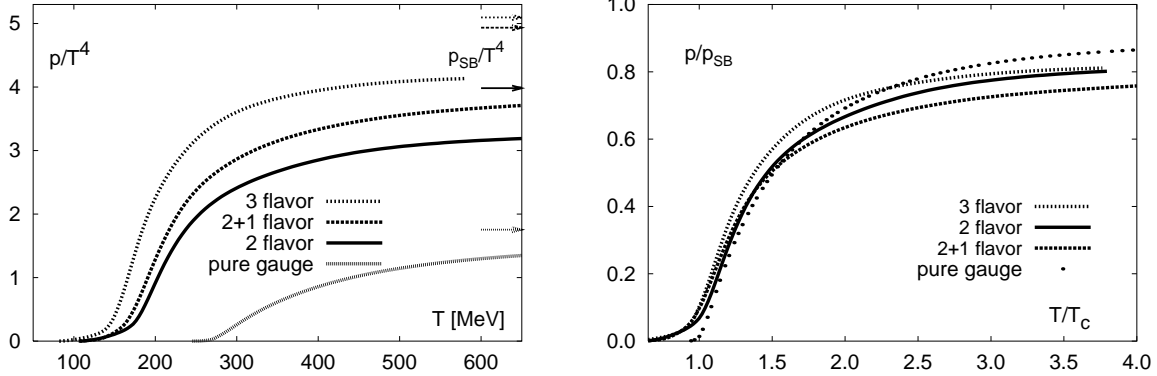


Figure 5: Left panel: Pressure (divided by T^4) as a function of temperature for the pure gauge theory and for QCD with two and three light flavors, as well as with two light and a four times heavier quark flavor (curve labelled “2 + 1”). Arrows denote the corresponding Stefan-Boltzmann values. For the “2+1” case, the arrow is slightly below the three-flavor case, due to the nonzero strange quark mass. Right panel: Pressure normalized to its corresponding Stefan-Boltzmann value as a function of temperature normalized to the corresponding transition temperature T_c for the four cases shown in the left panel. From Ref. [15].

integration of Eq. (40) with respect to the bare coupling β ,

$$\frac{p}{T^4} - \frac{p_1}{T_1^4} = -N_\tau^4 \int_{\beta_1}^{\beta} d\beta' (\langle \tilde{s}_A \rangle - \langle \tilde{s}_A \rangle_0) . \quad (41)$$

In order to determine the second term on the left-hand side, p_1/T_1^4 , one would like to choose a rather low value for the temperature T_1 . For temperatures $T_1 \ll m_H$, where m_H is the lightest hadronic particle, the pressure is exponentially small, $p_1/T_1^4 \sim \exp(-m_H/T_1)$. This argument holds to very good approximation in the pure gauge theory, since the lightest glueball state has a mass of order 1 GeV. It does not hold in full QCD in the chiral limit, where there are $N_f^2 - 1$ massless Goldstone particles, cf. discussion in Sec. 2.3.3. For lattice QCD calculations, however, chiral symmetry is always broken by a nonvanishing dynamical fermion mass, thus m_H is always positive. To very good approximation one may therefore set $p_1/T_1^4 \equiv 0$. Once the pressure is known, other thermodynamic quantities can be determined from thermodynamic identities, for more details see Ref. [15].

As discussed in Sec. 3.1, before one can draw definite conclusions about the thermodynamic properties of hot quark-gluon matter, one has to extrapolate the lattice data to the continuum limit (and hope that present-day lattices are sufficiently large to be close to the thermodynamic limit). This has been done in Fig. 5 which shows the pressure (normalized to T^4) as a function of temperature (in physical units) for the case of two light flavors, three light flavors, and the “2 + 1” case, i.e., two light plus one heavy flavor [75], in comparison to the pressure for the pure $[SU(3)_c]$ gauge theory [76].

One observes that the pressure is rather small at low temperatures. This is to be expected, as the contributions from hadronic resonances (or, in the pure gauge theory, from glueballs) to the pressure are exponentially suppressed, $p_H/T^4 \sim \exp(-m_H/T)$ for a hadron (glueball) of mass m_H . However, at the critical temperature T_c for the QCD transition (cf. Table 2), the pressure increases rapidly, approaching the so-called Stefan-Boltzmann limit p_{SB} for a system of quarks and gluons as $T \rightarrow \infty$. The Stefan-Boltzmann limit is the pressure for an ideal (i.e., non-interacting) ultrarelativistic gas of

particles. For an ultrarelativistic gas at $\mu = 0$, the temperature is the only scale with the dimension of energy, consequently $p_{\text{SB}}/T^4 = \text{const.}$. The value of this so-called Stefan-Boltzmann constant only depends on the number of degrees of freedom in the system. For an $[SU(N_c)]_c$ gauge theory with N_f massless quark flavors one obtains

$$\frac{p_{\text{SB}}}{T^4} = \left[2(N_c^2 - 1) + 2N_c N_f \frac{7}{4} \right] \frac{\pi^2}{90}. \quad (42)$$

Here, the first term in brackets is the contribution from the gauge fields, while the second corresponds to that from the matter fields. The factors of 2 in these terms arise from the spin degrees of freedom of massless gauge fields and fermions. The factor $N_c^2 - 1$ counts the number of gauge fields which are in the adjoint representation of the gauge group. The factor $N_c N_f$ counts the number of colors and flavors of the fermions which are in the fundamental representation of the gauge group. The factor 7/4 accounts for the difference between Bose-Einstein and Fermi-Dirac statistics and for the fact that at $\mu = 0$ there are as many antifermions as fermions. Finally, the factor $\pi^2/90$ is the value of the (dimensionless) Bose-Einstein integral $(1/6\pi^2) \int_0^\infty dx x^3 (e^x - 1)^{-1}$ occurring in the calculation of the pressure.

In all cases, the function p/T^4 approaches the Stefan-Boltzmann value for a gas of quarks and gluons, which indicates that there is indeed a transition from hadronic degrees of freedom to quark and gluon degrees of freedom, i.e., from hadronic matter to the QGP. From the behavior of the Polyakov loop and the chiral condensate discussed in Sec. 3.2, in the QGP color charges become deconfined and chiral symmetry is restored. However, the approach of the pressure to the corresponding Stefan-Boltzmann value is rather slow; even at temperatures $\sim 3T_c$, deviations are typically of the order of 20%. This indicates that at such temperatures the QGP cannot really be considered as a non-interacting gas of massless quarks and gluons.

In order to understand the deviations from the Stefan-Boltzmann values, one has to resort to analytic calculations of the pressure, taking into account interactions between quarks and gluons. In an analytic approach, deviations from the ideal-gas behavior are well under control and can be physically interpreted. For instance, in a perturbative calculation of the QCD pressure, deviations from the Stefan-Boltzmann limit are due to corrections proportional to powers of the strong coupling constant, see Sec. 4.1. Another possible explanation for the deviation of the pressure from p_{SB}/T^4 is that quarks and gluons are actually quasiparticles, i.e., they are not massless, but assume a thermal mass due to interactions with the hot environment, see Secs. 4.3 and 4.4.

An important step to understand the deviations from ideal-gas behavior might be the observation that, when normalizing the pressure to the corresponding Stefan-Boltzmann value and the temperature to the critical temperature, the curves p/p_{SB} as a function of T/T_c exhibit a universal behavior for the pure gauge theory and for QCD with various dynamical quark flavors, see right panel of Fig. 5. A possible explanation for this behavior is provided by the Polyakov-loop model of Ref. [68], see Sec. 4.5, where the dynamics of chiral symmetry restoration is exclusively driven by the dynamics of the deconfinement transition.

3.4 Heavy quark free energy

The behavior of the heavy quark free energy as a function of temperature is another indication for deconfinement in the QGP. The heavy quark free energy $F_{\bar{Q}Q}(R, T)$ is the free energy of a heavy quark and an antiquark, separated by a spatial distance R , at a temperature T [23]. It is related to the Polyakov-loop correlation function via

$$\exp\left(-\frac{F_{\bar{Q}Q}(R, T)}{T}\right) = \langle L(0) L^\dagger(\mathbf{x}) \rangle, \quad R \equiv |\mathbf{x}|, \quad (43)$$

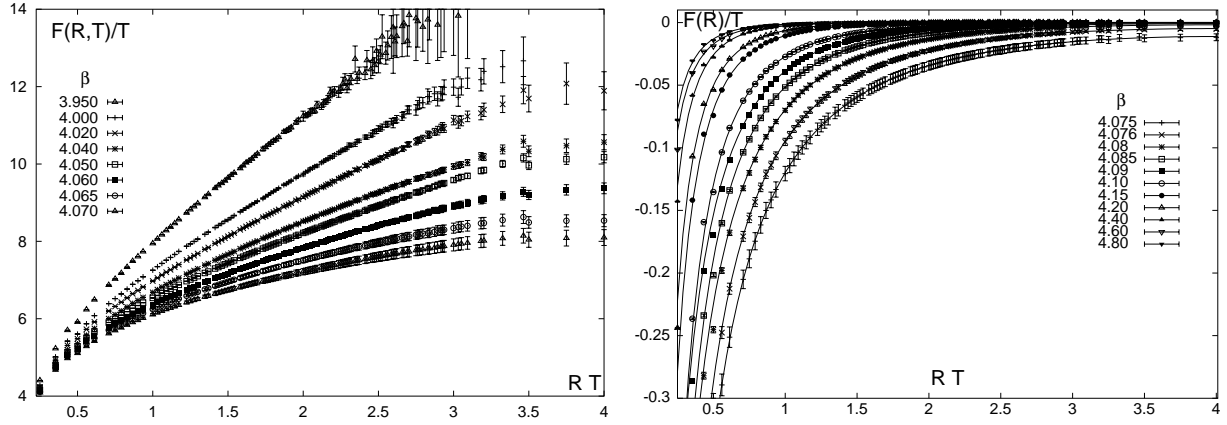


Figure 6: Left panel: The heavy quark free energy (in units of temperature) as a function of the distance (in units of inverse temperature) for various values of the bare coupling β in the confined phase. Right panel: The same for various values of β in the deconfined phase. In this phase, the Polyakov-loop correlation function of Eq. (43) is normalized to $\langle |L(0)|^2 \rangle$. Calculations are done for pure $[SU(3)_c]$ gauge theory on a $32^3 \times 4$ lattice. The critical bare coupling for this lattice is $\beta_c = 4.0729(3)$. From Ref. [77].

where $L(\mathbf{x})$ is the Polyakov-loop operator defined in Eq. (31). At $T = 0$, the heavy quark free energy is identical to the heavy quark potential, $V_{\bar{Q}Q}$, which is expected to have a form motivated by the string model,

$$V_{\bar{Q}Q}(R) = -\frac{\alpha(0)}{R} + \sigma R + \text{const.} \quad (44)$$

The second term ensures confinement of color charge due to the linear increase of $V_{\bar{Q}Q}$ with distance. The constant σ is the string tension. The first term is an attractive Coulomb-like contribution arising from fluctuations of the string.

Lattice QCD data [77] confirms these expectations, cf. Fig. 6. Below T_c (left panel of Fig. 6), at small distances the heavy quark free energy is dominated by an attractive Coulomb-like part, while at large distances it linearly rises with the distance, indicating confinement. The linear rise becomes less pronounced with increasing bare coupling β , indicating that the string tension decreases with temperature.

At temperatures above T_c , color charges are deconfined, i.e., the linearly rising part of the potential in Eq. (44) has to vanish, leaving only a Coulomb-like part. The latter is, however, screened due to the presence of a hot medium. This is confirmed by lattice QCD data above T_c (right panel of Fig. 6). It turns out [77] that a fit to the numerically computed potential can be achieved by the formula

$$\frac{F_{\bar{Q}Q}(R, T)}{T} = -\frac{c(T)}{(RT)^{d(T)}} e^{-\mu(T)R}, \quad (45)$$

where $\mu(T)$ is the temperature-dependent screening mass (or inverse screening length). This function is shown in Fig. 7.

While the qualitative picture of deconfinement and screening of color charges is certainly applicable, the deconfined gluon-plasma phase cannot be described perturbatively at temperatures in the range from T_c to a few times T_c . This is indicated by the fact that the fit function $d(T)$ in Eq. (45) is

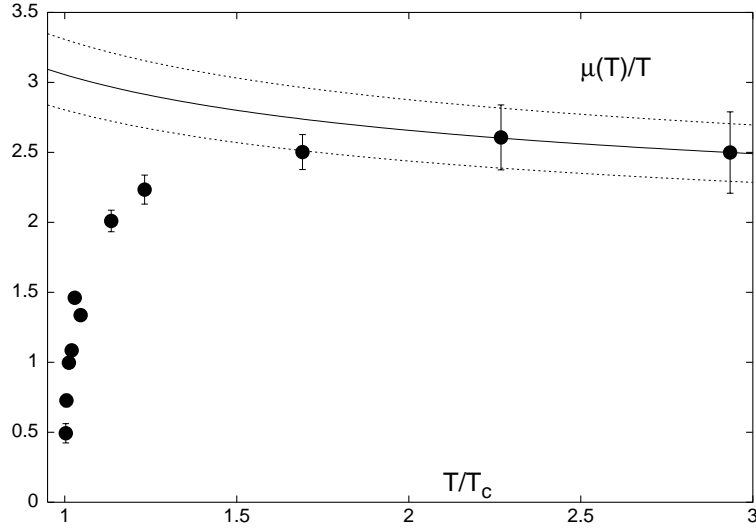


Figure 7: The temperature dependence of the screening mass $\mu(T)$ (in units of temperature) as obtained from a fit of Eq. (45) to the lattice data of Fig. 6. The solid line is a fit inspired by the perturbative expectation $\mu_{\text{pert.}}(T) = 2 m_D(T)$. From Ref. [77].

temperature-dependent [77] and always smaller than $\simeq 1.5$ in the range of temperatures considered here, while from perturbation theory one expects $d_{\text{pert.}} = 2$. Furthermore, the screening mass $\mu(T)$ deviates from the perturbative value $\mu_{\text{pert.}}(T) = 2 m_D(T)$, where $m_D(T) = gT$ is the Debye mass in a hot gluonic medium. The solid line in Fig. 7 represents a fit inspired by $\mu_{\text{pert.}}(T)$ to the two data points corresponding to the highest temperatures, for details see Ref. [77]. One observes that while the qualitative behavior of the data follows the perturbative expectation at large temperature, near T_c the data strongly deviate from the perturbative result. They even suggest that the screening mass goes to zero when $T \rightarrow T_c$. This is an indication for critical behavior and is naturally explained by the Polyakov-loop model of Ref. [68], see Sec. 4.5.

More recent developments in the study of the heavy quark free energy include a calculation in full QCD with dynamical quark flavors [70]. Below T_c , the string breaks when creation of dynamical quark-antiquark pairs becomes energetically favorable. Consequently, the heavy quark free energy saturates at larger distances instead of increasing linearly. In another recent paper [78] the color-singlet and color-octet contributions to the heavy quark free energy were studied separately within the pure gauge theory, using a novel prescription to renormalize the expectation value of the Polyakov loop. It was found that the singlet and octet contributions only deviate at smaller distances. As expected, the color-octet channel is repulsive, while the color-singlet channel is attractive.

3.5 Mesonic spectral functions

The correlation function of a mesonic state $G_H(\tau, \mathbf{x})$ is defined as

$$G_H(\tau, \mathbf{x}) \equiv \langle \bar{\psi}(0) \Gamma_H \psi(0) \bar{\psi}(\tau, \mathbf{x}) \Gamma_H \psi(\tau, \mathbf{x}) \rangle , \quad (46)$$

i.e., it is the overlap of a mesonic state with quantum numbers determined by the 4×4 Dirac matrix Γ_H at the origin with the same mesonic state at (τ, \mathbf{x}) . Fourier-transforming Eq. (46) with respect to the spatial variable, one obtains the mixed correlation function $G_H(\tau, \mathbf{p})$, which has the spectral

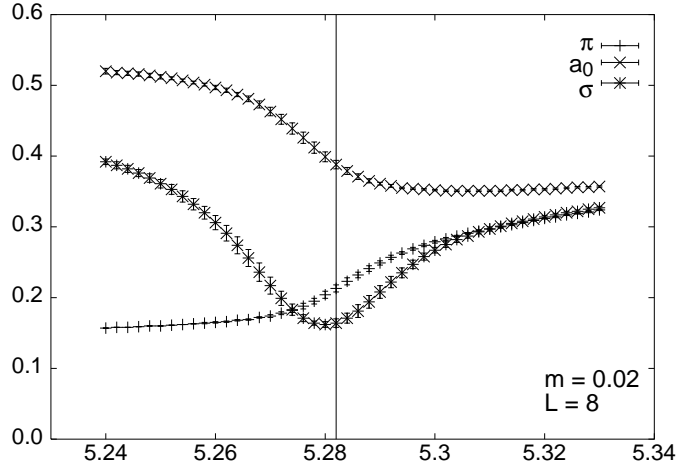


Figure 8: Mesonic masses as a function of the bare coupling, computed on an $8^3 \times 4$ lattice for QCD with $N_f = 2$ dynamical flavors. The vertical line indicates the critical bare coupling β_c for the phase transition. From Ref. [15].

representation

$$G_H(\tau, \mathbf{p}) = \int_0^\infty \frac{d\omega}{2\pi} \sigma_H(\omega, \mathbf{p}) \frac{\cosh \left[\omega \left(\tau - \frac{1}{2T} \right) \right]}{\sinh \left(\frac{\omega}{2T} \right)}. \quad (47)$$

Here, $\sigma_H(\omega, \mathbf{p})$ is the spectral density in the quantum number channel under consideration. Suppose the spectral density is dominated by a single, stable, mesonic state with mass m_H . In this case, $\sigma_H(\omega, 0) = \pi \lambda^2 \delta(\omega - m_H)/\omega$, where λ^2 is a constant with the dimension [MeV⁴]. Then, the susceptibility

$$\chi_H \equiv \frac{V}{T} \int_0^{1/T} d\tau \int_V d^3x G_H(\tau, \mathbf{x}) \quad (48)$$

assumes the value $\chi_H = (V/T) \lambda^2 m_H^{-2}$, i.e., it is proportional to the inverse mass (squared) of the meson. In a lattice QCD calculation, one can thus infer the mass of a mesonic state in a given quantum number channel from the corresponding susceptibility.

The masses for the pion, the σ meson, and the a_0 meson computed in this manner are shown in Fig. 8 as a function of the bare coupling (i.e., the temperature). The results indicate restoration of chiral symmetry, i.e., the mass of the pseudoscalar meson (pion) becomes degenerate with those of the scalar mesons (σ and a_0) at large temperature. The fact that the pion and the σ meson become degenerate in mass at smaller temperatures than the pion and the a_0 meson indicates that the $SU(2)_r \times SU(2)_\ell$ symmetry is restored prior to the $U(1)_A$ symmetry when increasing the temperature.

Instead of the susceptibility, one could also try to compute the complete spectral density $\sigma_H(\omega, \mathbf{p})$ of a mesonic state from lattice QCD data. An important motivation for such a calculation is the fact that the spectral density in the vector channel, $\sigma_V(\omega, \mathbf{p})$, is directly proportional to the rate of dilepton emission [79], which is an experimentally observable quantity [80],

$$\frac{dN_{\ell^+\ell^-}}{d^4X d\omega d^3p} = \frac{5\alpha^2}{27\pi^2} \frac{1}{e^{\omega/T} - 1} \frac{\sigma_V(\omega, \mathbf{p})}{\omega^2}. \quad (49)$$

To determine $\sigma_V(\omega, \mathbf{p})$, one would have to perform an inverse Laplace transformation of Eq. (47). This requires complete knowledge of the correlation function $G_V(\tau, \mathbf{p})$ on the left-hand side. On the lattice,

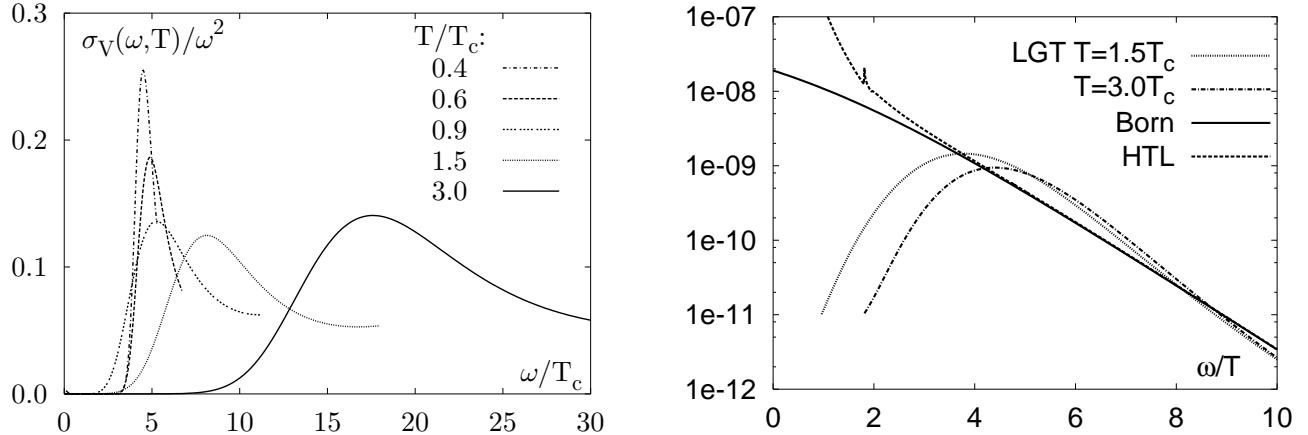


Figure 9: Left panel: The spectral density in the vector channel, divided by ω^2 , for various temperatures. Right panel: The dilepton rate computed in lattice QCD for two different temperatures as a function of energy (in units of temperature). Also shown is the Born approximation and the result from HTL-perturbation theory. From Ref. [16].

however, this function is only known at a few discrete points in τ -direction. Moreover, its value at these points is subject to statistical fluctuations. Consequently, a computation of $\sigma_V(\omega, \mathbf{p})$ via inversion of Eq. (47) with lattice data for $G_V(\tau, \mathbf{p})$ is impossible.

Nevertheless, a solution of this problem is provided by the so-called ‘‘Maximum Entropy Method’’ (MEM). The basic idea is to construct that particular spectral density $\sigma_H(\omega, \mathbf{p})$ under the integral in Eq. (47), which is the *most probable* one to yield a given correlation function $G_H(\tau, \mathbf{p})$ on the left-hand side of that equation; for details see Ref. [81]. Figure 9 shows the spectral function in the vector meson channel computed with this method [79] (left panel) and the corresponding dilepton rate (49) (right panel). One observes that the peak in the spectral density broadens and shifts towards larger energies as the temperature increases. Consequently, the dilepton rate is depleted for small dilepton energies. This behavior is in stark contrast to the dilepton emission rate computed in the Born approximation and in the so-called ‘‘hard thermal loop’’ (HTL-) resummation scheme, which are also shown in Fig. 9.

Finally, the low-energy behavior of the spectral density determines the value of transport coefficients in a hot medium [82]. I do not elaborate further on this point, as it concerns the non-equilibrium properties of the QGP, which are beyond the scope of the present review.

3.6 Nonzero Chemical Potential

As discussed in Sec. 3.1, for nonzero values of the quark chemical potential, $\mu \neq 0$, a straightforward evaluation of the QCD partition function on the lattice is not possible due to the sign problem of the fermion determinant. However, for sufficiently small μ progress has recently been made by applying methods which explicitly avoid the sign problem. Most notably among these are multiparameter reweighting [31], Taylor expansion around $\mu = 0$ [83], and analytic continuation from imaginary values of μ , where the fermion determinant is real-valued and positive, to real values of μ [84]. For the sake of brevity, here I only discuss the multiparameter-reweighting method; for a detailed comparison of all approaches see the review [16].

The multiparameter-reweighting method is based on the so-called Glasgow method [85]. The idea

of the Glasgow method is to treat the fermion determinant at nonzero μ in the partition function (35) as an *observable* rather than as a part of the integration measure. The integration measure itself is computed with a fermion determinant at $\mu = 0$, which is real-valued and positive and thus causes no problems when applying standard Monte Carlo methods to sample gauge field configurations,

$$\mathcal{Z}(N_\sigma, N_\tau, \beta, \tilde{m}, \tilde{\mu}) = \int \prod_{n,\mu} dU_{n,\mu} \frac{\det M(\tilde{m}, \tilde{\mu}, U)}{\det M(\tilde{m}, 0, U)} \det M(\tilde{m}, 0, U) e^{-\beta S_A} \equiv \left\langle \frac{\det M(\tilde{m}, \tilde{\mu}, U)}{\det M(\tilde{m}, 0, U)} \right\rangle_{\tilde{\mu}=0}. \quad (50)$$

Here, the expectation value $\langle \mathcal{O} \rangle_{\tilde{\mu}=0}$ of an operator \mathcal{O} is defined with respect to an ensemble of gauge fields and fermions at zero quark chemical potential.

This method is limited to small values of μ . In order to understand this, one has to remember the principle behind a Monte Carlo computation of the functional integral (50) [58]. A Monte Carlo computation assumes that in order to obtain a reasonable approximate value of the functional integral in Eq. (50) it suffices to sum only over (a few 10^2 to 10^4 of) the “most probable” gauge field configurations, rather than performing the integrals over the link variables $U_{n,\mu}$ explicitly. The “most probable” gauge field configurations are obviously those which minimize the action S_A . However, the most probable configurations at $\mu \neq 0$ are not the same as the ones at $\mu = 0$. Thus, approximating the partition function at $\mu \neq 0$ by configurations obtained for $\mu = 0$ becomes increasingly worse as μ increases. In other words, the “overlap” between the ensemble of most probable configurations at $\mu = 0$ and the ensemble that consists of the configurations which are actually most probable at $\mu \neq 0$ diminishes.

It has been recently realized [31] that a way to increase this overlap is to also include the exponential of the action into the operator which is averaged over the ensemble,

$$\mathcal{Z}(N_\sigma, N_\tau, \beta, \tilde{m}, \tilde{\mu}) \equiv \left\langle \frac{e^{-\beta S_A} \det M(\tilde{m}, \tilde{\mu}, U)}{e^{-\beta_0 S_A} \det M(\tilde{m}, 0, U)} \right\rangle_{\tilde{\mu}=0, \beta_0}, \quad (51)$$

i.e., the ensemble one averages over is generated at $\mu = 0$ and a value β_0 for the bare coupling. In this way, one not only reweights the ensemble in the parameter $\tilde{\mu}$, as in the Glasgow approach (50), but also in the bare coupling β (hence the name “multiparameter reweighting”).

How does one choose the second reweighting parameter β ? This depends on which physical question one asks. Suppose one wants to compute the QCD phase transition line for nonzero values of μ . One first generates an ensemble at $\tilde{\mu} = 0$ and $\beta_0 \equiv \beta_c$. This ensemble is “maximally” critical in the sense that it is generated at the phase transition point $(\beta, \tilde{\mu}) = (\beta_c, 0)$ (which corresponds to the point $(T, \mu) = (T_c, 0)$ in the continuum). For each nonzero value of $\tilde{\mu}$ one then determines β such that one remains on the phase transition line.

The criterion for “remaining on the phase transition line” is the position of the Lee-Yang zeroes $\beta_1^*, \beta_2^*, \dots$ of the partition function \mathcal{Z} in the complex β -plane [86]. For a given set of parameters $N_\sigma, N_\tau, \tilde{m}, \tilde{\mu}$, there are many Lee-Yang zeroes, i.e., roots of the equation $\mathcal{Z}(N_\sigma, N_\tau, \beta^*, \tilde{m}, \tilde{\mu}) = 0$. (In fact, the total number of Lee-Yang zeroes, M , increases linearly with the volume of the system, $M \sim N_\sigma^3$.) In the case of a first-order phase transition, one root, say β_1^* , has a vanishing imaginary part, i.e., it lies on the positive real β axis. Then the value of β which corresponds to the phase transition line in the $(\beta, \tilde{\mu})$ plane is $\beta \equiv \text{Re}\beta_1^*$.

Note that in a finite system, such as the space-time lattice considered in lattice QCD, all Lee-Yang zeroes have nonzero imaginary parts. Then one has to study lattices of different sizes and extrapolate to the infinite-volume limit. In Ref. [31], this is done via linear extrapolation in the variable $1/V$, $\beta_1^*(V) = \beta_1^*(\infty) + \alpha/V$. In the case of a crossover transition, the imaginary parts of the extrapolated Lee-Yang zeroes never vanish. In this case, the value of β corresponding to the phase transition line is determined by the real part of the Lee-Yang zero with the smallest imaginary part.

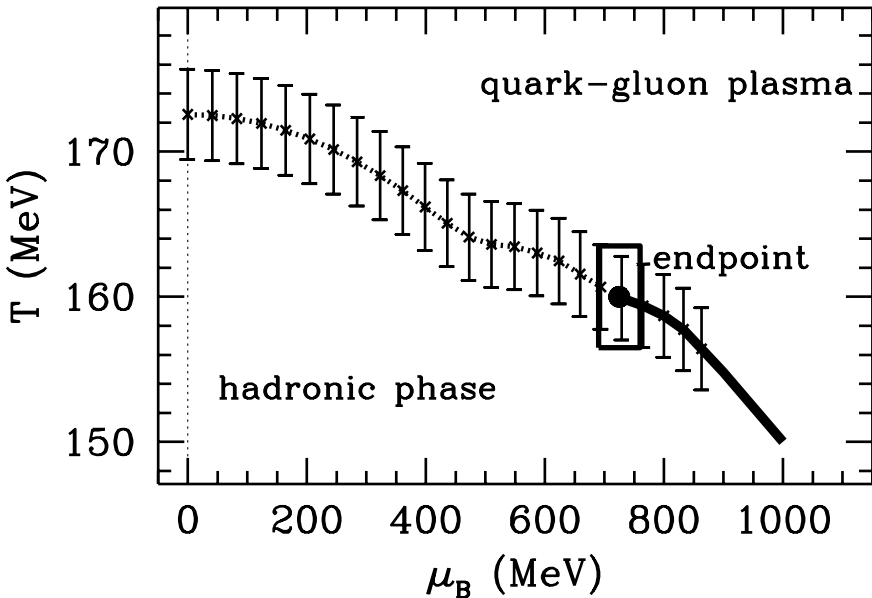


Figure 10: The QCD phase transition as computed in lattice QCD [31]. To the left of the critical point the transition is crossover, to the right it is of first order. At the critical point, the transition is of second order and in the universality class of the Ising model. Note that $\mu_B = 3\mu$.

The phase transition line calculated in this way is shown in Fig. 10. It agrees with the expectations discussed in Secs. 2.3.4, 3.2: there is a line of first-order phase transitions, ending at the point $(T, \mu)_{\text{cr}} = (160 \pm 3.5, 242 \pm 12)$ MeV, at which the transition is of second order. To the left of this point, the transition is crossover. One should mention that the lattice QCD calculation underlying Fig. 10 was done on fairly small lattice sizes, with probably unrealistically large quark masses. As discussed in Sec. 2.3.4, for smaller quark masses the endpoint should move towards the temperature axis. For three massless flavors, it should reach the temperature axis, since in this case the transition is of first order. For realistic quark masses, however, as discussed in Sec. 3.2 the transition is crossover at $\mu = 0$, and the line of first-order transitions should always end at some nonzero value of μ .

The position of the phase transition line determined by multiparameter reweighting is in good agreement with that computed by the other approaches mentioned previously, namely the Taylor expansion method, and method of analytic continuation from imaginary values of μ [16]. Recent developments [87] are the application of the multiparameter-reweighting method to compute the equation of state at nonzero quark chemical potential. Figure 11 shows the results for the pressure difference $\Delta p \equiv p(T, \mu) - p(T, 0)$, normalized to T^4 , as a function of T for various values of μ . There is a strong increase of Δp around the phase transition temperature. This increase is larger for larger values of μ .

Multiparameter reweighting, as well as the other aforementioned methods, is restricted to values of the quark chemical potential, which are not too large as compared to the temperature. In order to compute the partition function of QCD for large quark chemical potential at small or even zero temperature, and possibly study the color-superconducting phases of quark-gluon matter, one has to resort to other methods. A promising approach is the so-called meron-cluster algorithm which has been shown to solve the sign problem of the fermion determinant for the Hubbard and the Potts model [88]. For QCD, as of yet no solution has been found.

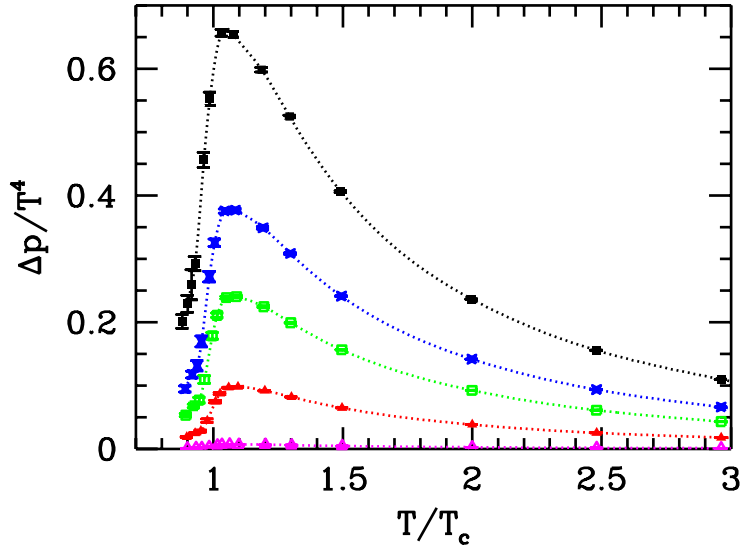


Figure 11: Δp as a function of T/T_c for various values of μ_B . From bottom to top, $\mu_B = 100, 210, 220, 310, 530$ MeV. From Ref. [87].

Another possibility is to study a model for QCD which does not have the sign problem. Such a model is, for instance, the NJL model which has been investigated on the lattice at $T = 0$ and $\mu \neq 0$ in Ref. [89]. Although this model has no color gauge symmetry which could be spontaneously broken, and thus strictly speaking cannot exhibit color superconductivity, quarks can still form Cooper pairs and the system may become superfluid. Figure 12 shows the chiral condensate, the baryon density, and the superfluid diquark condensate as a function of the baryon chemical potential, computed on the lattice and then extrapolated to the thermodynamic limit. One observes that, as the baryon density increases, the chiral condensate vanishes and the diquark condensate increases, signalling the onset of superfluid behavior. These results are in agreement with analytic calculations [38] for the NJL model in the mean-field approximation, which stimulated recent interest in color superconductivity.

4 Analytic Approaches

4.1 Perturbation Theory

The QCD partition function (1) can be expanded in a power series in the strong coupling constant g . In the following, I present the general idea behind this approach, neglecting contributions from gauge fixing and from Fadeev-Popov ghosts. Of course, these have to be properly accounted for in order to obtain the correct answer; for more details, see Ref. [10]. The first step is to split the QCD Lagrangian (2) into two terms, the non-interacting part, $\mathcal{L}_0 \equiv \mathcal{L}_{g=0}$, and the interaction part, $\mathcal{L}_I \equiv \mathcal{L} - \mathcal{L}_0$. Then, the QCD action $S \equiv \int_X \mathcal{L}$ can be written as

$$S = S_0 + S_I \equiv \int_X (\mathcal{L}_0 + \mathcal{L}_I) , \quad (52)$$

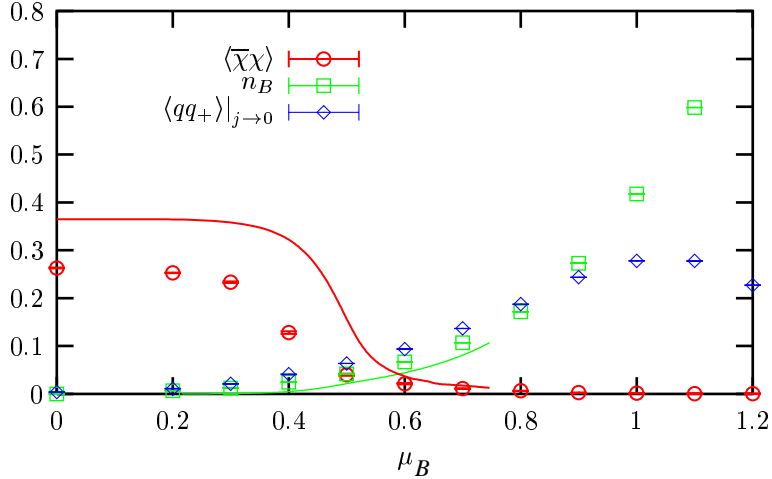


Figure 12: The chiral condensate, the baryon density, and the diquark condensate as a function of baryon chemical potential μ_B . The solid line is the chiral condensate computed analytically within the Hartree approximation. From Ref. [89].

$$\mathcal{L}_0 = \bar{\psi} \mathcal{G}_0^{-1} \psi + \frac{1}{2} A_\mu^a \Delta_0^{-1\mu\nu} A_\nu^b, \quad (53)$$

$$\mathcal{L}_I = g \bar{\psi} \gamma^\mu T^a \psi A_\mu^a + g f^{abc} \partial_\nu A_\mu^a A_\nu^b A_\nu^c - \frac{g^2}{4} f^{abc} f^{ade} A_\mu^b A_\nu^c A_\nu^d A_\nu^e. \quad (54)$$

Here $\mathcal{G}_0^{-1} \equiv i\gamma^\mu \partial_\mu - m$ is the free inverse quark propagator and $\Delta_0^{-1\mu\nu} \equiv (\square g^{\mu\nu} - \partial^\mu \partial^\nu) \delta_{ab}$ is the free inverse gluon propagator (which will eventually receive another contribution from the gauge fixing terms neglected here). The next step is to introduce source terms for fermions and gauge fields (which eventually have to be set to zero). One can then replace all fields in S_I in terms of functional derivatives with respect to the sources, and thus extract e^{S_I} from the functional integral. The functional integration over the exponential of the non-interacting part and the source terms is a Gaussian integral and can be performed exactly. The result is

$$\mathcal{Z} = \mathcal{Z}_0 \exp \left\{ S_I \left[\frac{\delta}{\delta \bar{\eta}}, \frac{\delta}{\delta \eta}, \frac{\delta}{\delta J_\mu^a} \right] \right\} \exp \left[\int_X \left(-\bar{\eta} \mathcal{G}_0 \eta - \frac{1}{2} J_\mu^a \Delta_0^{\mu\nu} J_\nu^b \right) \right] \Big|_{\bar{\eta}=\eta=J=0}, \quad (55)$$

where \mathcal{Z}_0 is the partition function for a system of non-interacting quarks and gluons. Obviously, the pressure $p_0 \equiv (T/V) \ln \mathcal{Z}_0$ is identical to the Stefan-Boltzmann pressure defined through Eq. (42), $p_0 \equiv p_{\text{SB}}$. The full pressure in QCD also receives contributions from the remaining two terms in Eq. (55). After introducing Feynman rules for propagators and vertices [10], these terms have a graphical representation as an infinite series of diagrams with no external legs. The diagrams can be sorted according to powers in the strong coupling constant g associated with the vertices. Thus, one obtains a perturbative series in powers of g .

Inspecting the topology of these diagrams, one would naively conclude that this perturbative series is an expansion in powers of g^2 . In fact, it turns out that this is only true at zero temperature [90]. At nonzero temperature, the expansion is in powers of g , rather than g^2 , due to the different infrared behavior of a field theory containing massless modes (such as gauge fields) at nonzero temperature. Roughly speaking, the difference arises from the infrared behavior of single-particle phase space, which, at zero temperature, is $\sim dk k^3$, while at nonzero temperature it is $\sim T dk k^2$. The missing power of

k at nonzero temperature leads to a completely different infrared behavior as compared to the zero-temperature case.

At zero temperature the theory is well-behaved in the infrared and the terms of the perturbative series are probably computable to all orders in g^2 [40]. Freedman and McLerran computed the series up to terms of order g^4 , for details see Ref. [90]. I do not present a more detailed discussion of their results at this point, as quark matter at zero temperature is a color superconductor, cf. Secs. 2.4.3 and 5. Color superconductivity is a nonperturbative phenomenon, which cannot be described in a purely perturbative calculation of the pressure.

At nonzero temperature, the infrared behavior of the theory leads to terms proportional to odd powers of g in the perturbative expansion (55) of the partition function. Technically, they arise from a resummation of an infinite subset of diagrams describing the screening of long-range electric fields. Moreover, there are infinitely many diagrams at order $O(g^6)$, and the perturbative expansion breaks down [10]. This is sometimes called the *Linde problem* of QCD, after his discoverer [11]. Nevertheless, what is perturbatively computable has been evaluated. These are all terms up to $O(g^5)$, and the terms of order $O(g^6 \ln g)$. How to obtain the latter is discussed in greater detail in Sec. 4.2. While the terms which are genuinely of order $O(g^6)$ cannot be computed perturbatively, they can in principle be evaluated via a lattice calculation.

At zero chemical potential, the pressure assumes the form

$$p = T^4 \left[c_0 + c_2 g^2 + c_3 g^3 + (c'_4 \ln g + c_4) g^4 + c_5 g^5 + c_6 g^6 \right]. \quad (56)$$

The coefficient c_0 is equal to the Stefan-Boltzmann constant (42). The coefficient c_2 arises from the lowest-order perturbative correction to the pressure of an ideal gas. It consists of two-loop diagrams, and was first computed by Shuryak [91]

$$c_2 = -\frac{N_c^2 - 1}{144} \left(N_c + \frac{5}{4} N_f \right). \quad (57)$$

The computation of the coefficient c_3 requires a nonperturbative resummation of plasmon ring diagrams in the infrared limit. This was first done correctly by Kapusta [92], with the result

$$c_3 = \frac{N_c^2 - 1}{36 \sqrt{3} \pi} \left(N_c + \frac{1}{2} N_f \right)^{3/2}. \quad (58)$$

The coefficient c'_4 has been computed by Toimela [93],

$$c'_4 = \frac{N_c^2 - 1}{48\pi^2} N_c \left(N_c + \frac{1}{2} N_f \right). \quad (59)$$

The coefficient c_4 is due to three-loop diagrams and has been computed by Arnold and Zhai [94],

$$\begin{aligned} c_4 = & -\frac{N_c^2 - 1}{(48\pi)^2} \left\{ -24 N_c \left(N_c + \frac{1}{2} N_f \right) \ln \left(\frac{N_c + N_f/2}{12\pi^2} \right) \right. \\ & + N_c^2 \left[\frac{22}{3} \ln \frac{\bar{\mu}}{4\pi T} + \frac{38}{3} \frac{\zeta'(-3)}{\zeta(-3)} - \frac{148}{3} \frac{\zeta'(-1)}{\zeta(-1)} - 4\gamma_E + \frac{64}{5} \right] \\ & + N_c N_f \left[\frac{47}{6} \ln \frac{\bar{\mu}}{4\pi T} + \frac{1}{6} \frac{\zeta'(-3)}{\zeta(-3)} - \frac{37}{3} \frac{\zeta'(-1)}{\zeta(-1)} - 4\gamma_E + \frac{1759}{120} + \frac{37}{10} \ln 2 \right] \\ & + N_f^2 \left[-\frac{5}{3} \ln \frac{\bar{\mu}}{4\pi T} + \frac{2}{3} \frac{\zeta'(-3)}{\zeta(-3)} - \frac{4}{3} \frac{\zeta'(-1)}{\zeta(-1)} - \gamma_E - \frac{1}{12} + \frac{22}{5} \ln 2 \right] \\ & \left. + \frac{N_c^2 - 1}{N_c} N_f \left[-\frac{105}{16} + 6 \ln 2 \right] \right\}. \end{aligned} \quad (60)$$

Here, $\zeta(x)$ is Riemann's zeta function, γ_E is the Euler-Mascheroni constant, and $\bar{\mu}$ is the renormalization scale in the \overline{MS} scheme, for details see Ref. [94]. The coefficient c_5 arises from corrections to the three-loop diagrams due to Debye screening of electric gluons. It has been computed by Zhai and Kastening [95] and by Braaten and Nieto [96],

$$\begin{aligned}
c_5 = & \frac{N_c^2 - 1}{9216 \sqrt{3} \pi^3} \left(N_c + \frac{1}{2} N_f \right)^{1/2} \left[N_c^2 \left(176 \ln \frac{\bar{\mu}}{4\pi T} + 176\gamma_E - 24\pi^2 - 494 + 264 \ln 2 \right) \right. \\
& + N_c N_f \left(56 \ln \frac{\bar{\mu}}{4\pi T} + 56\gamma_E + 36 - 64 \ln 2 \right) \\
& + N_f^2 \left(-16 \ln \frac{\bar{\mu}}{4\pi T} - 16\gamma_E + 8 - 32 \ln 2 \right) \\
& \left. - 36 \frac{N_c^2 - 1}{N_c} N_f \right]. \tag{61}
\end{aligned}$$

The coefficient c_6 contains terms $\sim \ln g$ and constant terms. The former contribute to order $O(g^6 \ln g)$ and can be evaluated perturbatively, while the latter are genuinely of order $O(g^6)$ and can only be computed e.g. via a lattice calculation, for more details, see Sec. 4.2. A perturbative computation of the pressure at nonzero chemical potential μ has not been done so far.

To be more explicit, consider pure $[SU(3)_c]$ gauge theory, i.e., $N_c = 3$, $N_f = 0$. The pressure up to terms of a given order in g is shown in the left panel of Fig. 13. The strong coupling constant g is taken to be running and evaluated at the scale $\bar{\mu}$. After applying the principle of fastest apparent convergence to minimize the two-loop corrections to the running of g , this scale is chosen as $\bar{\mu} \simeq 6.742 T$; for more details see [97]. The scale $\bar{\mu}$ also enters under the logarithms in Eqs. (60), (61). In principle, the complete result for the pressure, being a physically observable quantity, must be independent of the renormalization scale $\bar{\mu}$. The way this works out is that $\bar{\mu}$ under some logarithm, such as occurring in Eqs. (60), (61), is cancelled by a similar logarithm from the running of the coupling constant in a lower-order contribution. Nevertheless, while terms $\sim \ln \bar{\mu}$ must cancel, there still exist physical terms $\sim \ln g$, and here g has to be evaluated at the scale $\bar{\mu}$. The cancellation of the $\bar{\mu}$ -dependence holds for the complete result for p , but this does not happen if one terminates the perturbative expansion at some given order. This is the reason why, for instance, the $O(g^2)$ contribution to the pressure in Fig. 13 is not flat. Here the curvature arises from the logarithmic running of the strong coupling constant with the scale $\bar{\mu} \simeq 6.742 T$.

The perturbative series (56) converges badly. The second-order term $\sim c_2 g^2$ gives a negative contribution to the Stefan-Boltzmann pressure, which is less than 10% of p_{SB} at $T \sim 10^3 \Lambda_{\overline{MS}}$ and at most 40% of p_{SB} at $T \sim \Lambda_{\overline{MS}}$ ($\sim T_c$). However, the next contribution $\sim c_3 g^3$ is positive and so large that the pressure overshoots p_{SB} up to the largest values of T shown in Fig. 13. The terms of order g^4 are again small, but also positive, such that, to order $O(g^4)$, the pressure is larger than p_{SB} . The terms of order $O(g^5)$ are negative and so large in magnitude, that the pressure even vanishes at $T \simeq \Lambda_{\overline{MS}}$. Thus, naive perturbation theory is clearly not applicable for temperatures of order T_c .

In the sections following Sec. 4.2, several ways to improve the situation will be explained. All of them are based on the observation that the *odd* powers of g in the perturbative expansion (56) are responsible for the bad convergence properties, i.e., the latter are caused by the *infrared* properties of QCD. Note that there have also been attempts to improve the convergence properties of perturbation theory by using mathematical devices such as Padé approximates [98] and Borel resummation [99]. Here, I do not discuss these methods in more detail, because the physical problem of improving the description of the infrared sector of QCD cannot be solved in this way.

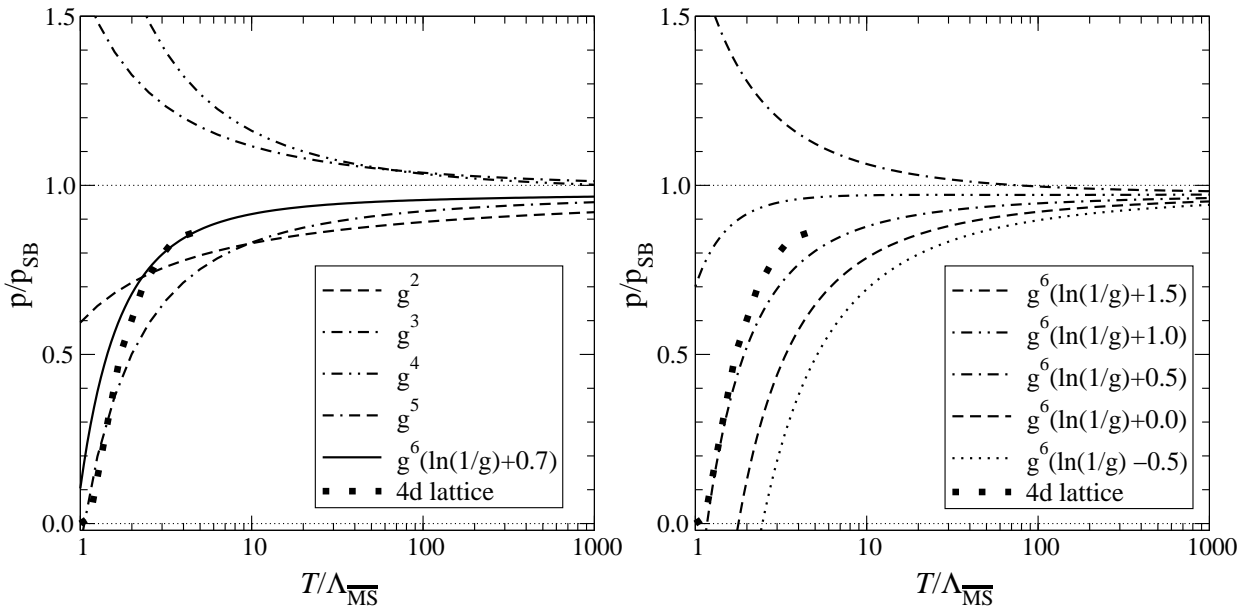


Figure 13: Left panel: Pressure (divided by T^4) as a function of temperature for the pure $[SU(3)_c]$ gauge theory. Several perturbative contributions (up to a given power in g) are shown, as well as lattice QCD data from Ref. [76]. Right panel: Sensitivity of the pressure to the value of the constant δ in the term $\sim g^6$. From Ref. [97].

4.2 Dimensional Reduction

Consider a quantum field theory at nonzero temperature in the limit $T \rightarrow \infty$. In this limit, the Euclidean time interval in the partition function (1) shrinks to zero, $1/T \rightarrow 0$. Consequently, the original 3+1-dimensional theory reduces to a theory in three spatial dimensions. This is called *dimensional reduction* [100]. What are the degrees of freedom in the dimensionally reduced theory? Recall that the compactification of the Euclidean time interval $[0, 1/T]$ at nonzero temperature leads to discrete energies for the field modes, the so-called Matsubara frequencies [10]. Bosonic degrees of freedom have periodic boundary conditions in Euclidean time, and thus their Matsubara frequencies are even multiples of πT , $\omega_n^b = 2n\pi T$, $n = 0, \pm 1, \pm 2, \dots$. On the other hand, fermionic degrees of freedom are antiperiodic in Euclidean time, and consequently their Matsubara frequencies are odd multiples of πT , $\omega_n^f = (2n+1)\pi T$, $n = 0, \pm 1, \pm 2, \dots$. As $T \rightarrow \infty$, all modes with nonzero Matsubara frequency become infinitely heavy, and are thus removed from the spectrum of physical excitations. These are *all* fermionic modes, and *all non-static* bosonic modes. Consequently, dimensional reduction leads to a theory of static bosonic fields in three spatial dimensions.

The dimensionally reduced theory can be viewed as an *effective* theory at energy scales much less than the temperature. Consider, for example, QCD in weak coupling, $g \ll 1$, where there is a distinct separation of energy scales, $g^2 T \ll gT \ll T$. The dimensionally reduced theory is then the effective theory for modes at energies of order $O(gT)$ which one obtains from the underlying theory, i.e., QCD, by integrating out modes at energy scales of order $O(T)$. One can then take this idea one step further and integrate out modes at energies of order $O(gT)$ and obtain an effective theory at an energy scale of order $O(g^2 T)$. It was suggested in Ref. [101] to apply this principle of constructing a series of effective theories to compute the pressure in QCD. This task was recently carried out to order $O(g^6)$ in a succession of papers [97]. In the following, I outline the idea and discuss the results, which are

also shown in Fig. 13. Note that the idea of constructing an effective theory valid on a certain energy scale has also been applied to non-Abelian transport theories [102]. As transport theory concerns non-equilibrium situations, a discussion of these aspects are beyond the scope of the present review.

After the first step of integrating out modes at energy scales of order $O(T)$, the pressure in QCD takes the form (at $\mu = 0$)

$$p(T) = p_T(T) + \frac{T}{V} \ln \left[\int \mathcal{D}A_i^a \mathcal{D}A_0^a \exp(-S_E) \right], \quad (62)$$

where $p_T(T)$ is the pressure of the modes at energy scales of order $O(T)$ and the remaining term is the contribution from modes at energy scales of order $O(gT)$. The argument of the logarithm is the partition function of the effective theory for these modes. Since the energy scale gT is that of the Debye mass, $m_D = gT$, which determines the screening length of static color-electric fields, quantities appearing in this partition function will be labelled with a subscript “ E ”. The action S_E of the effective theory is that of a three-dimensional non-Abelian gauge theory (i.e., consisting of the color-magnetic fields of the original theory) coupled to a Higgs field in the adjoint representation of the gauge group (corresponding to the static color-electric fields of the original theory) [97],

$$S_E = \int_V d^3x \mathcal{L}_E, \quad (63)$$

$$\mathcal{L}_E = \frac{1}{2} \text{Tr} \mathcal{F}_{ij}^2 + \text{Tr} [D_i, \mathcal{A}_0]^2 + m_E^2 \text{Tr} \mathcal{A}_0^2 + \lambda_E^{(1)} (\text{Tr} \mathcal{A}_0^2)^2 + \lambda_E^{(2)} \text{Tr} \mathcal{A}_0^4 + \dots. \quad (64)$$

Here, $\mathcal{F}_{ij} \equiv (i/g_E)[D_i, D_j] = F_{ij}^a T^a$, $D_i = \partial_i - ig_E \mathcal{A}_i$, and $\mathcal{A}_\mu \equiv A_\mu^a T^a$. There are five unknown quantities on the right-hand side of Eq. (62): the pressure p_T , the mass m_E of the adjoint Higgs field \mathcal{A}_0 and the coupling constants $g_E, \lambda_E^{(1)}, \lambda_E^{(2)}$. Their values have to be determined by “matching” the effective theory to the original theory at some matching energy scale. At this point, however, one can already determine their scaling behavior from counting dimensions. The pressure p_T is that of a 3+1-dimensional theory of modes with momenta of order $O(T)$. Thus, at nonzero temperature (see above) $p_T \sim T \int dk k^2 \sim T^4$. Since the action S_E has to be dimensionless, one can deduce the dimensionality of the fields \mathcal{A}_i from the kinetic term $\sim \mathcal{F}_{ij}^2$. As lengths have dimension T^{-1} , the fields have to scale as $\mathcal{A}_i \sim T^{1/2}$. The adjoint Higgs field must have the same dimension, $\mathcal{A}_0 \sim T^{1/2}$. From this one deduces that the mass term scales as $m_E \sim m_D = gT$, the coupling constant g_E scales $\sim gT^{1/2}$, and the four-point couplings behave as $\lambda_E^{(i)} \sim g^4 T$. The dots in Eq. (64) denote higher-order operators. One can show by power counting that they are not relevant if one is interested in a calculation of the pressure to order $O(g^6)$ [97].

The next step consists of integrating out modes at energy scales of order $O(gT)$. Since physics at this scale is determined by static color-electric fields, or in other words, by the adjoint Higgs field \mathcal{A}_0 , one has to integrate out this field,

$$\frac{T}{V} \ln \left[\int \mathcal{D}A_i^a \mathcal{D}A_0^a \exp(-S_E) \right] = p_E(T) + \frac{T}{V} \ln \left[\int \mathcal{D}A_i^a \exp(-S_M) \right]. \quad (65)$$

The term p_E is the pressure of modes with energy of order $O(gT)$. The argument of the logarithm on the right-hand side defines the partition function of an effective theory at energy scales of order $O(g^2 T)$. Since the energy scale $g^2 T$ is associated with the scale of the magnetic screening mass $m_M \sim g^2 T$ in non-Abelian gauge theories at nonzero temperature, quantities appearing in this partition function are labelled with a subscript “ M ”. The action S_M entering the partition function of the effective theory at an energy scale $O(g^2 T)$ is simply that for a three-dimensional non-Abelian field theory for color

magnetic fields,

$$S_M = \int d^3x \mathcal{L}_M , \quad (66)$$

$$\mathcal{L}_M = \frac{1}{2} \text{Tr} \mathcal{F}_{ij}^2 + \dots , \quad (67)$$

where $\mathcal{F}_{ij} \equiv (i/g_M)[D_i, D_j]$, $D_i = \partial_i - ig_M \mathcal{A}_i$, and $\mathcal{A}_i \equiv A_i^a T^a$. The two constants p_E , g_M on the right-hand side of Eq. (65) have to be determined by matching the effective theory at the energy scale $g^2 T$ to that at the energy scale gT . However, their scaling behavior can already be determined by power counting. The pressure p_E is again $\sim T \int dk k^2$, but now the integral runs only over modes with momenta of order $O(gT)$, thus $p_E \sim (gT)^3 T \sim m_E^3 T$. The dimensionality of the fields \mathcal{A}_i is the same as in the previous effective theory, thus $g_M \sim gT^{1/2} \sim g_E$. The dots in Eq. (67) denote higher-dimensional operators which are again irrelevant if one is interested in a computation of the pressure to order $O(g^6)$.

The final step is to compute the pressure of modes with energies of order $O(g^2 T)$,

$$p_M(T) \equiv \frac{T}{V} \ln \left[\int \mathcal{D}A_i^a \exp(-S_M) \right] . \quad (68)$$

From power counting one deduces that $p_M \sim T \int dk k^2 \sim (g^2 T)^3 T \sim g^6 T^4 \sim g_M^6 T$, since the integral runs over modes with momenta of order $O(g^2 T)$. Due to the Linde problem, this contribution cannot be obtained perturbatively. What one can evaluate [97] is the contribution of order $O(g^6 \ln g)$ to p_M , since this arises from ultraviolet divergences $\sim \ln(\bar{\mu}/m_M)$, instead from the nonperturbative infrared sector which yields a genuine $O(g^6)$ contribution to the pressure. The latter has to be evaluated e.g. via a lattice calculation.

The final answer for the pressure in QCD is then $p(T) = p_T(T) + p_E(T) + p_M(T)$. If one wants to determine the pressure to order $O(g^6 \ln g)$, one has to compute all terms appearing to this order in p_T , p_E , and p_M . This can be done perturbatively. The contributions to p_T constitute a power series in g^2 , and not in g . They are needed explicitly only to order $O(g^4)$, since the full $O(g^6)$ contribution to the pressure is nonperturbative in any case. One then evaluates all four-loop diagrams in the effective theory at scales gT , in order to determine p_E up to order $O(g^6 \ln g)$ [97]. As expected from power counting (see above), the lowest-order terms in p_E are $\sim m_E^3 T \sim g^3 T^4$. Finally one adds everything to the $O(g^6 \ln g)$ term from p_M . One obtains a well-defined expression for the pressure up to order $O(g^6 \ln g)$. The term which is genuinely of order $O(g^6)$ remains unknown. The result for the pressure in QCD is then given by Eq. (56) with the $O(g^6)$ contribution ($N_c = 3$, $N_f = 0$)

$$c_6 = N_c^3 \frac{N_c^2 - 1}{(4\pi^4)} \left[\left(\frac{215}{12} - \frac{805}{768} \pi^2 \right) \ln \frac{1}{g} + 8\delta \right] , \quad (69)$$

where δ is an unknown constant.

In the right panel of Fig. 13 the result for the pressure as a function of temperature is shown for various values of δ . Comparing to lattice QCD data for the pure $[SU(3)_c]$ gauge theory, the optimum value appears to be $\simeq 0.7$, since then the perturbative calculation nicely matches onto the results from the lattice computation, see left panel of Fig. 13. One also observes that for the optimum value, the pressure up to $O(g^6)$ is rather close to the result to order $O(g^2)$, unless the temperature is very close to T_c . This provides a certain amount of confidence that this perturbative evaluation of the pressure is reasonable.

4.3 Quasiparticle Models

In Sec. 4.2, the pressure of QCD was computed by evaluating the partition functions of various effective theories. This considerably improved the somewhat unsatisfactory situation of a purely perturbative evaluation of the pressure up to terms of order $O(g^5)$ as discussed in Sec. 4.1. Another way to improve the situation is based on the following observation. The result of Sec. 3.4 suggest that nonperturbative effects still influence the physics at temperatures in the range from T_c to a few times T_c . Consequently, a perturbative expansion of the pressure around the *perturbative* vacuum in terms of *massless* quarks and gluons seems inappropriate. What is obviously missing in a perturbative description of the QCD partition function are nonperturbative effects which, when decreasing the temperature from $T > T_c$, are responsible for the phase transition at T_c . This was realized a while ago and attempts were made to incorporate them into the properties of the physical degrees of freedom. In the following, I discuss two such attempts, the so-called “cut-off model” and a model which treats quarks and gluons as massive quasiparticles.

4.3.1 The cut-off model

Let us again restrict the discussion to the pure $[SU(3)_c]$ gauge theory. The cut-off model is motivated by the fact that QCD is an asymptotically free theory [1], i.e., only gluons with large momenta can be considered to be perturbative, while those with small momenta are subject to confinement. Quite similar to the effective-theory approach discussed in Sec. 4.2, one then introduces a cut-off momentum Λ to separate these two regions [103, 104]. Gluons with momenta larger than Λ are treated perturbatively, while gluons with momenta smaller than Λ are assumed to remain bound inside colorless objects (glueballs in the case of pure $[SU(3)_c]$ gauge theory). The dispersion relation for perturbative gluons then changes from the one for free massless particles, $\omega(\mathbf{k}) = |\mathbf{k}| = k$ to

$$\omega(\mathbf{k}) = \Theta(k - \Lambda) k . \quad (70)$$

Gluons with momenta $k < \Lambda$ are bound inside glueballs. The glueball mass scale M is of the order of 1 GeV. The contribution of glueballs to the thermodynamic functions is then exponentially suppressed $\sim \exp(-M/T)$, and can thus be neglected for the temperature range of interest.

The leading-order contribution to the pressure arises from non-interacting gluons with momenta $k > \Lambda$,

$$p_0^{\text{cut}}(T) = -2(N_c^2 - 1) T \int \frac{d^3 \mathbf{k}}{(2\pi)^3} \Theta(k - \Lambda) \ln \left[1 - \exp \left(-\frac{k}{T} \right) \right] . \quad (71)$$

One can also compute perturbative corrections to this leading-order result. To this end, one has to evaluate the standard diagrams of the perturbative expansion of the pressure as discussed in subsection 4.1, but with additional theta-functions like in Eq. (70) to restrict the phase space of the internal gluon lines. In Ref. [104] this has been done up to order $O(g^2)$. Due to the restricted phase space in the loop integrals, the perturbative corrections become relatively small compared to the zeroth-order contribution. In this sense, the perturbative series for particles with the dispersion relation (70) is better behaved than the original perturbative series when the cut-off $\Lambda = 0$.

Besides the cut-off Λ , the cut-off model has another parameter, the MIT bag constant B [105], which describes the energy difference between the perturbative and the nonperturbative vacuum. Fitting the parameters of the cut-off model to lattice QCD data for the pure $[SU(3)_c]$ gauge theory, quite reasonable agreement could be obtained. I do not explicitly show results from Ref. [104], because lattice data at that time were not yet extrapolated to the continuum limit. Consequently, the values for Λ and B obtained previously will quantitatively change once continuum-extrapolated data are used for the fit.

Nevertheless, on a qualitative level, the values for Λ necessary to fit the data were on the order a typical glueball mass $\Lambda \sim M \sim 1$ GeV. This value for Λ nicely confirms the consistency of the assumption underlying the cut-off model, namely that gluons with momenta $k < \Lambda \sim M$ are bound into glueballs of mass M . Moreover, if one interprets the cut-off model as an effective theory in the sense of Sec. 4.2, the physics cannot depend on the precise value of Λ . In other words, if one properly matches the effective theory for gluons with momenta $k > \Lambda$ to the effective theory for glueballs (i.e., gluons with momenta $k < \Lambda$), the cut-off would drop out. This matching procedure has not been done for the cut-off model. However, one may expect that a proper matching calculation would just confirm the result $\Lambda \sim M$ obtained from the fit to lattice QCD data. One may thus simply replace the unphysical parameter Λ by the physical value of the glueball mass M to obtain a model which is independent of the arbitrary (and thus unphysical) cut-off scale Λ . The cut-off model has not been applied to lattice data for full QCD, because then the assumption that all colorless objects are heavy and are negligible when computing thermodynamic functions breaks down (the pion mass is of the order of T_c).

The gluon dispersion relation (70) can be interpreted in the way that gluons with momenta below the cut-off momentum Λ have infinite mass, while those with momenta above Λ have zero mass. It is hard to believe that the true dispersion relation of gluons as computed in Yang-Mills theory would sustain the oversimplified and rather radical assumptions of the cut-off model. A more conservative model to improve our understanding of the thermodynamic properties of the QGP is explained in the following section.

4.3.2 Models with massive quasiparticles

In a hot and dense medium, particles attain a self-energy $\Pi(\omega, \mathbf{k})$, which (due to the breaking of Lorentz invariance) depends separately on energy ω and 3-momentum \mathbf{k} , as well as on the properties of the medium (i.e., its temperature T and chemical potential μ). If the imaginary part of the self-energy on the dispersion branch of the physical excitations is not too large compared to the real part, these excitations are called quasiparticles [106]. The simplest situation is when the self-energy is independent of energy and momentum, i.e., constant and real, corresponding to a mass term, which depends on T and μ , but not on the energy and the momentum of the particle. In this case, the dispersion relation for quasiparticles of mass m reads

$$\omega(\mathbf{k}) = \sqrt{\mathbf{k}^2 + m^2} . \quad (72)$$

The self-energies of quarks and gluons in QCD are certainly not constant (see also Sec. 4.4). Nevertheless, one can still simply *assume* that they are constant and explore the consequences. These so-called “massive quasiparticle models” have been investigated in great detail in the literature as a means to describe and interpret lattice QCD data on thermodynamic functions of QCD [107, 108, 109, 110]. The advantage of these models is that it is straightforward to extend them to nonzero quark chemical potential [111].

Here, as in the previous section let us only focus on a quasiparticle model for pure $[SU(3)_c]$ gauge theory. For the generalization to QCD with dynamical quarks, see Refs. [110, 111]. For the pure gauge theory, there are only massive gluon degrees of freedom and the pressure reads

$$p^{\text{mqp}}(T) = -DT \int \frac{d^3\mathbf{k}}{(2\pi)^3} \ln \left[1 - \exp \left(-\frac{\omega(\mathbf{k})}{T} \right) \right] - B , \quad (73)$$

with $\omega(\mathbf{k})$ given by Eq. (72). As in the cut-off model, an MIT bag constant is introduced to account for the difference between the perturbative and the nonperturbative vacuum.

Two comments regarding the pressure (73) are in order. First, while massless gluons have two transverse polarizations, massive gluons have an additional longitudinal polarization degree of freedom.

Therefore, one would naively argue that the constant D in Eq. (73) should assume the value $D = 3(N_c^2 - 1)$, instead of $D = 2(N_c^2 - 1)$, as for massless gluons. This is, however, not quite correct. First, the pressure (73) has to approach the correct Stefan-Boltzmann limit when $T \rightarrow \infty$. For three polarization degrees of freedom, the Stefan-Boltzmann pressure is a factor $3/2$ larger than the correct value. Another reason why this is incorrect is the following. In Sec. 4.4 we shall see that gluons indeed acquire a longitudinal degree of freedom in a hot or dense medium, but that the respective longitudinal spectral density vanishes rapidly for energies and momenta larger than gT . Thus, in a calculation of the pressure, which is dominated by modes with momenta of order T , one should in principle not count the longitudinal degrees of freedom. We shall therefore set $D = 2(N_c^2 - 1)$ in the following. (Note that Ref. [110] also investigated a scenario where D is a function of temperature.)

The second comment concerns the possibility to fit lattice QCD data with Eq. (73). It turns out that for constant mass and bag parameters, the quality of the fit is not satisfactory. Consequently, one needs to generalize the model (73) to allow for a temperature-dependent gluon mass, $m \rightarrow m(T)$. A convenient parametrization is motivated by the dispersion relation for transverse gluons at large momenta, which takes the form $\omega_t(k) = \sqrt{k^2 + m_{t\infty}^2}$, see Eq. (100). Consequently,

$$m(T) = \frac{g(T) T}{\sqrt{2}} , \quad g^2(T) = \frac{8\pi^2}{11 \ln [F(T/T_c, T_c/\Lambda_{\overline{MS}})]} , \quad F(x, y) = K(x) x y . \quad (74)$$

For a fixed value of $T_c/\Lambda_{\overline{MS}} \simeq 1.03 \pm 0.19$ for pure $[SU(3)_c]$ gauge theory [112], one only needs to know the function $K(T/T_c)$ in order to determine the mass, $m(T)$, and thus the kinetic term in the pressure (73). In Ref. [110] the function $K(T/T_c)$ is simply fit to reproduce lattice QCD data. A surprisingly good fit is obtained with the functional form $K(x) = 18/[18.4 \exp(-0.5 x^2) + 1]$, see Fig. 14. Once the gluon mass is a function of temperature, thermodynamical consistency requires the bag parameter to depend on the temperature as well, $B \rightarrow B(T)$. The functional form of $B(T)$ can be uniquely determined from $m(T)$; for details see Ref. [110].

4.4 HTL/HDL-Resummed Perturbation Theory

Apparently, the idea that quarks and gluons are quasiparticles works rather well to describe the thermodynamic functions of the QGP. Therefore, it seems appropriate to put this concept onto a more formal basis. In fact, the quasiparticle excitations in the QGP are well known in the weak-coupling limit, $g \ll 1$, and for temperatures and/or chemical potentials much larger than the quasiparticles' energies and momenta. At nonzero temperature, these quasiparticles form the basis of the so-called “hard thermal loop” (HTL-) resummation scheme [13, 113]. At zero temperature, but large quark chemical potential, there is an equivalent approach, the so-called “hard dense loop” (HDL-) resummation scheme [13, 114]. From the quasiparticle excitation spectrum, one can also construct the equation of state. All this will be discussed in detail in the following.

4.4.1 The excitation spectrum in a hot and dense medium

How does one determine the spectrum of physical excitations in a hot and/or dense medium? I shall illustrate this explicitly for the case of gluons. The case of quarks can be considered analogously, I only briefly report on the results at the end of this section. The outline of the procedure is the following. First, one computes the gluon self-energy, $\Pi_{ab}^{\mu\nu}(\omega, \mathbf{p})$. From the self-energy, one then determines the full gluon propagator, $\Delta_{ab}^{\mu\nu}(\omega, \mathbf{p})$. From the gluon propagator, one then deduces the spectral density, which provides all information about the excitation spectrum in a hot and/or dense medium. Quite surprisingly, it turns out that one can follow this procedure in complete generality, without actually

Fig.4. $SU(3)$, $N_c=0$ --- EOS + Lattice QCD data

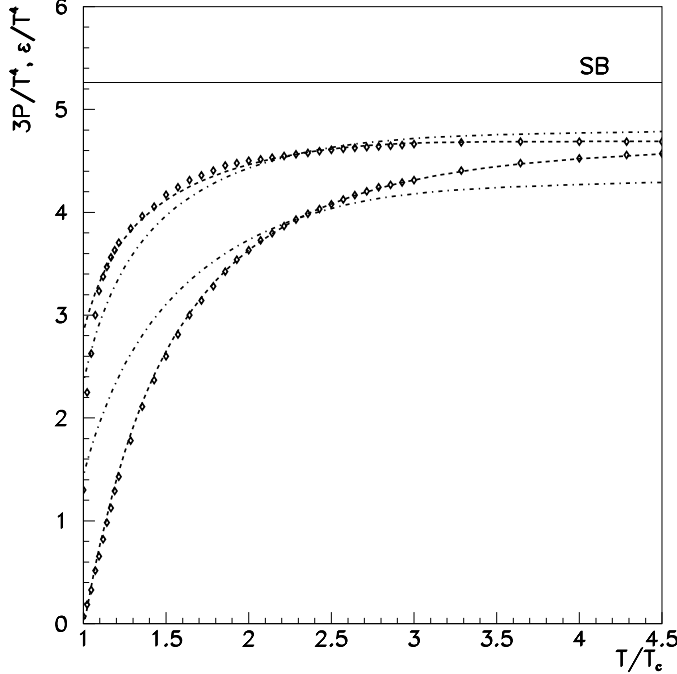


Figure 14: The temperature dependence of $3p/T^4$ and ϵ/T^4 in pure $[SU(3)_c]$ gauge theory. Symbols are lattice QCD data from [76]. The dashed lines are a fit within the massive gluon model. The dash-dotted lines represent the contribution of the kinetic term in Eq. (73). The horizontal line is the Stefan-Boltzmann limit. (Since for an ultrarelativistic ideal gas $\epsilon \equiv 3p$, this limit is the same for the functions $3p/T^4$ and ϵ/T^4 .) From Ref. [110].

specifying $\Pi_{ab}^{\mu\nu}$ until the very end. Although the derivation is somewhat formal, it is nevertheless a rather instructive exercise and will therefore be discussed in more detail [115]. Note that, in a medium, Lorentz symmetry is explicitly broken, and all quantities depend separately on energy ω and momentum \mathbf{p} . Nevertheless, to abbreviate the notation, I shall frequently use the 4-vector $P^\mu \equiv (\omega, \mathbf{p})$ to characterize this dependence. Note also that, at nonzero temperature, one usually computes in Euclidean space time, i.e., all energies are discrete Matsubara frequencies on the *imaginary* energy axis. However, in order to determine the physical excitation spectrum, one has to analytically continue to *real* energies, $i\omega_n \rightarrow \omega + i\eta$. This $i\eta$ prescription produces the *retarded* Greens functions [106]. When writing real energies ω in the following, the $i\eta$ prescription will be suppressed.

The self-energy $\Pi_{ab}^{\mu\nu}$ can be decomposed according to its tensor structure. First of all, if the color $[SU(3)_c]$ gauge symmetry is not broken, one may assume that the gluon self-energy is diagonal in adjoint color, $\Pi_{ab}^{\mu\nu} \equiv \delta_{ab} \Pi^{\mu\nu}$. (In a color superconductor, this is in general no longer the case, for examples see Sec. 5.4.) It thus suffices to consider $\Pi^{\mu\nu}$. The next step is to decompose $\Pi^{\mu\nu}$ in terms of tensors, multiplied by scalar functions of ω and \mathbf{p} [13]. Let us define

$$E^{\mu\nu} \equiv \frac{P^\mu P^\nu}{P^2} \quad (75)$$

as the projector onto the subspace parallel to P^μ . Then one chooses a vector orthogonal to P^μ , for instance

$$N^\mu \equiv \left(\frac{\omega p^2}{P^2}, \frac{\omega^2 \mathbf{p}}{P^2} \right) \equiv (g^{\mu\nu} - E^{\mu\nu}) f_\nu , \quad (76)$$

with $f^\mu = (0, \mathbf{p})$. Now one defines the tensors

$$B^{\mu\nu} = \frac{N^\mu N^\nu}{N^2} , \quad C^{\mu\nu} = N^\mu P^\nu + P^\mu N^\nu , \quad A^{\mu\nu} = g^{\mu\nu} - B^{\mu\nu} - E^{\mu\nu} . \quad (77)$$

With the help of these tensors one can write the gluon self-energy as

$$\Pi^{\mu\nu} = \Pi^a A^{\mu\nu} + \Pi^b B^{\mu\nu} + \Pi^c C^{\mu\nu} + \Pi^e E^{\mu\nu} . \quad (78)$$

The scalar functions $\Pi^{a,b,c,e}$ can be obtained by suitable projections of $\Pi^{\mu\nu}$ onto the respective tensor structures.

Using the explicit form of N^μ , one convinces oneself that the tensor $A^{\mu\nu}$ projects onto the spatially transverse subspace orthogonal to P^μ ,

$$A^{00} = A^{0i} = 0 , \quad A^{ij} = -(\delta^{ij} - \hat{p}^i \hat{p}^j) . \quad (79)$$

This means that the self-energy function Π^a determines the excitation spectrum of the spatially transverse gluon fields

$$A_{\perp\mu}^a(P) \equiv A_\mu^\nu A_\nu^a(P) . \quad (80)$$

As $A^{\mu\nu}$ projects onto a two-dimensional subspace, there are two degrees of freedom associated with $A_{\perp\mu}^a$. In the vacuum, these are the only physical degrees of freedom, since gluons are massless.

The tensor $B^{\mu\nu}$ projects onto the spatially longitudinal subspace orthogonal to P^μ ,

$$B^{00} = -\frac{p^2}{P^2} , \quad B^{0i} = -\frac{\omega p^i}{P^2} , \quad B^{ij} = -\frac{\omega^2}{P^2} \hat{p}^i \hat{p}^j . \quad (81)$$

Consequently, the polarization function Π^b determines the excitation spectrum of the longitudinal gluon degree of freedom,

$$A_N^a(P) \equiv \frac{N^\mu A_\mu^a(P)}{N^2} , \quad (82)$$

which becomes a physical degree of freedom in a medium.

The spatially transverse and spatially longitudinal gluon fields $A_{\perp\mu}^a$ and A_N^a are the only physical degrees of freedom. There is an unphysical degree of freedom associated with the projection onto P^μ ,

$$A_{\parallel}^a(P) \equiv \frac{P^\mu A_\mu^a(P)}{P^2} . \quad (83)$$

The scalar function Π^e is the self-energy of this unphysical degree of freedom. It will be seen that gauge fixing ultimately removes this degree of freedom from the theory. A nonvanishing Π^c indicates that the spatially longitudinal, physical gluon degree of freedom A_N^a mixes with the unphysical degree of freedom A_{\parallel}^a . Before extracting the physical excitation spectrum, one has to remove this mixing term, as will be discussed below.

Now use the tensor decomposition (78) to determine the full gluon propagator $\Delta_{ab}^{\mu\nu}$. Since the free inverse gluon propagator

$$\Delta_0^{-1\mu\nu} \equiv \delta_{ab}(P^2 g^{\mu\nu} - P^\mu P^\nu) \equiv \delta_{ab} P^2 (A^{\mu\nu} + B^{\mu\nu}) \quad (84)$$

is diagonal in adjoint colors, so is the full inverse gluon propagator, $\Delta^{-1\mu\nu} \equiv \delta_{ab} \Delta^{-1\mu\nu}$. One obtains

$$\Delta^{-1\mu\nu} \equiv \Delta_0^{-1\mu\nu} + \Pi^{\mu\nu} \equiv (P^2 + \Pi^a) A^{\mu\nu} + (P^2 + \Pi^b) B^{\mu\nu} + \Pi^c C^{\mu\nu} + \Pi^e E^{\mu\nu} . \quad (85)$$

In an effective action, this inverse propagator is the coefficient of the term quadratic in the gauge fields. In momentum space (and choosing a normalization such that $A_\mu^a(P)$ retains dimensions of energy),

$$S_2 = -\frac{1}{2} \frac{V}{T} \sum_P \sum_{a=1}^{N_c^2-1} \left\{ A_{\perp\mu}^a(-P) [P^2 + \Pi^a(P)] A^{\mu\nu} A_{\perp\nu}^a(P) - A_N^a(-P) [P^2 + \Pi^b(P)] N^2 A_N^a(P) \right. \\ \left. - A_{\parallel}^a(-P) \Pi^c(P) N^2 P^2 A_N^a(P) - A_N^a(-P) \Pi^c(P) N^2 P^2 A_{\parallel}^a(P) \right. \\ \left. - A_{\parallel}^a(-P) \Pi^e(P) P^2 A_{\parallel}^a(P) \right\} , \quad (86)$$

where $\sum_P \equiv (V/T) f_P$. The physical excitation spectrum can be most easily extracted from a diagonalized inverse gluon propagator, i.e., the term which mixes the physical field component A_N^a with the unphysical component A_{\parallel}^a has to be eliminated. This can be done as follows. Remember that in the partition function one functionally integrates the exponential of the action (a part of which is S_2 in Eq. (86)) over all gauge field components, including A_{\parallel}^a . For the purpose of diagonalizing the inverse gluon propagator one may simply redefine the integration variable

$$A_{\parallel}^a(P) \rightarrow \hat{A}_{\parallel}^a(P) \equiv A_{\parallel}^a(P) + \frac{\Pi^c(P) N^2}{\Pi^e(P)} A_N^a(P) . \quad (87)$$

This redefinition does not change the physics (as it only involves the unphysical component of the gauge field) and diagonalizes the action S_2 in the components of the gauge field,

$$S_2 = -\frac{1}{2} \frac{V}{T} \sum_P \sum_{a=1}^{N_c^2-1} \left\{ A_{\perp\mu}^a(-P) [P^2 + \Pi^a(P)] A^{\mu\nu} A_{\perp\nu}^a(P) - A_N^a(-P) [P^2 + \hat{\Pi}^b(P)] N^2 A_N^a(P) \right. \\ \left. - \hat{A}_{\parallel}^a(-P) \Pi^e(P) P^2 \hat{A}_{\parallel}^a(P) \right\} , \quad (88)$$

where

$$\hat{\Pi}^b(P) \equiv \Pi^b(P) - \frac{[\Pi^c(P)]^2 N^2 P^2}{\Pi^e(P)} . \quad (89)$$

From Eq. (88) one can read off the inverse gluon propagator in diagonal form. However, in order to be able to invert it, it is necessary to fix the gauge. (To see this, consider the case where $\Pi^e = 0$. Then, the inverse propagator has a zero eigenvalue and is not invertible). For the sake of simplicity, let us choose covariant gauge, where the gauge fixing term in the action only involves the unphysical components of the gauge field,

$$S_{\text{gf}} = \frac{1}{2\lambda} \frac{V}{T} \sum_P \sum_{a=1}^{N_c^2-1} \hat{A}_{\parallel}^a(-P) P^2 P^2 \hat{A}_{\parallel}^a(P) . \quad (90)$$

Adding S_{gf} to S_2 , one reads off the (gauge-fixed) inverse gluon propagator

$$\Delta^{-1\mu\nu}(P) = [P^2 + \Pi^a(P)] A^{\mu\nu} + [P^2 + \hat{\Pi}^b(P)] B^{\mu\nu} + \left[\frac{1}{\lambda} P^2 + \Pi^e(P) \right] E^{\mu\nu} , \quad (91)$$

which can be straightforwardly inverted, since $A^{\mu\nu}$, $B^{\mu\nu}$, and $E^{\mu\nu}$ are projectors,

$$\Delta^{\mu\nu}(P) = \Delta_t(P) A^{\mu\nu} - \Delta_\ell(P) \frac{p^2}{P^2} B^{\mu\nu} + \frac{\lambda}{P^2 + \lambda \Pi^e(P)} E^{\mu\nu} , \quad (92)$$

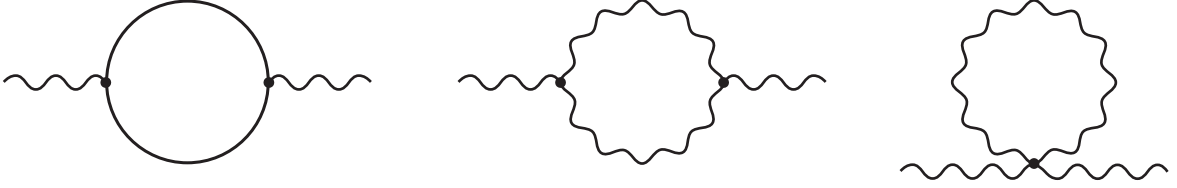


Figure 15: The one-loop diagrams contributing to the gluon self-energy (possible ghost contributions are not shown).

where the transverse and longitudinal propagators are defined as

$$\Delta_t(P) \equiv \frac{1}{P^2 + \Pi^a(P)} \equiv \frac{1}{P^2 - \Pi_t(P)} , \quad \Delta_\ell(P) \equiv -\frac{P^2}{p^2} \frac{1}{P^2 + \hat{\Pi}^b(P)} = -\frac{1}{p^2 - \Pi_\ell(P)} , \quad (93)$$

with the transverse and longitudinal polarization functions $\Pi_t \equiv -\Pi^a$ and $\Pi_\ell \equiv -(p^2/P^2)\hat{\Pi}^b$. The last term in Eq. (92) can be removed from the spectrum of physical excitations by the gauge choice $\lambda = 0$. The physical excitations are described by the transverse and longitudinal propagators defined in Eq. (93). From these one can derive the corresponding spectral densities in the usual way [13]

$$\rho_t(\omega, \mathbf{p}) \equiv \frac{1}{\pi} \text{Im} \Delta_t(\omega + i\eta, \mathbf{p}) , \quad \rho_\ell(\omega, \mathbf{p}) \equiv \frac{1}{\pi} \text{Im} \Delta_\ell(\omega + i\eta, \mathbf{p}) . \quad (94)$$

All that is left is to actually specify the form of the polarization functions Π_t and Π_ℓ . In the weak-coupling limit, $g \ll 1$, this can be done via a one-loop calculation of these functions. To this end, one has to compute the diagrams shown in Fig. 15 using standard methods [10, 13]. Note, however, that the result depends in general on the choice of gauge and thus cannot determine the physical excitation spectrum, which is by definition independent of the choice of gauge. However, it was noticed many years ago [116], that the high-temperature limit $T \gg \omega, p$ of the polarization functions is actually independent of the choice of gauge,

$$\text{Re} \Pi_t(\omega, \mathbf{p}) = \frac{3}{2} m_g^2 \left[\frac{\omega^2}{p^2} + \left(1 - \frac{\omega^2}{p^2}\right) \frac{\omega}{2p} \ln \left| \frac{\omega + p}{\omega - p} \right| \right] , \quad (95)$$

$$\text{Im} \Pi_t(\omega, \mathbf{p}) = -\pi \frac{3}{4} m_g^2 \frac{\omega}{p} \left(1 - \frac{\omega^2}{p^2}\right) \Theta(p - \omega) , \quad (96)$$

$$\text{Re} \Pi_\ell(\omega, \mathbf{p}) = -3 m_g^2 \left(1 - \frac{\omega}{2p} \ln \left| \frac{\omega + p}{\omega - p} \right| \right) , \quad (97)$$

$$\text{Im} \Pi_\ell(\omega, \mathbf{p}) = -\pi \frac{3}{2} m_g^2 \frac{\omega}{p} \Theta(p - \omega) , \quad (98)$$

where the gluon mass parameter at a given T and μ is

$$m_g^2 = g^2 \left[\frac{2N_c + N_f}{18} T^2 + \frac{N_f}{6\pi^2} \mu^2 \right] . \quad (99)$$

This result is not restricted to the high-temperature limit, in fact it holds as long as either T or μ is much larger than ω and p . Thus, it also describes gluonic quasiparticle excitations at $T = 0$ and high density. It is only this gauge-invariant high- T (or high- μ) limit of the one-loop polarization functions, which is relevant for the HTL- (or HDL-) resummation scheme discussed in Sec. 4.4.2.

What is the physical meaning of the result (95) – (98)? The condition $T, \mu \gg \omega, p$ implies that there is a separation of scales, just like in the construction of the effective theories in Sec. 4.2. The temperature (or the chemical potential) sets a “hard” energy scale, while the external energy and momentum are “soft”. As will be seen in Sec. 4.4.2, this separation of scales forms the basis of the HTL- (or HDL-) resummation scheme. In this scheme, energies of order gT (or $g\mu$, in the HDL-resummation scheme) are “soft”, while energies of order T (or μ , respectively) are “hard”. In the loops in Fig. 15, one integrates over the internal loop momentum, \mathbf{k} , but the result must be finite, as there are no other ultraviolet divergences at nonzero T and/or μ than those already known from the vacuum. Therefore, the ultraviolet regularization must be provided by the distribution functions of quarks and gluons, which decrease exponentially with temperature. (At $T = 0$ and $\mu \neq 0$, the gluon distribution function vanishes, while the quark distribution function is a step function $\sim \Theta(\mu - k)$, which cuts off momenta $k > \mu$). On the other hand, the phase space in the loop integral grows $\sim \int dk k^2$. One thus expects that the *dominant* contribution to the loop integral comes from “hard” momenta of order T (or, at $T = 0$ and $\mu \neq 0$, from momenta close to the Fermi surface, $k \sim \mu$). For dimensional reasons, and including factors of g from the vertices, $\Pi \sim g^2 T^2$ (or $\sim g^2 \mu^2$, at $T = 0$ and $\mu \neq 0$). This gives rise to the prefactor $\sim m_g^2$ in Eqs. (95) – (98). The “soft” external energy and momentum cannot significantly alter the kinematics in the loop, where the dominant contribution comes from “hard” momenta. In fact, it suffices to expand the integrands of the loop integrals to leading order in these external quantities. This gives rise to the particular dependence on ω and p of the result (95) – (98). The essential approximation which leads to this result is the assumption that internal momenta are exclusively “hard”. Therefore, the loops computed under this assumption are called “*hard thermal loops*” (or “*hard dense loops*”, at $T = 0$ and $\mu \neq 0$).

From the self-energies one can construct the propagators (93) and the spectral densities (94), respectively. Following Ref. [117] it turns out that the propagators have poles above the light-cone, $\omega > p$, and a cut below, $\omega < p$. In the spectral densities, the poles become δ -functions. These determine the excitation branches $\omega(p)$. Since a δ -function has no width, the quasiparticles corresponding to these excitation branches are *stable*, i.e., they have an infinite lifetime. (This changes if one computes beyond one-loop order.) The excitation branches are above the light-cone, i.e., they correspond to time-like, propagating gluons. In the left panel of Fig. 16 they are shown for transverse and longitudinal gluon modes. For large momenta, the longitudinal mode has an exponentially vanishing residue [117]. In contrast, the transverse mode has a finite residue and a dispersion relation which approaches the form

$$\omega_t(p) \rightarrow \sqrt{p^2 + m_{t\infty}^2} , \quad m_{t\infty}^2 \equiv \frac{3}{2} m_g^2 . \quad (100)$$

The cuts in the propagator become continuous distributions in the spectral density. They provide Landau-damping for space-like gluons.

Performing a similar exercise for quarks [118], one obtains the spectrum of fermionic quasiparticle excitations. It turns out that there are twice as many excitation branches as expected. There are in fact *two* solutions for positive energies, $\omega_{\pm}(p)$, determined by the equation

$$\omega_{\pm}(p) = \pm p \pm \frac{m_f^2}{p} \left[1 - \frac{\omega_{\pm}(p) \mp p}{2p} \ln \left(\frac{\omega_{\pm}(p) + p}{\omega_{\pm}(p) - p} \right) \right] , \quad (101)$$

where the fermionic mass parameter (squared) is

$$m_f^2 = g^2 \frac{N_c^2 - 1}{16 N_c} \left(T^2 + \frac{\mu^2}{\pi^2} \right) . \quad (102)$$

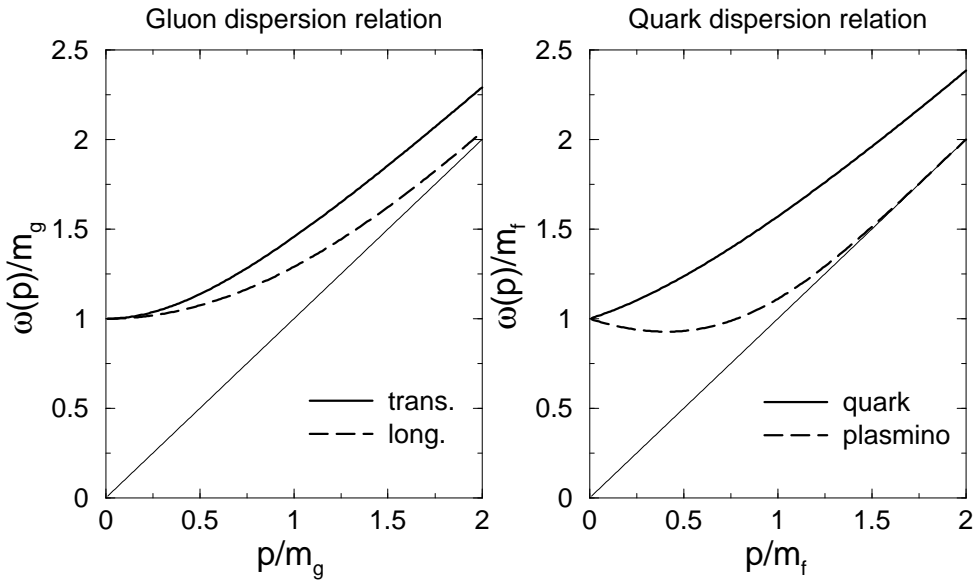


Figure 16: The excitation branches for gluons (left panel) and quarks (right panel) in a hot and/or dense medium. For gluons, energy and momenta are shown in units of the gluon mass parameter, m_g . For quarks, energy and momenta are shown in units of the fermion mass parameter, m_f .

These two solutions are shown in the right panel of Fig. 16. (The two solutions for negative energies mirror the above solutions below the p axis.) The solution $\omega_-(p)$ corresponds to a quasiparticle with the opposite chirality than the one associated with the solution $\omega_+(p)$. This peculiar quasiparticle is commonly called the “plasmino”. Note that, while the ordinary quasiparticle dispersion branch $\omega_+(p)$ has a positive group velocity $d\omega_+(p)/dp > 0$, the plasmino branch has negative group velocity at small momenta. For large momenta, the residue of the plasmino branch becomes exponentially small, while the one for the ordinary quasiparticle remains finite and its dispersion relation approaches the form

$$\omega_+(p) \rightarrow \sqrt{p^2 + m_{f\infty}^2}, \quad m_{f\infty}^2 = 2 m_f^2. \quad (103)$$

The quark propagator also features a cut below the light-cone, which gives rise to Landau damping. Finally, note that the fermionic quasiparticle spectrum in Fig. 16 is shown for energies and momenta much smaller than either temperature and/or chemical potential. However, at $T = 0$ and large μ , this kinematic region is irrelevant, as it reflects the situation at the bottom of the Fermi sea. At $T = 0$ and large μ , the *relevant* fermionic excitations are those around the Fermi surface, where $p \simeq \mu$. The excitation spectrum for this case will be discussed in more detail in Sec. 5.2.

4.4.2 HTL/HDL-resummation scheme

The HTL-resummation scheme and its counterpart at $T = 0$ and nonzero μ , the HDL-resummation scheme, are explained in great detail in textbooks on field theory at nonzero temperature and density (see, for instance, Ref. [13]). Therefore, for more details, I refer the interested reader to the literature and restrict myself here to a short discussion of the general idea behind these methods.

As already discussed in Sec. 4.1, due to the infrared behavior of gauge theories at nonzero temperature, naive perturbation theory breaks down. We have seen in Sec. 4.4.1 that loop calculations involve

propagators of the form

$$\Delta(\omega, \mathbf{p}) \sim \frac{1}{\omega^2 - p^2 + \Pi(\omega, \mathbf{p})}. \quad (104)$$

The leading-order terms in the one-loop self-energy arise from “hard” particles with momenta $k \sim T$ inside the loop. Together with factors of the coupling constant arising from the vertices, the self-energy is $\Pi \sim g^2 T^2$. Therefore, as long as either ω or p are “hard”, i.e., of order T , the self-energy Π in the propagator (104) can be *neglected*. However, for “soft” ω and p of order gT , the self-energy is of the same order of magnitude as the first two terms in the denominator and *cannot* be neglected.

This observation forms the basis of the so-called HTL-resummation scheme [13, 113] in field theories at nonzero temperature. In simple words it states that whenever the energy and the momentum of a propagator in a given diagram is “soft”, one has to use the “dressed” propagator (104) including the self-energy Π , and if either energy or momentum is “hard”, one may use the “bare” propagator $\Delta_0(\omega, \mathbf{p}) = 1/(\omega^2 - p^2)$ without the self-energy Π . How does the name “HTL-resummation scheme” arise? The dressed propagator is the solution of the Dyson-Schwinger equation

$$\Delta = \Delta_0 - \Delta_0 \Pi \Delta. \quad (105)$$

Iterating this equation, one realizes that it stands for an infinite series of diagrams; consequently the solution (104) is a *resummed* propagator. As explained in Sec. 4.4.1, the quantity which is resummed is the self-energy Π computed in the HTL approximation, i.e., one resums HTL’s.

It is now also easy to see why naive perturbation theory breaks down at nonzero temperature. Imagine a diagram with n vertices, such that naive perturbation theory would tell us that this diagram is of order $O(g^n)$. Now imagine that there is a loop in this diagram with propagators of the type (104) and that the dominant contribution to this loop arises not from the “hard” region of phase space, i.e., from momenta of order T , as in HTL’s, but from the “soft” region, i.e., from momenta $k \sim gT$. The contribution of the propagator (104) to the diagram is then $\sim 1/(g^2 T^2)$, instead of $\sim 1/T^2$. This cancels two powers of the coupling constant in the naive perturbative counting scheme. The diagram is thus actually of order $O(g^{n-2})$ (or even of lower order, if other propagators contribute additional powers of g^{-2}). The occurrence of the additional energy scale T (or μ , at $T = 0$) compared to the vacuum invalidates the naive perturbative counting scheme.

For gauge theories, the Ward identities require to extend the HTL-resummation scheme from propagators to vertices as well. For physical quantities which are determined by computing diagrams with at least one loop, depending on whether the dominant contribution in the loop arises from the hard or the soft region of phase space, one may be required to use only bare propagators, resummed propagators, or both resummed propagators and resummed vertices. The major success of the HTL-resummation scheme was the proof that the leading-order result for the gluon-damping rate is independent of the gauge and positive [119].

4.4.3 The equation of state for quasiparticles in HTL/HDL approximation

The objective of this section is to apply our knowledge from Sec. 4.4.1 about the quasiparticle excitation spectrum in QCD to determine the equation of state at high temperature and/or density. What one obviously needs is a thermodynamically consistent way to construct the pressure including information about the spectral density of the quasiparticles. Obviously, classical statistical mechanics, such as applied in Sec. 4.3.2, is of no use; we need a field-theoretical approach. The method of choice is the so-called “Cornwall-Jackiw-Tomboulis” (CJT) formalism [120]. The CJT formalism determines the effective action of a theory as a functional of the one- and two-point functions. The stationary values of the effective action yield the expectation value of the field and the full propagator. The stationarity

conditions are Dyson-Schwinger equations for these quantities. The CJT formalism is particularly useful for theories with spontaneously broken symmetries, see Sec. 4.6. For unbroken symmetries, the CJT formalism is equivalent to the so-called Φ -functional approach [121].

Let us elaborate on this in somewhat greater detail. In the CJT formalism the effective action of a theory with bosonic fields ϕ and corresponding propagators Δ , as well as fermionic fields $\bar{\psi}, \psi$ with propagators G reads

$$\begin{aligned}\Gamma[\phi, \bar{\psi}, \psi, \Delta, G] &= I[\phi, \bar{\psi}, \psi] - \frac{1}{2} \text{Tr} \ln \Delta^{-1} - \frac{1}{2} \text{Tr} (D^{-1} \Delta - 1) \\ &+ \text{Tr} \ln G^{-1} + \text{Tr} (S^{-1} G - 1) + \Gamma_2[\phi, \bar{\psi}, \psi, \Delta, G].\end{aligned}\quad (106)$$

Here, $I[\phi, \bar{\psi}, \psi]$ is the classical action and all traces are taken in the functional sense. The quantities D^{-1} and S^{-1} are the inverse tree-level propagators for bosons and fermions, respectively,

$$D^{-1}(X, Y) \equiv -\frac{\delta I[\phi, \bar{\psi}, \psi]}{\delta \phi(X) \delta \phi(Y)}, \quad S^{-1}(X, Y) \equiv -\frac{\delta I[\phi, \bar{\psi}, \psi]}{\delta \bar{\psi}(X) \delta \psi(Y)}. \quad (107)$$

The functional Γ_2 is the sum of all two-particle irreducible (2PI) diagrams without external legs and with internal lines given by the propagators Δ and G . The stationarity conditions which determine the expectation value of the bosonic field, φ , as well as the full propagators for bosons, \mathcal{D} , and for fermions, \mathcal{G} , read

$$\frac{\delta \Gamma[\phi, \bar{\psi}, \psi, \Delta, G]}{\delta \phi(X)} = \frac{\delta \Gamma[\phi, \bar{\psi}, \psi, \Delta, G]}{\delta \Delta(X, Y)} = \frac{\delta \Gamma[\phi, \bar{\psi}, \psi, \Delta, G]}{\delta G(X, Y)} = 0 \quad (108)$$

In principle, there are also stationarity conditions for the fermionic fields $\bar{\psi}$ and ψ , but their solution is always trivial, as fermionic fields are not classical and thus cannot assume a nonzero expectation value.

Inserting the explicit form of Γ from Eq. (106) into the last two equations of (108), one obtains the Dyson-Schwinger equations for the full propagators for bosons, \mathcal{D} , and fermions, \mathcal{G} ,

$$\mathcal{D}^{-1} = D^{-1} + \Pi, \quad \mathcal{G}^{-1} = S^{-1} + \Sigma, \quad (109)$$

where the bosonic and fermionic self-energies are

$$\Pi \equiv -2 \frac{\delta \Gamma_2[\phi, \bar{\psi}, \psi, \Delta, G]}{\delta \Delta}, \quad \Sigma \equiv \frac{\delta \Gamma_2[\phi, \bar{\psi}, \psi, \Delta, G]}{\delta G}. \quad (110)$$

The right-hand sides of these equations have to be taken at the stationary point $\phi = \varphi, \bar{\psi} = \psi = 0, \Delta = \mathcal{D}, G = \mathcal{G}$. According to their definition (110), the self-energies are obtained from the set of 2PI-diagrams Γ_2 by opening one internal line.

For translationally invariant systems, $\phi(X) \equiv \phi = \text{const.}, \Delta(X, Y) \equiv \Delta(X - Y), G(X, Y) \equiv G(X - Y)$, and it is advantageous to work in energy-momentum space instead of in space-time. The effective action is, up to a sign and a factor of the four-dimensional volume of the system, V/T , equal to the effective potential,

$$V[\phi, \bar{\psi}, \psi, \Delta, G] \equiv -\frac{T}{V} \Gamma[\phi, \bar{\psi}, \psi, \Delta, G]. \quad (111)$$

At the stationary point, the effective potential is, again up to a sign, equal to the thermodynamic pressure. Utilizing the stationarity conditions (109) and the definitions (110),

$$p \equiv -V[\varphi, \mathcal{D}, \mathcal{G}] = -U(\varphi) - \frac{1}{2} \text{Tr} \ln \mathcal{D}^{-1} + \frac{1}{2} \text{Tr} \Pi \mathcal{D} + \text{Tr} \ln \mathcal{G}^{-1} - \text{Tr} \Sigma \mathcal{G} - V_2[\varphi, \mathcal{D}, \mathcal{G}]. \quad (112)$$

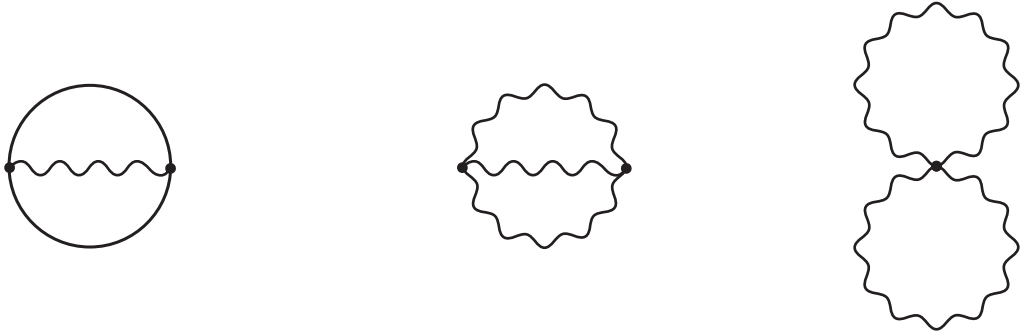


Figure 17: The two-loop approximation to Γ_2 (possible ghost contributions are not shown).

Here, $U(\varphi)$ is the tree-level potential, $V_2 \equiv -(T/V)\Gamma_2$, and $\text{Tr } A \equiv \int_K \text{tr } A(\omega_n, \mathbf{k})$, where tr runs over possible internal indices (Lorentz, Dirac, color, flavor, etc.) of A .

Equation (112) is the desired result. All one has to do is to apply it to QCD. In QCD, there is no spontaneously broken symmetry (unless one considers color superconductivity, see Sec. 5), and thus $U(\varphi) \equiv 0$. The bosons are the gluons and the fermions are the quarks. Of course, one also has to account for ghost degrees of freedom. These look like another fermion contribution in Eq. (112), but the corresponding Matsubara sum in Tr has to run over *even* multiples of πT [10].

This sounds much simpler than it is to realize in practice. The difficulty obviously lies in solving the Dyson-Schwinger equations for the gluon and quark propagators. It is clear that, as V_2 consists of an infinite set of diagrams, one can never aspire to solve the problem exactly. However, a great advantage of the CJT formalism is that the solutions of the Dyson-Schwinger equations (109) are self-consistent and conserving, even if one truncates this infinite set. Any truncation defines a meaningful many-body approximation scheme (for a well-known example, the Hartree approximation, see Sec. 4.6). Let us therefore imagine we only take a finite subset of all diagrams in V_2 , for instance the one consisting of the two-loop diagrams shown in Fig. 17. This subset is particularly interesting, because when computing the self-energies according to Eq. (110) one obtains these self-energies to one-loop order. As discussed in Sec. 4.4.1, the high-temperature (high-density) limit of the one-loop self-energies defines the HTL (HDL) approximation, which is already known to provide a physically interesting, meaningful, and gauge-invariant quasiparticle excitation spectrum. Another advantage of restricting V_2 to a set of two-loop diagrams is that the entropy density $s \equiv \partial p / \partial T$ and the quark number density $n \equiv \partial p / \partial \mu$ assume the particularly simple form [122]

$$s = -\text{tr} \int \frac{d^4 K}{(2\pi)^4} \frac{\partial n(\omega)}{\partial T} \left[\text{Im} \ln \mathcal{D}^{-1} - \text{Im} \Pi \text{Re} \mathcal{D} \right] - 2 \text{tr} \int \frac{d^4 K}{(2\pi)^4} \frac{\partial f(\omega)}{\partial T} \left[\text{Im} \ln \mathcal{G}^{-1} - \text{Im} \Sigma \text{Re} \mathcal{G} \right], \quad (113)$$

$$n = -2 \text{tr} \int \frac{d^4 K}{(2\pi)^4} \frac{\partial f(\omega)}{\partial \mu} \left[\text{Im} \ln \mathcal{G}^{-1} - \text{Im} \Sigma \text{Re} \mathcal{G} \right], \quad (114)$$

where $K^\mu \equiv (\omega, \mathbf{k})$ and $n(\omega) \equiv (e^{\omega/T} - 1)^{-1}$ is the Bose-Einstein distribution function, while $f(\omega) \equiv [e^{(\omega-\mu)/T} + 1]^{-1}$ is the Fermi-Dirac distribution function. While one has to compute two-loop diagrams to obtain the pressure (112), the entropy and quark number densities (113,114) are essentially one-loop quantities and thus much simpler to calculate.

However, even when restricting V_2 to the simple subset of Fig. 17, the solution of the Dyson-Schwinger equations is highly nontrivial (see also Sec. 4.6). Let us suppose, however, that it can be

achieved. Then there is still the issue whether the propagators thus obtained obey the Ward identities. In general, this is not the case [123], and a cure of this problem would most likely require a self-consistent calculation of the three- and four-point functions on top of the two-point functions. An extension of the CJT formalism in this direction was proposed in Ref. [124], but since that work considers only scalar field theories, it is not clear whether this approach also applies to gauge theories in a way which preserves the Ward identities. Another question is the gauge invariance of the solution. Fortunately, as shown in Ref. [123], the gauge dependence always enters at an order which is higher than the truncation order. Finally, there is the issue of renormalizability. For scalar theories, renormalizability was demonstrated in Ref. [125]. For gauge theories, it still remains an open question.

In order to make progress, one has to simplify the solution of the problem. Instead of a completely self-consistent solution of the Dyson-Schwinger equations (109), as a first educated guess one might simply use the self-energies in the HTL (or HDL) approximation to compute the propagators entering the pressure (112). Since this approximation is independent of the choice of gauge, gauge invariance is not an issue anymore. There is also another advantage: since the HTL- (HDL-) approximated self-energies are just the high- T (high- μ) limit of the *one-loop* self-energies, Eqs. (113,114) for the entropy and quark number densities apply. These expressions are completely ultraviolet safe and thus do not require normalization. They are one-loop quantities and thus simpler to compute than the pressure which contains two-loop diagrams. From the entropy and quark number densities one can always deduce the pressure via an integration with respect to T and μ .

This approach has been followed in Ref. [126], where a detailed discussion of the results and their interpretation can be found. In particular, since the self-consistent approach is based on a partial resummation of a subset of perturbative diagrams, i.e., a reorganization of the perturbative series, it is possible to compare with standard perturbation theory (Sec. 4.1) by re-expanding the results in powers of g ; for more details, see Ref. [17, 126]. Here, I restrict myself to a discussion of one of the main results, namely the pressure for pure $[SU(3)]_c$ gauge theory as computed in this approach in comparison to lattice QCD data, cf. Fig. 18. One observes that the agreement at large temperatures is quite good, and that deviations occur only below $T \simeq 2.5 T_c$. The quality of reproducing lattice QCD data is comparable to that in the perturbative approach of Sec. 4.2. However, a distinct advantage of the self-consistent approximation scheme is that the physical interpretation of the results in terms of a gas of quasiparticles is much more appealing.

Note that a very similar approach has been pursued in Ref. [127], utilizing directly the expression (112) for the pressure, with propagators in the HTL approximation and a suitably modified V_2 . Another related approach is so-called “HTL-resummed perturbation theory” [128]. Here, the pressure of the pure gauge theory is computed to two-loop order with HTL-resummed propagators. A variational procedure like that of Ref. [130] is applied to determine the gluon mass parameter. The pressure computed from this approach is closer to the Stefan-Boltzmann limit and fails to agree with lattice QCD data in the region of temperatures from T_c to several times T_c , cf. Fig. 18. The reason for the differences between this approach and the one of Ref. [126] lies in the way the perturbative series is reorganized when resumming certain subsets of diagrams. The differences can be explained by re-expanding the results in powers of g [17]. Finally, note that HTL-resummed perturbation theory was also applied to one-loop order in a computation of the pressure at $T = 0$ and nonzero μ [131].

4.5 Polyakov-Loop Model

The pressure, normalized to the appropriate Stefan-Boltzmann limit, as a function of temperature, normalized to the appropriate critical temperature, shows a universal behavior, see right panel of Fig. 5. Since the normalized pressure for full QCD with dynamical fermions looks the same as for the

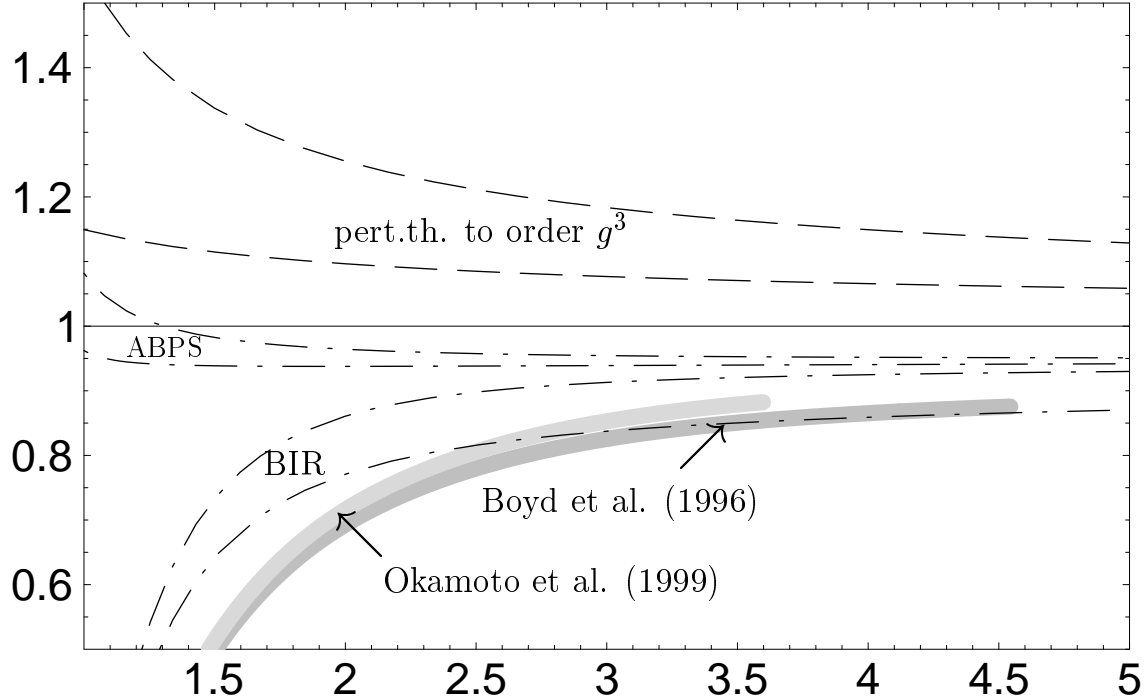


Figure 18: The pressure, normalized to the Stefan-Boltzmann limit, as a function of temperature, normalized to the critical temperature. Different resummation methods are compared to lattice QCD results for pure $[SU(3)_c]$ gauge theory. The band labelled ‘‘pert.th. to order g^3 ’’ is the order $O(g^3)$ perturbative result computed in Sec. 4.1 and shown in Fig. 13. The band labelled ‘‘ABPS’’ is the two-loop HTL-resummed pressure from Ref. [128]. The band labelled ‘‘BIR’’ is the result from Ref. [126]. Bands arise from varying the renormalization scale $\bar{\mu}$ within certain limits. Lattice data from Refs. [76, 129] are shown as grey bands.

pure gauge theory (i.e., without dynamical fermions), a natural conclusion would be to assume that the dynamics of the gluons drives the QCD phase transition, not that of the fermions. Consequently, the order parameter for the transition in full QCD should be the same as in the pure gauge theory, i.e., the Polyakov loop, see Sec. 2.3.2. For an $[SU(N_c)_c]$ gauge symmetry, the Polyakov loop (7) is invariant under $[SU(N_c)_c]$ gauge transformations, up to an element of the center of the gauge group, $Z(N_c)$, $L(\mathbf{x}) \rightarrow \exp(2\pi i/N_c) L(\mathbf{x})$. The effective theory for the Polyakov loop consists of all possible terms invariant under $Z(N_c)$ transformations [68],

$$\mathcal{L}_{\text{eff}} = c_0 |\nabla L|^2 + c_2 |L|^2 + c_3 [L^3 + (L^*)^3] - c_4 (|L|^2)^2 + \dots, \quad (115)$$

where the dots denote higher-order terms (which will be neglected in the following). For $N_c = 2$, one would have $c_3 = 0$, because L^3 is not $Z(2)$ -symmetric. For $N_c = 3$, it is precisely this cubic term which drives the transition first order [24], see also Sec. 2.3.2.

The ground state of the theory, $L_0 \equiv \langle L(\mathbf{x}) \rangle$ (which is assumed to be real), is determined by the global minimum of the effective potential

$$V_{\text{eff}}(L) = -c_2 |L|^2 - c_3 [L^3 + (L^*)^3] + c_4 (|L|^2)^2. \quad (116)$$

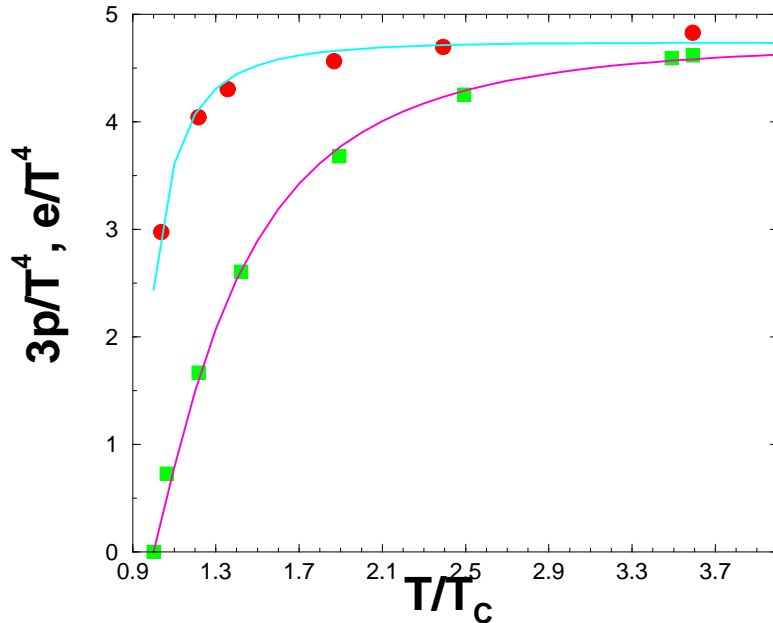


Figure 19: The functions $3p/T^4$ (lower curve) and ϵ/T^4 (upper curve) as a function of T/T_c . Fit of the thermodynamic functions of the Polyakov-loop model to lattice data (shown as circles and boxes) for the pure $[SU(3)_c]$ gauge theory.

The Polyakov loop L is dimensionless, therefore all coupling constants in Eq. (116) carry dimension [energy]⁴. Since the only dimensionful scale is set by the temperature, one may pull out a factor T^4 from the right-hand side of Eq. (116) and after appropriately renaming the constants write

$$V_{\text{eff}}(L) = b_4 T^4 \left\{ -b_2 |L|^2 - b_3 [L^3 + (L^*)^3] + (|L|^2)^2 \right\}, \quad (117)$$

where the new coupling constants are dimensionless. In order to have a potential that is bounded from below for large values of L , one has to assume $b_4 > 0$. For the moment take $b_3 = 0$ (for $N_c = 2$, $b_3 \equiv c_3/(b_4 T^4)$ must always vanish). Then the sign of b_2 drives the transition. Below the transition, $T < T_c$, there is confinement, which can only be achieved if the curvature of V_{eff} at the origin is positive, $b_2 < 0$, such that the global minimum is at $L_0 = 0$. Above the transition, $T > T_c$, there is deconfinement, which is achieved by a negative curvature of V_{eff} at the origin, $b_2 > 0$, giving rise to a nonvanishing $L_0 = \pm\sqrt{b_2/2}$. The constant b_2 is therefore a function of temperature, $b_2 = b_2(T)$, while in the simplest version of the Polyakov-loop model, b_3 and b_4 are assumed to be constant. Through the temperature dependence of b_2 , L_0 also becomes a function of temperature, $L_0 \equiv L_0(T)$. At $T = T_c$, one must have $b_2(T_c) = 0$, i.e., L_0 vanishes continuously at T_c , and one has a second-order phase transition. A nonvanishing b_3 (which is allowed for $N_c = 3$) turns this second-order transition into a first-order transition. Lattice QCD data indicate that the transition for pure $[SU(3)_c]$ gauge theory has a comparatively small latent heat, i.e., the transition is only *weakly* of first order. This suggests that the constant b_3 is small.

Now remember that the pressure is, up to sign, equal to the value of the effective potential at its minimum

$$\frac{p}{T^4} \equiv -\frac{V_{\text{eff}}(L_0)}{T^4} = \frac{b_4}{2} L_0^2 (b_2 + b_3 L_0). \quad (118)$$

For $N_c = 2$, where $b_3 = 0$, one has $p/T^4 = b_4 b_2(T)^2/4$, where the explicit value of L_0 was used. The physical interpretation of this result is quite astonishing: the pressure in QCD, as calculated on the lattice, cf. Fig. 5, is *not* determined by the *kinetic* energy of a gas of weakly interacting quasiparticles, as advocated in Secs. 4.3, 4.4, but is simply given by the *potential* for the Polyakov loop (at the respective minimum). All that one has to know is $L_0(T)$ (or, equivalently, $b_2(T)$, under the assumption that this is the only coupling constant which depends on temperature), and the pressure in QCD can be immediately computed from Eq. (118). Comparing Figs. 3 and 5, this conjecture is at least qualitatively correct. Quantitatively, it is not as simple: not only is the absolute value of L_0 as calculated on the lattice subject to renormalization, also the constants b_2, b_3 , and b_4 are not known. In the meantime, one can at least convince oneself that there are no principal obstacles for this interpretation: one may insert the value of L_0 (which is only a function of b_2 and b_3) into Eq. (118) and simply fit b_3, b_4 , as well as $b_2(T)$ to lattice QCD data. The result of this fit is $b_3 = 4/3$, $b_4 \simeq 0.1515$, $b_2(x) = 2(1 - 1.11/x)(1 + 0.265/x)^2(1 + 0.300/x)^3 - 0.974$, where $x \equiv T/T_c$. The pressure and the energy density obtained from this fit are shown in Fig. 19.

The Polyakov-loop model also allows to predict other physical observables, for instance, the ratio of screening masses related to the correlation function of the real and the imaginary part of the Polyakov loop [68]. Decompose the Polyakov loop into its real and imaginary part, $L \equiv R + iI$. In analogy to Eq. (43), the correlation functions for the real and imaginary part are then defined as $\langle R(0) R(\mathbf{x}) \rangle$ and $\langle I(0) I(\mathbf{x}) \rangle$, respectively. In the deconfined phase, one expects them to decrease exponentially with the distance,

$$\langle R(0) R(\mathbf{x}) \rangle \sim \exp(-m_R |\mathbf{x}|), \quad \langle I(0) I(\mathbf{x}) \rangle \sim \exp(-m_I |\mathbf{x}|), \quad (119)$$

where m_R, m_I are the corresponding screening masses. In weak coupling, one can make a definite prediction for these masses. To this end, expand L in powers of g to leading nontrivial order. One obtains $R \sim 1 - g^2/(T^2 N_c) \text{Tr} \mathcal{A}_0^2$. Thus, the correlation function for the real part involves the exchange of two static \mathcal{A}_0 fields, which are Debye screened. One therefore expects $\langle R(0) R(\mathbf{x}) \rangle \sim \exp(-2m_D |\mathbf{x}|)$. Analogously, $\langle I(0) I(\mathbf{x}) \rangle \sim \exp(-3m_D |\mathbf{x}|)$. Thus, the perturbative prediction for the screening masses is $m_R = 2m_D$, $m_I = 3m_D$, and $m_I/m_R = 3/2$.

In general, because of the renormalization of the Polyakov loop it is not as simple to obtain an answer for the absolute values of m_R and m_I . However, in the ratio m_I/m_R one expects unknown factors to cancel out [68]. The Polyakov-loop model makes a definite prediction for this ratio. First, write the potential (116) in terms of R and I . As usual, the curvature of the effective potential in the ground state provides the masses. Consequently, computing the curvature in R - and in I -direction, one obtains

$$m_R^2 \sim -b_2 - 6b_3 L_0 + 6L_0^2, \quad m_I^2 \sim -b_2 + 6b_3 L_0 + 2L_0^2. \quad (120)$$

I have refrained from writing the constant of proportionality, which also provides the correct dimension for $m_{R,I}$, because this constant will drop out anyway in the ratio m_I/m_R . Let us compute the ratio close to T_c . In the case of a first-order transition, at $T = T_c$ the effective potential V_{eff} has two minima, one at the origin and one at $L_0 \neq 0$, which are degenerate and separated by an energy barrier. The condition $V_{\text{eff}}(0) = V_{\text{eff}}(L_0)$ gives $L_0 = -b_2/b_3$, which together with the condition that L_0 is the nontrivial minimum of V_{eff} , $L_0^2 = (3b_3 L_0 + b_2)/2$, allows to express all quantities in Eq. (120) in terms of, say $b_3 L_0$. This yields $m_I/m_R = 3$. This value differs from the perturbative expectation by a factor of two, and is a definite prediction of the Polyakov-loop model which can be tested, for instance, on the lattice.

Another particularly appealing aspect of the Polyakov-loop model is that it correctly describes the behavior of the screening masses when approaching T_c from above, cf. Fig. 7. Near T_c , the temperature dependence of b_2 and L_0 cause the screening masses m_R, m_I to decrease, in agreement with lattice QCD

data. The fact that the perturbative prediction completely fails to reproduce this behavior was already mentioned in Sec. 3.4.

Finally, let us remark that the Polyakov-loop model may also naturally explain why the chiral symmetry restoration transition occurs at the same temperature as the deconfinement transition. There is nothing to prevent the effective theory (115) from having a term $\sim c|L|^2 \text{Tr } \Phi^\dagger \Phi$, where Φ is the chiral condensate and $c > 0$ a constant. Thus, when $|L|$ condenses (in the deconfined phase), this term suppresses condensation of Φ on account of the positive coupling constant c , effectively restoring the chiral symmetry. Thus, chiral symmetry restoration and deconfinement occur at the same temperature.

4.6 Linear Sigma Models with Hadronic Degrees of Freedom

In Sec. 3.2 we have seen that the QCD transition is most likely crossover for small values of the chemical potential μ . Therefore, there is no real distinction between hadronic degrees of freedom on the one side and quark and gluon degrees of freedom on the other side of the transition. Consequently, there is no compelling reason why the thermodynamic properties of QCD around the phase transition should be described in terms of quarks and gluons; a hadronic description should be equally adequate.

Let us assume that, somewhat contrary to the idea behind the Polyakov-loop model discussed in Sec. 4.5, the QCD transition is driven by chiral symmetry restoration instead of deconfinement. In this case, the order parameter for the transition is the chiral condensate, see Sec. 2.3.3, and the effective theory is given by the linear sigma model (13). The degrees of freedom in this effective theory are the fluctuations of the order parameter field Φ around the ground state, $\langle \Phi \rangle$. Physically, these fluctuations correspond to the scalar and pseudoscalar mesons. Following the above line of arguments, this effective theory could therefore not only serve to understand the dynamics of chiral symmetry restoration, it could equally well be used to describe the thermodynamic properties of QCD around the phase transition.

Of particular interest is the question how chiral symmetry restoration is exhibited in the meson mass spectrum. In the framework of lattice QCD, this was discussed in Sec. 3.5. Here, I explain how to answer this question using the effective theory (13) at nonzero temperature. The standard definition of a particle mass is via the pole of the propagator at zero momentum. Consequently, the goal is to determine the mesonic propagators. The method of choice is obviously the CJT formalism discussed in Sec. 4.4.3, because this approach allows to compute the full propagator from the stationary points of the effective action Γ , cf. Eq. (108), or in other words, from the Dyson-Schwinger equations (109). Of course, the solution of these equations requires Γ_2 , i.e., the complete set of 2PI diagrams. For practical purposes, a solution of the Dyson-Schwinger equations is therefore impossible. However, as already discussed in Sec. 4.4.3, one may truncate Γ_2 at some given order. Such a truncation defines a many-body approximation, within which a solution of the Dyson-Schwinger equations becomes feasible.

The most simple, nontrivial truncation of Γ_2 is to include only the set of double-bubble diagrams shown on the left in Fig. 20. The self-energies (110) computed from these diagrams consist only of the tadpole diagrams shown on the right-hand side of Fig. 20. This is the well-known Hartree approximation [106]. In general, all particle species in a particular effective theory contribute via tadpole diagrams to the self-energy of a given particle species. Since the tadpole diagrams do not have any dependence on the external momentum, the self-energies are (temperature-dependent) constants in the Hartree approximation. They simply shift the meson masses as compared to their vacuum values. In principle, the Dyson-Schwinger equations (109) for the propagators are coupled integral equations, but in the Hartree approximation, they reduce to a system of coupled fix-point equations for the meson masses. While numerically much simpler than solving integral equations, the solution can still be a formidable task, if the underlying chiral symmetry group is large. For an $O(4)$ chiral symmetry, this problem was solved in Refs. [132, 133]. The $U(3)_r \times U(3)_\ell$ case was discussed in Ref. [134]. The cases $U(2)_r \times U(2)_\ell$

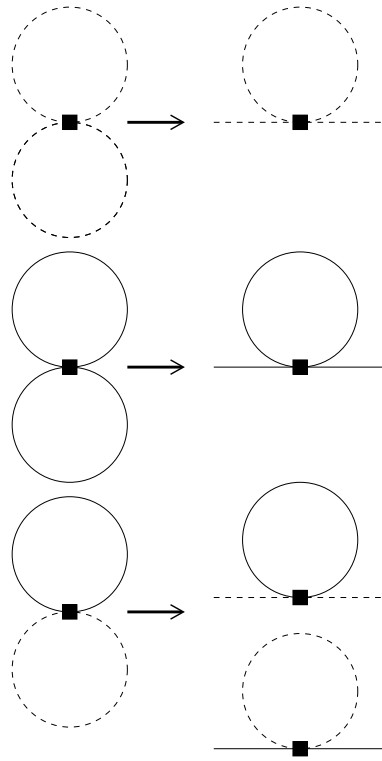


Figure 20: Double-bubble diagrams (left-hand side), where full lines denote scalar mesons and dashed lines denote pseudoscalar mesons. Cutting the bubbles produces the tadpole-diagram contributions to the self-energies shown on the right-hand side. The tadpole diagrams constitute the so-called Hartree approximation.

as well as $U(4)_r \times U(4)_\ell$ were investigated in Ref. [135]. (The $U(1)_V$ of baryon number is always trivially respected in these models, cf. the discussion in Sec. 2.3.3. Nevertheless, in order to simplify the notation I include it in characterizing the symmetry of a particular chiral effective theory.)

In Fig. 21 the masses for the scalar and pseudoscalar mesons are shown as a function of temperature, calculated within the framework of linear sigma models with $O(4)$, $U(2)_r \times U(2)_\ell$, $U(3)_r \times U(3)_\ell$, and $U(4)_r \times U(4)_\ell$ chiral symmetry. The different subpanels show the masses of the respective chiral partners. In the non-strange sector, these are (a) the σ meson and the pion, and (b) the a_0 and the η meson. In the strange sector, these are (c) the κ meson and the kaon, and (d) the f_0 and the η' meson. Finally, in the charmed meson sector one has (e) the scalar D_0 and D_{s0} meson and the pseudoscalar D and D_s meson, and (f) the η_c and χ_{c0} meson. One observes that in all cases the chiral transition occurs at temperatures of the order of 200 – 300 MeV. For the results shown in Fig. 21 realistic, nonzero values for the quark masses were assumed, and consequently the transition is crossover, cf. the discussion in Sec. 2.3.4. Figure 21 also allows to compare the results for models with different chiral symmetry. For instance, Fig. 21 (a) nicely demonstrates the effect of enlarging the symmetry group. In general, the higher the symmetry, the more particle species contribute via tadpole diagrams to the mass of a particular species, and consequently the larger is its mass at a given temperature. Furthermore, one can learn from all subpanels that the difference between the $U(3)_r \times U(3)_\ell$ and the $U(4)_r \times U(4)_\ell$ model is at best marginal. The reason is that the additional charmed meson degrees of freedom in the latter are so heavy that the contribution of the respective tadpole diagrams is exponentially suppressed

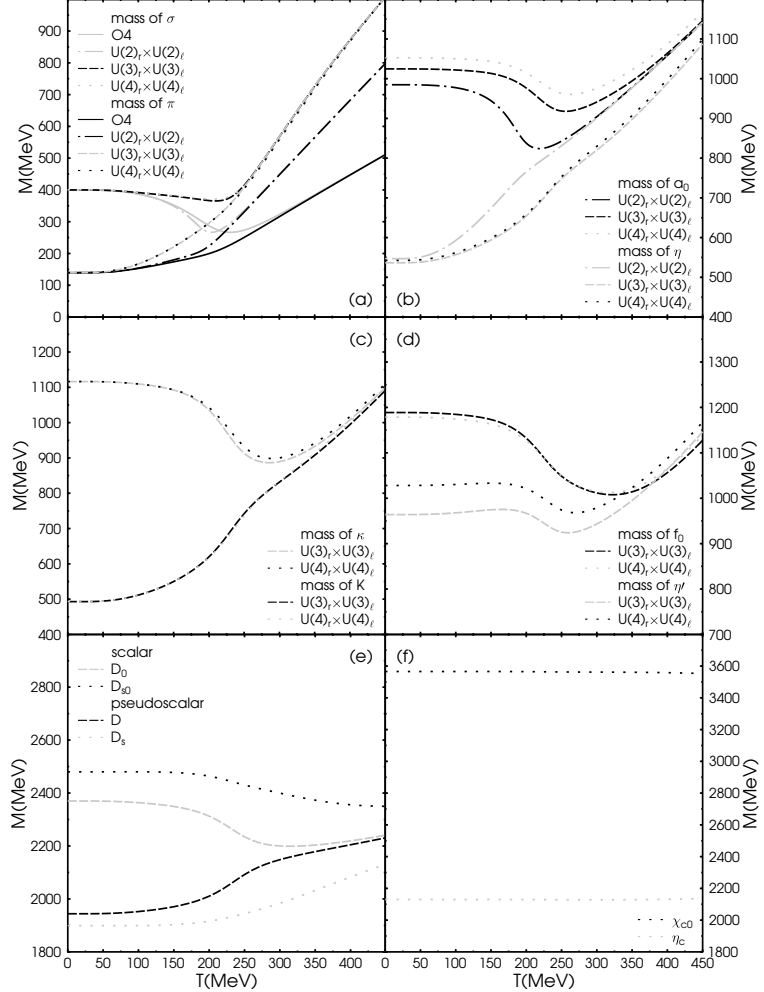


Figure 21: Scalar and pseudoscalar meson masses as a function of temperature in the Hartree approximation, for effective theories models with different chiral symmetry: $O(4)$, $U(2)_r \times U(2)_l$, $U(3)_r \times U(3)_l$, and $U(4)_r \times U(4)_l$. Chiral partners are shown in the same panel to demonstrate that their masses become degenerate at high temperature. From Ref. [135].

$\sim \exp(-m/T)$. Consequently, they only minimally influence the behavior of the non-charmed mesons in the temperature range considered here. In turn, in this temperature range the charmed meson masses change little from their vacuum values, cf. Fig. 21 (e), (f).

Lattice QCD calculation cannot be done in the chiral limit, because as the quark mass decreases, the computation of the fermion determinant becomes more and more difficult. The only way to make predictions about the chiral limit is to extrapolate data obtained for nonzero quark masses. This is computationally expensive, as it requires calculations at several different values of the quark mass. In contrast, in the framework of linear sigma models, taking the chiral limit actually simplifies the calculation. A comparison between quantities computed in lattice QCD and extrapolated to the chiral limit with the corresponding values obtained in linear sigma models is therefore straightforward. Let us discuss two examples. The first is the critical temperature for the chiral transition. The way to identify the critical temperature is the following. For a first-order phase transition, look for the temperature where two minima of the effective potential become degenerate. For a second-order transition, the criterion is a vanishing second derivative of the potential in one direction in order parameter space (indicating a massless degree of freedom and critical behavior). It should be mentioned that the Hartree approx-

Table 3: The critical temperature T_c for the chiral transition, computed for various chiral effective theories in the chiral limit with and without $U(1)_A$ anomaly [135], in comparison to results from lattice QCD, extrapolated to the chiral limit. For $N_f = 2$ flavors, the QCD results for Wilson and Kogut-Susskind fermions from Table 2 have been averaged, assuming uncorrelated statistical errors.

Chiral model	T_c with $U(1)_A$ anomaly	T_c without $U(1)_A$ anomaly	LQCD
$O(4)$	(159.5 ± 0.2) MeV	N/A	(172 ± 9) MeV
$U(2)_r \times U(2)_\ell$	(154.5 ± 0.2) MeV	(149.2 ± 0.2) MeV	(172 ± 9) MeV
$U(3)_r \times U(3)_\ell$	(165.5 ± 0.2) MeV	(147.5 ± 0.2) MeV	(154 ± 8) MeV

imation does not always reproduce the correct order of the transition as predicted from universality arguments. (Aside from that, being a mean-field type approximation, it always fails to predict the correct critical exponents.) For instance, for the $O(4)$ model and the $U(2)_r \times U(2)_\ell$ model with $U(1)_A$ anomaly, the transition should be of second order, but the Hartree approximation predicts a first-order transition. For the $U(2)_r \times U(2)_\ell$ model without $U(1)_A$ anomaly, as well as for the $U(N_f)_r \times U(N_f)_\ell$ models with $N_f \geq 3$, the Hartree approximation predicts a first-order transition in agreement with universality arguments. In chiral effective theories, one can simply “switch off” the $U(1)_A$ anomaly by setting the constant $c = 0$ in Eq. (14). This is not possible for lattice QCD: the $U(1)_A$ anomaly may or may not be present, depending on how strongly instantons are screened at T_c . This question has been studied on the lattice [136], with the result that the $U(1)_A$ anomaly is not completely absent at the critical temperature, but at least rapidly decreasing.

The critical temperatures obtained in various chiral models, with and without the $U(1)_A$ anomaly, are shown in Table 3 in comparison to the results from lattice QCD, cf. Table 2. Two things are noteworthy. First, the values of the critical temperature obtained in chiral models are rather close to the ones computed in lattice QCD. This is surprising given the fact that chiral effective theories only contain a certain subset of the degrees of freedom of full QCD, do not describe confinement, and moreover are treated here in the framework of a very simple many-body approximation. Second, the ordering of the critical temperatures as a function of quark flavors is the same in lattice QCD and chiral models *without* $U(1)_A$ anomaly, but the opposite in chiral models *with* $U(1)_A$ anomaly. This also lends support to the above mentioned results [136] regarding the rapid decrease of the $U(1)_A$ anomaly near T_c .

The second example is the investigation of the quark-mass diagram. Figure 22 shows this diagram as determined within a $U(3)_r \times U(3)_\ell$ linear sigma model [137]. Of course, the linear sigma model does not have quark degrees of freedom. Nonzero quark masses correspond to a term of the form (15) in the Lagrangian, where the matrix H is proportional to the quark mass matrix. Since the vacuum expectation value of Φ is a diagonal matrix, the matrix H must also be diagonal. If one assumes $SU(2)_V$ isospin symmetry, $H = h_0 T_0 + h_8 T_8$. Consequently, $m_q = a(h_0 + h_8/\sqrt{2})$, $m_s = b(h_0 - \sqrt{2}h_8)$. The fields h_0 , h_8 can be determined from the vacuum values for the pion and kaon masses, as well as the pion and kaon decay constants. Then, setting $m_q = 10$ MeV, $m_s = 150$ MeV fixes the values for the

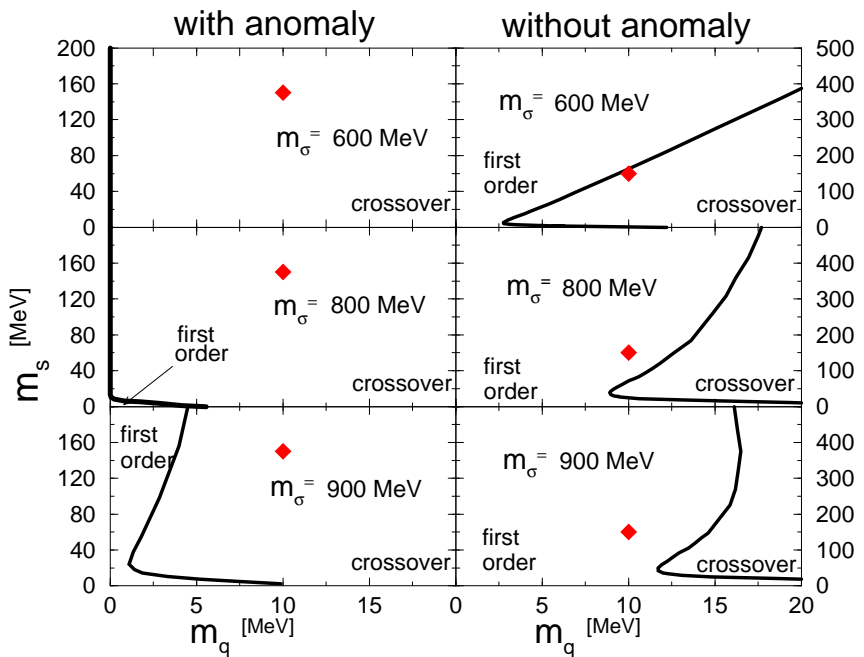


Figure 22: The quark-mass diagram computed in a $U(3)_r \times U(3)_\ell$ chiral model [137], with or without $U(1)_A$ anomaly for different values of the σ meson mass in vacuum. The physical point $(m_q, m_s) = (10, 150)$ MeV is shown as a diamond.

constants of proportionality a and b ; for details see Ref. [137].

One observes in Fig. 22 that the position of the line of second-order phase transitions between the first-order region around the origin and the crossover region depends sensitively on the value of the σ meson mass in vacuum. However, the physical point is always in the crossover region, if the $U(1)_A$ anomaly is present. Without the $U(1)_A$ anomaly, the transition could be of first order, if the σ meson is sufficiently heavy.

Recently, there have been attempts to go beyond the Hartree approximation by including diagrams with more complicated topologies in Γ_2 [125, 138]. In this case, a self-consistent calculation becomes technically rather difficult, because these topologies lead to momentum-dependent self-energies, so that the Dyson-Schwinger equations turn from simple fix-point equations for the masses into integral equations for the full propagators. Moreover, momentum-dependent self-energies have in general nonzero imaginary parts, such that quasiparticles, which are stable in the Hartree approximation, develop a finite decay width. The spectral density carries the complete information of the spectral properties of the quasiparticles in the system. It is therefore natural to solve the Dyson-Schwinger equations for the full propagators as self-consistency equations for the respective spectral densities. Work in this direction is in progress [139].

5 Color Superconductivity

5.1 Derivation of the Gap Equation

As discussed in Sec. 2.4.3, there is compelling evidence that quark matter at high density and sufficiently low temperature is a color superconductor [37, 38]. While the color quantum numbers of a Cooper pair

are determined by the attractive gluon interaction in the color-antitriplet channel, there are still many different ways to combine flavor and spin quantum numbers, giving rise to a plethora of possible color-superconducting phases. In general, the energetically most favorable phase will prevail at a given T and μ . In order to decide which is the most favorable phase one has to compute the gain in condensation energy when forming Cooper pairs. To this end, one has to calculate the color-superconducting gap parameter. In general, the larger the gap, and the more degrees of freedom participate in forming Cooper pairs, the larger the gain condensation energy. The gap is computed from a so-called *gap equation*. In this section, I shall outline the derivation of this equation.

Consider the QCD action

$$S \equiv S_A + S_F + g \int_X \bar{\psi}(X) \gamma^\mu T_a \psi(X) A_\mu^a(X) , \quad (121)$$

where S_A is the gauge field action (including ghost and gauge fixing contributions) and

$$S_F = \int_X \bar{\psi}(X) (i\gamma \cdot \partial_X + \mu\gamma_0 - m) \psi(X) \quad (122)$$

is the action for non-interacting fermion fields in the presence of a chemical potential. For reasons which will become clear in the following, S_F and the quark-gluon coupling is rewritten in terms of ordinary quark fields, $\bar{\psi}$, ψ , and their *charge-conjugate* counterparts, $\bar{\psi}_C \equiv \psi^T C$, $\psi_C \equiv C \bar{\psi}^T$, where $C \equiv i\gamma^2\gamma_0$ is the charge conjugation matrix. To this end, introduce the so-called Nambu-Gor'kov basis, with the $2 \cdot 4 N_c N_f$ -dimensional quark spinors

$$\Psi \equiv \begin{pmatrix} \psi \\ \psi_C \end{pmatrix} , \quad \bar{\Psi} \equiv (\bar{\psi}, \bar{\psi}_C) . \quad (123)$$

For the fermion action one then obtains

$$S_F = \frac{1}{2} \int_{X,Y} \bar{\Psi}(X) \mathcal{S}_0^{-1}(X, Y) \Psi(Y) , \quad (124)$$

where

$$\mathcal{S}_0^{-1} \equiv \begin{pmatrix} [G_0^+]^{-1} & 0 \\ 0 & [G_0^-]^{-1} \end{pmatrix} , \quad [G_0^\pm]^{-1}(X, Y) \equiv -i(i\gamma \cdot \partial_X \pm \mu\gamma_0 - m) \delta^{(4)}(X - Y) , \quad (125)$$

is the free inverse fermion propagator in the Nambu-Gor'kov basis. The quark-gluon coupling becomes

$$\bar{\psi}(X) \gamma^\mu T_a \psi(X) A_\mu^a(X) = \frac{1}{2} \bar{\Psi}(X) \Gamma_a^\mu \Psi(X) A_\mu^a(X) , \quad (126)$$

where

$$\Gamma_a^\mu \equiv \begin{pmatrix} \gamma^\mu T_a & 0 \\ 0 & -\gamma^\mu T_a^T \end{pmatrix} \quad (127)$$

is the Nambu-Gor'kov matrix which couples the corresponding quark spinors to gluon fields.

Now add a bilocal source term to the QCD action,

$$S[\mathcal{K}] \equiv S + \int_{X,Y} \bar{\Psi}(X) \mathcal{K}(X, Y) \Psi(Y) , \quad (128)$$

where, in the Nambu-Gor'kov basis,

$$\mathcal{K} \equiv \begin{pmatrix} \sigma^+ & \varphi^- \\ \varphi^+ & \sigma^- \end{pmatrix} . \quad (129)$$

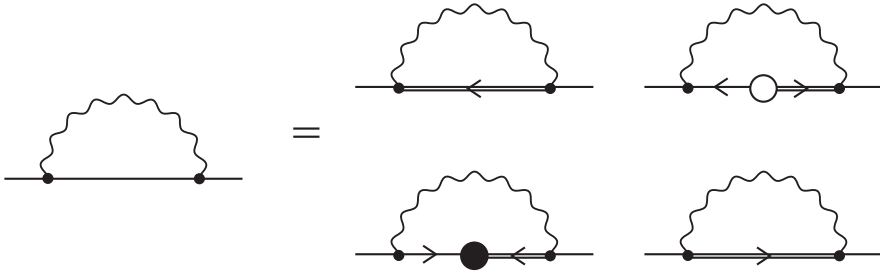


Figure 23: The quark self-energy. Writing out the individual components in the Nambu-Gor'kov basis one obtains the diagrams on the right-hand side.

Here, σ^+ and σ^- are sources which couple to adjoint quark spinors and quark spinors, while φ^+ couples to two quark spinors (remember that $\bar{\psi}_C \sim \psi^T$) and φ^- couples to two adjoint quark spinors, respectively ($\psi_C \sim \bar{\psi}^T$). Charge-conjugation invariance of the action relates the sources σ^+ and σ^- : $\sigma^- \equiv C[\sigma^+]^\dagger C^{-1}$. The action must also be real-valued, which leads to the condition $\varphi^- \equiv \gamma_0[\varphi^+]^\dagger \gamma_0$.

The next step is to derive the effective action from the partition function of QCD in the presence of the external source \mathcal{K} ,

$$\mathcal{Z}[\mathcal{K}] = \int \mathcal{D}A_\mu^a \mathcal{D}\bar{\Psi} \mathcal{D}\Psi \exp S[\mathcal{K}] . \quad (130)$$

The details of this derivation are beyond the scope of this review, but the interested reader can readily convince himself that, in the presence of bilocal sources, this problem is solved precisely by the CJT formalism [120] discussed in Sec. 4.4.3. Consequently, if one takes into account that in the present case there is no nonvanishing expectation value for a one-point function, and if one adapts Eq. (106) to the notation of this section, the effective action reads

$$\Gamma[\Delta, \mathcal{S}] = -\frac{1}{2} \text{Tr} \ln \Delta^{-1} - \frac{1}{2} \text{Tr} (\Delta_0^{-1} \Delta - 1) + \text{Tr} \ln \mathcal{S}^{-1} + \text{Tr} (\mathcal{S}_0^{-1} \mathcal{S} - 1) + \Gamma_2[\Delta, \mathcal{S}] , \quad (131)$$

where Δ_0 is the free and Δ the full gluon propagator, and \mathcal{S} is the full fermion propagator in the Nambu-Gor'kov basis. The full propagators for the physical situation (where $\mathcal{K} = 0$) are obtained from the stationarity conditions (108). These conditions are Dyson-Schwinger equations of the type (109),

$$\Delta^{-1} = \Delta_0^{-1} + \Pi , \quad \mathcal{S}^{-1} = \mathcal{S}_0^{-1} + \Sigma . \quad (132)$$

(In a slight abuse of notation, we also denote the full gluon propagator at the stationary point of $\Gamma[\Delta, \mathcal{S}]$ by Δ and, similarly, the full quark propagator by \mathcal{S} .)

In order to proceed one has to make an approximation for Γ_2 . As in Sec. 4.4.3, the discussion will be restricted to the set of diagrams shown in Fig. 17, however, with the quark propagators in the quark loop now given by the Nambu-Gor'kov propagator \mathcal{S} . The gluon self-energy is computed as $\Pi = -2 \delta \Gamma_2 / \delta \Delta$, i.e., by cutting a gluon line in the diagrams of Fig. 17. Thus, Π is given by the diagrams shown in Fig. 15 (with Nambu-Gor'kov propagators \mathcal{S} in the quark loop). The quark self-energy in the Nambu-Gor'kov basis is

$$\Sigma \equiv \begin{pmatrix} \Sigma^+ & \Phi^- \\ \Phi^+ & \Sigma^- \end{pmatrix} \equiv \frac{\delta \Gamma_2[\Delta, \mathcal{S}]}{\delta \mathcal{S}} . \quad (133)$$

It is given by the diagram shown on the left-hand side in Fig. 23. The diagonal components Σ^\pm correspond to the ordinary self-energies for particles and charge-conjugate particles. In space-time, $\Sigma^+(X, Y)$ ($\Sigma^-(X, Y)$) has a particle (charge-conjugate particle) entering at X and another particle

(charge-conjugate particle) emerging at Y . On the other hand, the off-diagonal components Φ^\pm have to be interpreted as follows: a particle (charge-conjugate particle) enters $\Phi^+(X, Y)$ ($\Phi^-(X, Y)$) at X and a *charge-conjugate particle* (an *ordinary particle*) emerges at Y . This is typical for systems with a fermion-fermion condensate in the ground state [106]. The self-energies Φ^\pm symbolize this condensate. Note that the two off-diagonal components are related in the same way as the bilocal sources φ^\pm in Eq. (129), i.e., $\Phi^- \equiv \gamma_0 [\Phi^+]^\dagger \gamma_0$. In the following, also the term *gap matrix* will be used for Φ^+ .

In momentum space, the self-energy is given by

$$\Sigma(K) = -g^2 \int_Q \Gamma_a^\mu \mathcal{S}(Q) \Gamma_b^\nu \Delta_{\mu\nu}^{ab}(K - Q) . \quad (134)$$

This equation can be decomposed in terms of its Nambu-Gor'kov components. To this end, let us first determine the full Nambu-Gor'kov quark propagator by formally inverting the Dyson-Schwinger equation (132) for the quark propagator [140],

$$\mathcal{S} = \begin{pmatrix} G^+ & \Xi^- \\ \Xi^+ & G^- \end{pmatrix} , \quad (135)$$

where

$$G^\pm \equiv \left\{ [G_0^\pm]^{-1} + \Sigma^\pm - \Phi^\mp \left([G_0^\mp]^{-1} + \Sigma^\mp \right)^{-1} \Phi^\pm \right\}^{-1} , \quad (136)$$

$$\Xi^\pm \equiv - \left([G_0^\mp]^{-1} + \Sigma^\mp \right)^{-1} \Phi^\pm G^\pm . \quad (137)$$

Here G^+ (G^-) is the propagator for quasiparticles (charge-conjugate quasiparticles). Besides these quantities describing the ordinary propagation of quasiparticles, there are also off-diagonal, or “anomalous” propagators Ξ^\pm in Eq. (135). These anomalous propagators are typical for superconducting systems [106] and account for the possibility that in the presence of a Cooper-pair condensate, symbolized by Φ^\pm , a fermion can always be absorbed in the condensate, while its charge-conjugate counterpart is emitted from the condensate and continues to propagate.

In terms of its Nambu-Gor'kov components, the quark self-energy is

$$\Sigma^+(K) = -g^2 \int_Q \gamma^\mu T_a G^+(Q) \gamma^\nu T_b \Delta_{\mu\nu}^{ab}(K - Q) , \quad (138)$$

$$\Sigma^-(K) = -g^2 \int_Q \gamma^\mu T_a^T G^-(Q) \gamma^\nu T_b^T \Delta_{\mu\nu}^{ab}(K - Q) , \quad (139)$$

$$\Phi^+(K) = g^2 \int_Q \gamma^\mu T_a^T \Xi^+(Q) \gamma^\nu T_b \Delta_{\mu\nu}^{ab}(K - Q) , \quad (140)$$

$$\Phi^-(K) = g^2 \int_Q \gamma^\mu T_a \Xi^-(Q) \gamma^\nu T_b^T \Delta_{\mu\nu}^{ab}(K - Q) . \quad (141)$$

The integrals in these equations are shown diagrammatically on the right-hand side of Fig. 23. In these diagrams, a normal full propagator G^+ (G^-) is denoted as a double line with an arrow pointing to the left (right). According to Eq. (137), the anomalous propagators Ξ^+ and Ξ^- consist of a combination of propagators $\left([G_0^\pm]^{-1} + \Sigma^\pm \right)^{-1}$, gap matrices Φ^\pm , and full propagators G^\pm . This combination is explicitly drawn on the right-hand side of Fig. 23, with propagators $\left([G_0^\pm]^{-1} + \Sigma^\pm \right)^{-1}$ as single lines with arrows pointing left/right, and gap matrices Φ^\pm as full/empty circles. Inserting these self-energies (and the corresponding one for the gluons) into the Dyson-Schwinger equations (132) one obtains a coupled set of integral equations which has to be solved self-consistently. In particular, the Dyson-Schwinger

equations for the off-diagonal components Φ^\pm of the inverse propagator \mathcal{S}^{-1} , i.e., Eqs. (140) and (141), are the *gap equations* for the color-superconducting condensate.

A completely self-consistent solution of the Dyson-Schwinger equations is technically too difficult to be feasible, and one has to make certain approximations. It turns out that in weak coupling a well-controlled, approximate solution is possible. This will be demonstrated in Sec. 5.3. Prior to that, I shall discuss the excitation spectrum in a superconductor, which follows from the poles of the quark propagator (135).

5.2 Excitation spectrum

In order to find the quasiparticle excitations, one has to determine the poles of G^\pm and Ξ^\pm . For an arbitrary quark mass m , this is a formidable task, see Ref. [141]. For our purpose it is sufficient to consider the ultrarelativistic limit, $m = 0$, where the situation simplifies considerably [142]. Let us also focus exclusively on G^+ ; the poles of G^- and Ξ^\pm can be determined accordingly (in fact, they have precisely the same poles). In order to proceed, we need to specify the color, flavor, and Dirac structure of the inverse free propagators $[G_0^\pm]^{-1}$, and of the self-energies Σ^\pm and Φ^\pm . The inverse propagators $[G_0^\pm]^{-1}$ are diagonal in color and flavor space. To determine the Dirac structure, it is convenient to Fourier transform them into energy-momentum space and then to expand them in terms of projectors onto states of positive or negative energies, $\Lambda_{\mathbf{k}}^e \equiv (1 + e \gamma_0 \boldsymbol{\gamma} \cdot \mathbf{k})/2$, $e = \pm$,

$$[G_0^\pm]^{-1}(K) = \boldsymbol{\gamma} \cdot K \pm \mu \gamma_0 = \gamma_0 \sum_{e=\pm} [k_0 - (ek \mp \mu)] \Lambda_{\mathbf{k}}^e. \quad (142)$$

For the weak-coupling solution discussed in Sec. 5.3 it turns out that it suffices to compute the self-energies Σ^\pm neglecting effects from the breaking of the $[SU(3)_c]$ color symmetry due to condensation of Cooper pairs. Then, the self-energies are diagonal in color and flavor space, and one only needs to know their Dirac structure. One may expand them in terms of Dirac matrices,

$$\Sigma^\pm = s_0^\pm \gamma^0 + \mathbf{s}^\pm \cdot \boldsymbol{\gamma} + \dots. \quad (143)$$

Other Dirac structures are simply abbreviated by dots. It turns out that, in weak coupling, the dominant contribution to the quark self-energy arises from the exchange of almost static (i.e., Landau-damped) magnetic gluons and, in momentum space, is [143]

$$\Sigma^+(K) = \Sigma^-(K) \simeq \gamma_0 \bar{g}^2 \left(k_0 \ln \frac{M^2}{k_0^2} + i\pi |k_0| \right), \quad (144)$$

where $\bar{g} \equiv g/(3\sqrt{2}\pi)$ and $M^2 \equiv (3\pi/4)m_g^2$. The imaginary part gives rise to a finite lifetime of quasiparticle excitations off the Fermi surface [140], but in weak coupling this contributes to the color-superconducting gap only at sub-subleading order. (How to count orders in weak coupling will be discussed in detail in Sec. 5.3). There are other contributions at sub-subleading order which have not been reliably computed so far. Only the subleading order terms are under complete analytic control. They determine the prefactor of the color-superconducting gap to order $O(1)$. The sub-subleading contributions contribute to the prefactor at order $O(g)$. Therefore, in the following the imaginary part will be neglected and only the real part will be kept, which, for $\ln(M/k_0) \sim 1/g$ contributes at subleading order to the color-superconducting gap [144]. Defining the wave function renormalization factor

$$Z(k_0) \equiv \left(1 + \bar{g}^2 \ln \frac{M^2}{k_0^2} \right)^{-1}, \quad (145)$$

Table 4: The structure of the matrices $\mathcal{M}_\mathbf{k}$ and $L_\mathbf{k}$ in various color-superconducting phases, $(\tau_2)^{fg} \equiv i\epsilon^{fg}$, $(J_k)_{ij} \equiv -i\epsilon_{ijk}$, $(I^h)^{fg} \equiv -i\epsilon^{fgh}$, and $\boldsymbol{\gamma}_\perp(\mathbf{k}) \equiv \boldsymbol{\gamma} - \boldsymbol{\gamma} \cdot \mathbf{k} \mathbf{k}$. For the matrix $L_\mathbf{k}$ in the CSL phase, the second term is a matrix in color space, formed by the dyadic product of the two vectors $\hat{\mathbf{k}} + \boldsymbol{\gamma}_\perp(\mathbf{k})$ and $\hat{\mathbf{k}} - \boldsymbol{\gamma}_\perp(\mathbf{k})$, and a matrix in Dirac space, formed by the product of the two $\boldsymbol{\gamma}_\perp(\mathbf{k})$ matrices. The last two columns show the two eigenvalues λ_r of $L_\mathbf{k}$ and their degeneracy d_r (counting color-flavor degrees of freedom in the 2SC and CFL phases, and color-Dirac degrees of freedom in the two spin-one phases).

phase	$\mathcal{M}_\mathbf{k}$	$L_\mathbf{k}$	$\lambda_1 (d_1)$	$\lambda_2 (d_2)$
2SC	$\gamma_5 \tau_2 J_3$	$(J_3)^2 (\tau_2)^2$	1 (4)	0 (2)
CFL	$\gamma_5 \mathbf{I} \cdot \mathbf{J}$	$(\mathbf{I} \cdot \mathbf{J})^2$	4 (8)	1 (1)
CSL	$\mathbf{J} \cdot [\hat{\mathbf{k}} + \boldsymbol{\gamma}_\perp(\mathbf{k})]$	$\mathbf{1} + [\hat{\mathbf{k}} + \boldsymbol{\gamma}_\perp(\mathbf{k})] [\hat{\mathbf{k}} - \boldsymbol{\gamma}_\perp(\mathbf{k})]$	4 (4)	1 (8)
polar	$J^3 [\hat{k}^z + \gamma_\perp^z(\mathbf{k})]$	$(J_3)^2$	1 (8)	0 (4)

the effect of the quark self-energy is to shift the poles in the propagator, $k_0 \rightarrow k_0/Z(k_0)$. Note that the logarithm renders a normal-conducting system a non-Fermi liquid [145].

The color, flavor, and Dirac structure of the off-diagonal self-energies Φ^\pm is less trivial. As they symbolize the Cooper-pair condensate, they must have the quantum numbers of the particular channel where condensation occurs. For the purpose of illustration, I specify this structure for the four color-superconducting phases already discussed in Sec. 2.4.3. Let us furthermore only consider parity-even spin-zero and spin-one condensates. In this case, one may expand the gap matrix Φ^+ (in momentum space) as follows [49],

$$\Phi^+(K) = \sum_{e=\pm} \phi^e(K) \mathcal{M}_\mathbf{k} \Lambda_\mathbf{k}^e, \quad (146)$$

where ϕ^e , the so-called *gap function*, is a scalar function of 4-momentum and $\mathcal{M}_\mathbf{k}$ is a matrix in color, flavor, and Dirac space, which is determined by the symmetries of the color-superconducting order parameter (cf. Sec. 2.4.3). An important property is that it commutes with the energy projectors, $[\mathcal{M}_\mathbf{k}, \Lambda_\mathbf{k}^e] = 0$.

In Table 4 the explicit expressions for $\mathcal{M}_\mathbf{k}$ are listed for the four phases considered here. For these expressions, I have used the fact that a color antitriplet is totally antisymmetric and thus has a representation in terms of the antisymmetric Gell-Mann matrices λ_2 , λ_5 , and λ_7 . These Gell-Mann matrices form an $SO(3)$ subgroup of $SU(3)$, and are thus identical to the generators of $SO(3)$, $(J_1, J_2, J_3) \equiv \mathbf{J}$. These matrices were finally used in Table 4 to parametrize that the gap matrix Φ^+ is a color-antitriplet. Similarly, τ_2 (the only Pauli matrix which is antisymmetric) symbolizes that the gap in the 2SC phase is a flavor singlet. The Dirac matrix γ_5 in the 2SC and CFL cases is necessary to obtain even parity. For the CFL case, the flavor-antitriplet nature is represented by another set of generators $(I^1, I^2, I^3) \equiv \mathbf{I}$ of $SO(3)$. Color-flavor locking is obtained by a scalar product of \mathbf{I} with \mathbf{J} , cf. also Table 1. For the two spin-one phases, the CSL phase and the polar phase, the order parameter is a 3-vector, see Sec. 2.4.3,

but the gap matrix is a scalar. This requires it to be proportional to a scalar product of the order parameter with another 3-vector. There are only two other 3-vectors (in momentum space), the direction of momentum of the quark in the Cooper pair, $\hat{\mathbf{k}}$, and the vector γ . Consequently, Φ^+ has to be proportional to a linear combination of these two 3-vectors. It is convenient [39] to use the projection of γ onto the subspace orthogonal to $\hat{\mathbf{k}}$, $\gamma_{\perp}(\mathbf{k})$, because then $\mathcal{M}_{\mathbf{k}}$ commutes with the energy projectors. Finally, color-spin locking requires a scalar product of \mathbf{J} with this linear combination of 3-vectors. In the polar phase, one may independently choose a direction for the gap in color space and in space-time. Conveniently, one chooses the 3- (anti-blue) direction in color space and the z -direction in space-time.

In order to proceed, however, one does not require the explicit form of $\mathcal{M}_{\mathbf{k}}$ in the various phases. The existence of the decomposition (146) and the commutation property of $\mathcal{M}_{\mathbf{k}}$ with the energy projectors is sufficient to derive the quasiparticle spectrum as a function of the absolute magnitude of the gap function, $|\phi^e(K)|$. To see this, compute $\Phi^- \equiv \gamma_0 [\Phi^+]^\dagger \gamma_0$ and, together with Φ^+ and $[G_0^-]^{-1} + \Sigma^-$, the quantity

$$\Phi^- \left([G_0^-]^{-1} + \Sigma^- \right)^{-1} \Phi^+ \left([G_0^-]^{-1} + \Sigma^- \right) = \sum_{e=\pm} |\phi^e(K)|^2 L_{\mathbf{k}} \Lambda_{\mathbf{k}}^{-e} , \quad (147)$$

where

$$L_{\mathbf{k}} \equiv \gamma_0 \mathcal{M}_{\mathbf{k}}^\dagger \mathcal{M}_{\mathbf{k}} \gamma_0 \quad (148)$$

is another central quantity for the quasiparticle excitation spectrum. Expressions for the matrix $L_{\mathbf{k}}$ in the various phases are also listed in Table 4. Note that also $L_{\mathbf{k}}$ commutes with the energy projectors, $[L_{\mathbf{k}}, \Lambda_{\mathbf{k}}^e] = 0$. Since $L_{\mathbf{k}}$ is hermitian, it has real eigenvalues, λ_r , and can be expanded in terms of a complete set of orthogonal projectors, $\mathcal{P}_{\mathbf{k}}^r$,

$$L_{\mathbf{k}} = \sum_r \lambda_r \mathcal{P}_{\mathbf{k}}^r . \quad (149)$$

In the four phases considered here, there are only two distinct eigenvalues and therefore two distinct projectors. The eigenvalues are also listed in Table 4, and the projectors can be expressed in terms of $L_{\mathbf{k}}$ via

$$\mathcal{P}_{\mathbf{k}}^{1,2} = \frac{L_{\mathbf{k}} - \lambda_{2,1}}{\lambda_{1,2} - \lambda_{2,1}} . \quad (150)$$

Obviously, also these projectors commute with the energy projectors, $[\mathcal{P}_{\mathbf{k}}^{1,2}, \Lambda_{\mathbf{k}}^e] = 0$. It is now straightforward to compute the full propagator by inverting the term in curly brackets in Eq. (136), since the projectors $\mathcal{P}^r \Lambda_{\mathbf{k}}^e$ form a complete, orthogonal set in color, flavor, and Dirac space,

$$G^+(K) = \left[[G_0^-]^{-1}(K) + \Sigma^-(K) \right] \sum_{e,r} \mathcal{P}_{\mathbf{k}}^r \Lambda_{\mathbf{k}}^{-e} \frac{1}{[k_0/Z(k_0)]^2 - [\epsilon_{\mathbf{k},r}^e(\phi^e)]^2} , \quad (151)$$

where

$$\epsilon_{\mathbf{k},r}^e(\phi^e) = \left[(ek - \mu)^2 + \lambda_r |\phi^e|^2 \right]^{1/2} . \quad (152)$$

Obviously, the poles of the full propagator are located at $k_0 \equiv \pm Z(k_0) \epsilon_{\mathbf{k},r}^e(\phi^e)$. Because of the k_0 dependence of the gap function $\phi^e(K)$, this is a condition which has to be solved self-consistently.

In order to get an impression what the excitation spectrum of the quasiparticles in a superconductor looks like, let us for the moment approximate $\phi^e(K) \equiv \phi = \text{const.}$, and also set $Z(k_0) \equiv 1$ (corrections are of order $O(\bar{g})$). Let us also neglect the fact that there are two different sets of excitation branches depending on the value of λ_r . In Fig. 24 the excitation spectrum is shown for non-interacting massless fermions as well as for quasiparticles in a superconductor. The dispersion branches for the quasiparticle

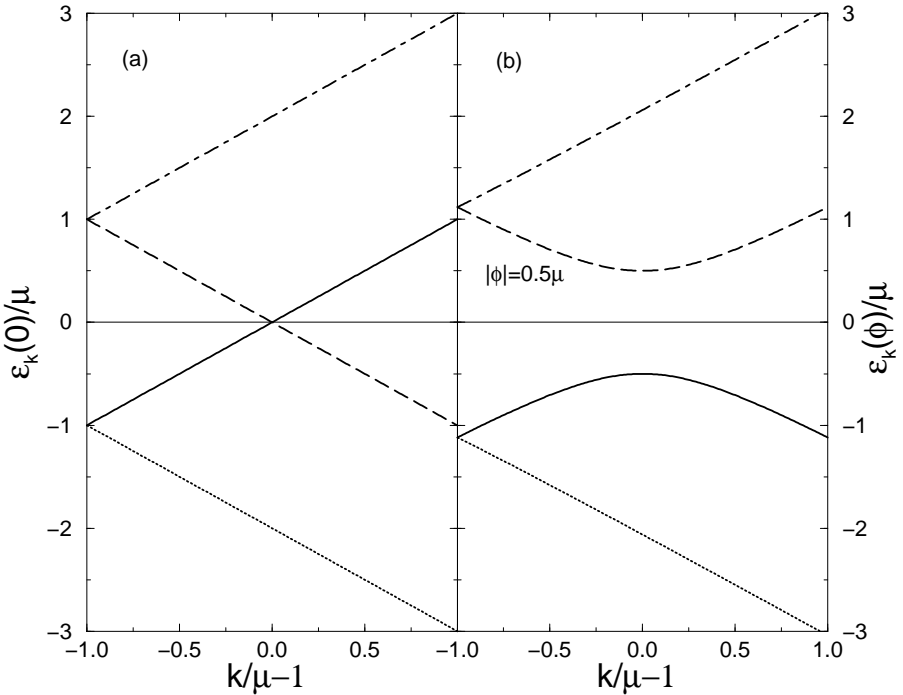


Figure 24: The excitation spectrum for (a) non-interacting massless particles and (b) quasi-particles in a superconductor. The value of the gap function $\phi^e(K)$ is assumed to be constant, $\phi = 0.5 \mu$. The excitation energies for non-interacting particles are $\epsilon_{\mathbf{k}}(0) = k - \mu$ for particles (solid), $\epsilon_{\mathbf{k}}(0) = \mu - k$ for holes (dashed), $\epsilon_{\mathbf{k}}(0) = -(k + \mu)$ for antiparticles (dotted), and $\epsilon_{\mathbf{k}}(0) = k + \mu$ for antiparticle-holes (dash-dotted). The excitation energies for quasi-particles are $\epsilon_{\mathbf{k}}(\phi) = -\sqrt{(k - \mu)^2 + \phi^2}$ for quasiparticles (solid), $\epsilon_{\mathbf{k}}(\phi) = \sqrt{(k - \mu)^2 + \phi^2}$ for quasiparticle-holes (dashed), $\epsilon_{\mathbf{k}}(\phi) = -\sqrt{(k + \mu)^2 + \phi^2}$ for quasi-antiparticles (dotted), and $\epsilon_{\mathbf{k}}(\phi) = \sqrt{(k + \mu)^2 + \phi^2}$ for quasi-antiparticle-holes (dash-dotted) [142].

excitations corresponding to negative energies, $e = -$, i.e., the quasi-antiparticles and quasi-antiparticle-holes, hardly differs from the non-interacting antiparticle or antiparticle-hole branches. As we shall see in Sec. 5.3, in weak coupling, $\phi \ll \mu$, such that to very good approximation $\epsilon_{\mathbf{k},r}^- \simeq k + \mu$. On the other hand, the dispersion branches for the quasiparticle excitations corresponding to positive energies, $e = +$, differ considerably from the non-interacting particle or hole branches. The most notable feature is an energy gap at the Fermi surface, $k = \mu$, between the quasiparticle and quasiparticle-hole branches. This indicates that, in a superconductor, it costs an energy 2ϕ to excite quasiparticle-quasiparticle-hole pairs at the Fermi surface. In contrast, in a non-interacting system it costs no energy to excite particle-hole pairs at the Fermi surface. The superconducting state is thus energetically favored compared to the normal-conducting (non-interacting) state. As a rule of thumb, the more fermionic excitations branches develop a gap (the more fermions form Cooper pairs), and the larger the associated gap, the lower is the ground state energy, and the more energetically favored is the particular superconducting state.

In the CFL and CSL case, there are two different excitation branches with two different gaps, $\epsilon_{\mu,1}^+(\phi) = \sqrt{\lambda_1} \phi \equiv 2\phi$ and $\epsilon_{\mu,2}^+(\phi) = \sqrt{\lambda_2} \phi \equiv \phi$. Consequently, it costs twice the amount of energy

to excite quasiparticle excitations from the first branch than from the second. In the 2SC and polar phases, there also two different excitation branches, but the one corresponding to unpaired fermionic excitations is gapless, $\epsilon_{\mu,2}^+ = 0$. In the next section, the gap equation (140) for the gap function $\phi^e(K)$ will be solved, which allows us to determine the magnitude of the gap at the Fermi surface.

5.3 Solution of the Gap Equation

In order to solve the gap equation (140), insert Eqs. (146) and (151) into Eq. (137) for Ξ^+ ,

$$\Xi^+(K) = - \sum_{e,r} \gamma_0 \mathcal{M}_k \gamma_0 \mathcal{P}_k^r \Lambda_k^{-e} \frac{\phi^e(K)}{[k_0/Z(k_0)]^2 - [\epsilon_{k,r}^e(\phi^e)]^2} . \quad (153)$$

(By the way, this result demonstrates the claim made earlier that G^+ and Ξ^+ have the same poles.) Now insert this equation into the gap equation (140), multiply from the right with $\mathcal{M}_k^\dagger \Lambda_k^e$, and trace over color, flavor, and Dirac space. The result is an equation for the scalar gap function $\phi^e(K)$,

$$\phi^e(K) = g^2 T \sum_n \int \frac{d^3 q}{(2\pi)^3} \sum_{e',s} \frac{\phi^{e'}(Q)}{[q_0/Z(q_0)]^2 - [\epsilon_{q,s}^{e'}(\phi^{e'})]^2} \Delta_{\mu\nu}^{ab}(K-Q) \mathcal{T}_{ab,s}^{\mu\nu,ee'}(\mathbf{k}, \mathbf{q}) , \quad (154)$$

where

$$\mathcal{T}_{ab,s}^{\mu\nu,ee'}(\mathbf{k}, \mathbf{q}) = - \frac{\text{Tr} [\gamma^\mu T_a^T \gamma_0 \mathcal{M}_q \gamma_0 \mathcal{P}_q^s \Lambda_q^{-e'} \gamma^\nu T_b \mathcal{M}_k^\dagger \Lambda_k^e]}{\text{Tr} [\mathcal{M}_k \mathcal{M}_k^\dagger \Lambda_k^e]} . \quad (155)$$

The form of this gap equation is the same for all color-superconducting phases considered here. The difference lies in the excitation spectrum and the structure of the term $\mathcal{T}_{ab,s}^{\mu\nu,ee'}(\mathbf{k}, \mathbf{q})$.

At this point it is convenient to explain the power counting scheme in weak coupling, $g \ll 1$. The right-hand side of Eq. (154) has a prefactor g^2 . Consequently, in order to satisfy the equality, after performing the integral there have to be terms $\sim \phi/g^2$, which together with the prefactor produce a term $\sim O(\phi)$, i.e., which is of the same order as the left-hand side. These are the so-called terms of *leading order* in the gap equation. Then there are terms of so-called *subleading order*. These enter the right-hand side of the gap equation at order $O(g\phi)$. The terms of so-called *sub-subleading order* are $\sim O(g^2\phi)$. It turns out that only the terms of leading and subleading order can be reliably calculated in weak coupling.

In order to proceed, one has to make further approximations. As shown in Ref. [146], to leading and subleading order one does not need the fully self-consistent gluon propagator; it suffices to employ the gluon propagator in HDL approximation, cf. Sec. 4.4.1. The HDL gluon propagator is diagonal in adjoint colors, $\Delta_{\mu\nu}^{ab} \equiv \delta^{ab} \Delta_{\mu\nu}$. For the sake of definiteness, I choose pure Coulomb gauge, where

$$\Delta_{00}(P) = \Delta_\ell(P) , \quad \Delta_{0i}(P) = 0 , \quad \Delta_{ij}(P) = \Delta_t(P) (\delta_{ij} - \hat{p}_i \hat{p}_j) , \quad (156)$$

with $P \equiv K - Q$ and the longitudinal and transverse propagators $\Delta_{\ell,t}$ introduced in Eq. (93). In fact, it is not even necessary to use the full form of the HDL propagator. In weak coupling, power counting along the lines of argument given above reveals [39, 57, 147] that the dominant, leading-order contribution to the gap equation comes from almost static, Landau-damped magnetic gluons. Their propagator may be approximated by

$$\Delta_t^{\text{LDM}}(P) \simeq \frac{p^4}{p^6 + M^4 \omega^2} \Theta(M - p) , \quad (157)$$

where $M^2 = (3\pi/4)m_g^2$. To subleading order, there are two contributions, from non-static magnetic gluons,

$$\Delta_t^{\text{NSM}}(p) \simeq \frac{1}{p^2} \Theta(p - M) , \quad (158)$$

and from static electric gluons,

$$\Delta_{00}^{\text{SE}}(p) \simeq -\frac{1}{p^2 + 3m_g^2} . \quad (159)$$

All other terms in the HDL gluon propagator contribute to sub-subleading order.

In pure Coulomb gauge, one only needs the 00-component, $\mathcal{T}_{ab,s}^{00,ee'}(\mathbf{k}, \mathbf{q})$, and the transverse projection of the ij -components of the tensor $\mathcal{T}_{ab,s}^{\mu\nu,ee'}(\mathbf{k}, \mathbf{q})$,

$$\mathcal{T}_{ab,s}^{t,ee'}(\mathbf{k}, \mathbf{q}) \equiv -(\delta_{ij} - \hat{p}_i \hat{p}_j) \mathcal{T}_{ab,s}^{ij,ee'}(\mathbf{k}, \mathbf{q}) , \quad (160)$$

where the extra minus sign is convention. In Ref. [49] it was shown that one can write these components in terms of a power series in $p^2/(kq)$, where $p \equiv |\mathbf{k} - \mathbf{q}|$, with coefficients $\eta_{2m}^{\ell,t}$ which depend on k, q and the product ee' , and an overall normalization factor a_s which is the same for the 00- and the transverse component. The series over m start at $m = -1$ and, for spin-zero and spin-one gaps, terminate at $m = 2$. The normalization factors satisfy the constraint $\sum_s a_s = 1$.

Performing the Matsubara sum in Eq. (154) one then obtains

$$\begin{aligned} \phi^e(\epsilon_{\mathbf{k},r}^e, k) &= \frac{g^2}{16\pi^2 k} \int_{\mu-\delta}^{\mu+\delta} dq q \sum_{e',s} a_s Z(\epsilon_{\mathbf{q},s}^{e'}) \frac{\phi^{e'}(\epsilon_{\mathbf{q},s}^{e'}, q)}{\epsilon_{\mathbf{q},s}^{e'}} \tanh\left(\frac{\epsilon_{\mathbf{q},s}^{e'}}{2T}\right) \sum_m \int_{|k-q|}^{k+q} dp p \left(\frac{p^2}{kq}\right)^m \\ &\times \left\{ -2 \Delta_{00}^{\text{SE}}(p) \eta_{2m}^{\ell} + \left[2 \Delta_t^{\text{NSM}}(p) + \Delta_t^{\text{LDM}}\left(\epsilon_{\mathbf{q},s}^{e'} + \epsilon_{\mathbf{k},r}^e, p\right) + \Delta_t^{\text{LDM}}\left(\epsilon_{\mathbf{q},s}^{e'} - \epsilon_{\mathbf{k},r}^e, p\right) \right] \eta_{2m}^t \right\} . \end{aligned} \quad (161)$$

Several approximations have been made to obtain this result. First, the integration over q has been restricted to a narrow interval of length 2δ around the Fermi surface, $\delta \sim M$. It turns out that this approximation is good to subleading order; due to the momentum dependence of the gap function, the value of the cut-off affects the color-superconducting gap parameter only at sub-subleading order [39]. Second, when evaluating the Matsubara sum via contour integration, to subleading order the value of the poles $q_0 = \pm Z(q_0) \epsilon_{\mathbf{q},s}^{e'}$ may be approximated by $q_0 \simeq \pm \epsilon_{\mathbf{q},s}^{e'}$ everywhere except in the residue of the contour integral. The single factor of $Z(q_0)$ under the integral arises from the residue. In the argument of $Z(q_0)$, one may also make the approximation $q_0 \simeq \pm \epsilon_{\mathbf{q},s}^{e'}$, since the logarithm in q_0 in Eq. (145) gives at most a subleading contribution to the integral [49, 144]. Third, the gap function was assumed to be an even function of energy, $\phi^e(k_0) \equiv \phi^e(-k_0)$ [39]. Fourth, the gap function was assumed to be isotropic in momentum space, $\phi^e(\mathbf{k}) \equiv \phi^e(k)$ [49]. Finally, the imaginary part of ϕ^e was neglected [39].

How do the leading, $\sim O(\phi)$, and subleading, $\sim O(g\phi)$, terms arise? To this end, one has to power-count the different contributions to the integral in Eq. (161). One uses the fact (which will be confirmed below) that in weak coupling, $\phi \sim \mu \exp(-1/g)$. Neglecting all subtleties regarding different excitation branches, and setting $\epsilon_{\mathbf{q},s}^{e'} \equiv \epsilon_{\mathbf{q}}^{e'} \equiv \sqrt{(e'q - \mu)^2 + \phi^2}$, for $e' = +$ the integral over q gives rise to a term

$$\int_{\mu-\delta}^{\mu+\delta} \frac{dq}{\epsilon_{\mathbf{q}}^+} \equiv 2 \int_0^\delta \frac{d\xi}{\sqrt{\xi^2 + \phi^2}} = 2 \ln\left(\frac{\delta + \sqrt{\delta^2 + \phi^2}}{\phi}\right) \simeq 2 \ln\left(\frac{2\delta}{\phi}\right) \sim \ln\left[\frac{g}{\exp(-1/g)}\right] \sim \frac{1}{g} , \quad (162)$$

where I have substituted the variable $\xi \equiv q - \mu$ and used the fact that $\delta \sim M \sim g\mu \gg \phi \sim \mu \exp(-1/g)$. The logarithm appearing in the estimate (162) is called the ‘‘BCS-logarithm’’, because it also appears in standard BCS theory [106]. For $e' = -$, the BCS-logarithm does not occur, as $\epsilon_{\mathbf{q}}^- \simeq q + \mu$, such that

Table 5: The normalization factors a_s , the coefficients $\eta_{2m}^{\ell,t}$, and the constant d from Eq. (165) in various color-superconducting phases. In the polar phase, ϑ is the angle between the direction of the color-superconducting order parameter and the momentum of the quarks in the Cooper pair.

phase	a_1	a_2	η_0^ℓ	η_2^ℓ	η_4^ℓ	η_0^t	η_2^t	η_4^t	d
2SC	1	0	$\frac{2}{3}$	$-\frac{1}{6}$	0	$\frac{2}{3}$	$\frac{1}{6}$	0	0
CFL	$\frac{1}{3}$	$\frac{2}{3}$	$\frac{2}{3}$	$-\frac{1}{6}$	0	$\frac{2}{3}$	$\frac{1}{6}$	0	0
CSL	$\frac{2}{3}$	$\frac{1}{3}$	$\frac{2}{3}$	$-\frac{7}{18}$	$\frac{1}{18}$	$\frac{2}{3}$	$-\frac{5}{18}$	0	5
polar	1	0	$\frac{2}{3}$	$-\frac{2+\cos^2\vartheta}{6}$	$\frac{1+\cos^2\vartheta}{24}$	$\frac{2}{3}$	$-\frac{2-\cos^2\vartheta}{6}$	$\frac{1-3\cos^2\vartheta}{24}$	$\frac{3}{2}(3+\cos^2\vartheta)$

the integral is parametrically only of order $\delta/\mu \sim M/\mu \sim g$ (provided that the gap function ϕ^- falls off sufficiently fast that one may restrict the integral to a narrow range around the Fermi surface).

For the leading-order contribution to the gap equation, we need another term which is also $\sim 1/g$, such that this term and the BCS-logarithm combine to give a contribution $\sim 1/g^2$ which cancels the prefactor g^2 in front of the integral in Eq. (161). To estimate the order of magnitude of the remaining terms, one notes that the coefficients $\eta_{2m}^{\ell,t}$ are parametrically at most of order $O(1)$ [49], such that they can be neglected for the purpose of power counting. The term $\sim 1/g$ which we are looking for arises from the term $m = 0$ in the sum over m in conjunction with the Landau-damped magnetic gluon propagator. Abbreviating $\omega_\pm \equiv \epsilon_{\mathbf{q},s}^{e'} \pm \epsilon_{\mathbf{k},r}^e$, one estimates

$$\int_{k-q}^{k+q} dp p \Delta_t^{\text{LDM}}(\omega_\pm, p) = \int_{k-q}^M dp \frac{p^5}{p^6 + M^4 \omega_\pm^2} = \frac{1}{6} \ln \left[\frac{M^6 + M^4 \omega_\pm^2}{(k-q)^6 + M^4 \omega_\pm^2} \right] \sim \ln \left(\frac{M^2}{\omega_\pm^2} \right), \quad (163)$$

where the approximation $k \simeq q$ was used. (Only when $k - q \simeq 0$, the logarithm may become large, see argument below. Otherwise, if $k - q \sim M$, the logarithm is only of order $O(1)$, not $O(1/g)$.) If either $e = -$ or $e' = -$, or both $e = e' = -$, the logarithm is parametrically of order $O(1)$, and not $\sim 1/g$. Consequently, the only case of interest is if both $e = e' = +$. In this case, $\omega_\pm \sim \phi$, and the logarithm is large, $\ln(\mu/\phi) \sim 1/g$.

One readily convinces oneself that the p integral over the other terms in Eq. (161) gives at most a contribution of order $O(1)$. In combination with the BCS-logarithm, this leads to a subleading contribution in the gap equation. From the quasi-antiparticle poles, $e' = -$, one does not obtain a large BCS-logarithm, but a term $\sim g$. With the prefactor and a factor of ϕ from the gap function under the integral, their contribution to the gap equation is of order $g^3\phi$, i.e., even beyond sub-subleading order. In the following, one may therefore safely neglect the contribution from quasi-antiparticles when computing the gap for the quasiparticle excitations, $e = +$.

In order to proceed, one performs the p integrals, which can be done exactly [49], but only need to be known to order $O(1)$. One furthermore analyzes the coefficients $\eta_{2m}^{\ell,t}$ and realizes [49] that, to subleading order, one may approximate $k \simeq q \simeq \mu$ in the expressions for these coefficients. Thus,

they become pure numbers of order $O(1)$. Moreover, to subleading order the coefficients $\eta_{-2}^{\ell,t} \equiv 0$ and need not be considered further. I list the coefficients for $m = 0, 1, 2$ in Table 5 together with the normalization factors a_s for the four color-superconducting phases considered here. The final result for the gap equation can be written in the concise form [49] (let us omit the superscript “+” for the sake of simplicity)

$$\phi(\epsilon_{\mathbf{k},r}, k) = \bar{g}^2 \int_0^\delta d(q - \mu) \sum_s a_s Z(\epsilon_{\mathbf{q},s}) \frac{\phi(\epsilon_{\mathbf{q},s}, q)}{\epsilon_{\mathbf{q},s}} \tanh\left(\frac{\epsilon_{\mathbf{q},s}}{2T}\right) \frac{1}{2} \ln\left(\frac{b^2 \mu^2}{|\epsilon_{\mathbf{q},s}^2 - \epsilon_{\mathbf{k},r}^2|}\right) , \quad (164)$$

which is exact to subleading order. In Eq. (164) we have introduced

$$b \equiv \tilde{b} \exp(-d) , \quad \tilde{b} \equiv 256\pi^4 \left(\frac{2}{N_f g^2}\right)^{5/2} , \quad d = -\frac{6}{\eta_0^t} [\eta_2^\ell + \eta_2^t + 2(\eta_4^\ell + \eta_4^t)] . \quad (165)$$

The N_f -dependence of b arises from the corresponding dependence of the gluon mass parameter m_g , cf. Eq. (99). The values for the constant d are also listed in Table 5. For the spin-zero color-superconducting phases, $d = 0$, due to an accidental cancellation of the coefficients η_2^ℓ and η_2^t . This does not happen in the spin-one phases and, consequently, $d \neq 0$.

In order to solve Eq. (164), one makes the following approximation which was first proposed by Son [147] and is valid to subleading order,

$$\frac{1}{2} \ln\left(\frac{b^2 \mu^2}{|\epsilon_{\mathbf{q},s}^2 - \epsilon_{\mathbf{k},r}^2|}\right) \simeq \Theta(\epsilon_{\mathbf{q},s} - \epsilon_{\mathbf{k},r}) \ln\left(\frac{b\mu}{\epsilon_{\mathbf{q},s}}\right) + \Theta(\epsilon_{\mathbf{k},r} - \epsilon_{\mathbf{q},s}) \ln\left(\frac{b\mu}{\epsilon_{\mathbf{k},r}}\right) . \quad (166)$$

The remainder of the calculation is technical, but straightforward and given in detail in Ref. [49]. To summarize the steps, a suitable substitution of variables allows to rewrite the gap equation (164), which is an integral equation, in terms of Airy's differential equation [49, 144]. The result for the gap function has the form

$$\phi(x_r) \equiv \phi_0 F(x_r) , \quad (167)$$

where ϕ_0 is the value of the gap function at the Fermi surface, i.e., the color-superconducting gap parameter or “gap”, and $F(x_r)$ parametrizes the momentum dependence of the gap function. The variable x_r is defined as

$$x_r \equiv \bar{g} \ln\left(\frac{2b\mu}{k - \mu + \epsilon_{\mathbf{k},r}}\right) . \quad (168)$$

At the Fermi surface, $k = \mu$, one has $x_r \equiv x_r^* = \bar{g} \ln[2b\mu/(\sqrt{\lambda_r} \phi_0)] = \pi/2 + O(\bar{g}) \sim O(1)$. If one moves away from the Fermi surface, x_r stays of order $O(1)$, as long as the momentum difference from the Fermi surface is $|k - \mu| \sim O(\phi)$. When $|k - \mu| \sim M$ or larger, $x_r \sim O(\bar{g})$. The precise form of the function $F(x_r)$ is not very illuminating (it consists of a combination of Airy functions [49, 144]), and thus will not be discussed here. All one needs to know is that it has a narrow peak in an interval $|k - \mu| \sim O(\phi)$ around the Fermi surface. At the Fermi surface, $x_r \equiv x_r^*$, the function $F(x_r)$ assumes the value $F(x_r^*) \equiv 1 + O(\bar{g}^2)$. At a distance $|k - \mu| \sim M$ from the Fermi surface, $F(x_r) \sim O(\bar{g})$. If one neglects the factor $Z(\epsilon_{\mathbf{q},s})$ in Eq. (164), the differential equation satisfied by the gap function is that of the harmonic oscillator and, consequently, the solution of the gap equation becomes simpler and more amenable to interpretation: $F(x_r) \equiv \sin x_r$ [39, 147].

The value of the gap function at the Fermi surface is

$$\phi_0 = 2 b b'_0 \mu \exp\left(-\frac{\pi}{2\bar{g}}\right) (\lambda_1^{a_1} \lambda_2^{a_2})^{-1/2} . \quad (169)$$

Table 6: The value of the gap function at the Fermi surface, ϕ_0 in units of its value in the 2SC phase, and the critical temperature, in units of its value expected from BCS theory, Eq. (28), and in units of the critical temperature in the 2SC phase, $T_c^{2\text{SC}}$.

phase	$\phi_0/\phi_0^{2\text{SC}}$	T_c/T_c^{BCS}	$T_c/T_c^{2\text{SC}}$
2SC	1	1	1
CFL	$2^{-1/3}$	$2^{1/3}$	1
CSL	$2^{-2/3} e^{-d}$	$2^{2/3}$	e^{-d}
polar	e^{-d}	1	e^{-d}

The constant $b'_0 \equiv \exp[-(\pi^2 + 4)/8]$ arises from the wave function renormalization factor $Z(\epsilon_{\mathbf{q},s})$ in Eq. (164) [57, 144]. The result (169) differs from the standard BCS result in the power of the coupling constant g in the exponent. In weak-coupling BCS theory, $\phi_0 \sim \exp(-1/g^2)$, while here $\phi_0 \sim \exp(-1/g)$. The difference in the parametric dependence on g arises from the long-range nature of magnetic gluon exchange. In BCS theory, the attractive interaction is assumed to be short-range (point-like or at least exponentially screened). On the other hand, in QCD static magnetic gluon exchange is not screened [13]. Almost static magnetic gluons are dynamically screened, but the screening is rather weak. It gives rise to the large logarithm (163) in addition to the BCS logarithm (162). This reduces the power of g in the exponent.

In Table 6 I list the value of the gap ϕ_0 in units of its value in the 2SC phase. For the spin-one gaps, the nonzero value of the constant d leads to a strong suppression $\sim e^{-d} \sim 10^{-2} - 10^{-3}$ as compared to the spin-zero gaps. In the CFL and CSL phases, the second gapped excitation leads to a nontrivial factor $(\lambda_1^{a_1} \lambda_2^{a_2})^{-1/2} < 1$, which reduces the gap as compared to the 2SC and polar phases where there is only a single gapped excitation.

The result (169) is rigorously valid in weak coupling, i.e., for asymptotically large quark chemical potentials, where the value of the strong coupling constant evaluated at the scale μ is small, $g(\mu) \ll 1$. However, for phenomenology it is of considerable interest to determine the gap also at values of μ which might occur in nature, for instance in the core of compact stellar objects. To this end, one extrapolates the weak-coupling result (169) to large values of $g(\mu) \sim O(1)$. Such an extrapolation has to be considered under the caveat that the sub-subleading terms are not really small for $g(\mu) \sim 1$ and could lead to large deviations of the actual value of the gap from the subleading result (169). Nevertheless, the computation of ϕ_0 at $g(\mu) \ll 1$ is a well-posed problem with a definite result, and so is its extrapolation to large values of $g(\mu)$. In this sense, this approach should be considered to be more reliable than *ad hoc* calculations within NJL-type models which are very popular in the description of color-superconducting quark matter [18].

For the running of the strong coupling constant g with μ/Λ , where Λ is the QCD scale parameter, I take the standard 3-loop formula [35]. I assume that there are only $N_f = 3$ active quark flavors involved in the running of the coupling constant, so that in order to obtain the correct value of $g(\mu)$ at the mass of the Z boson, one has to adjust the QCD scale parameter, $\Lambda = 364$ MeV. I also take $N_f = 3$

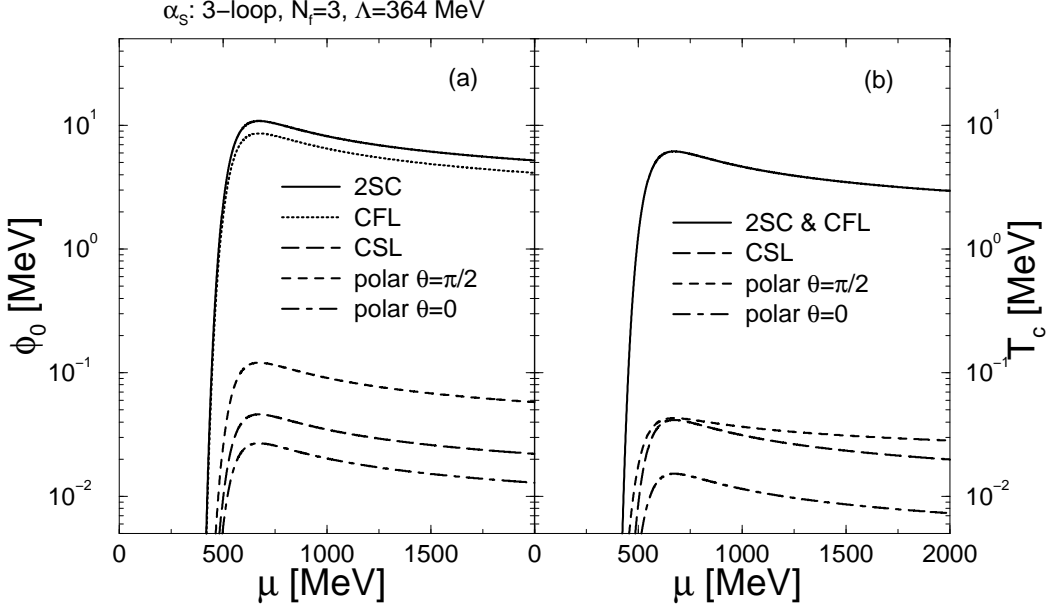


Figure 25: (a) The gap and (b) the critical temperature as a function of the quark chemical potential. Solid curves are for the 2SC phase, and dotted curves for the CFL phase. (In the case of the critical temperature, both curves coincide). The long-dashed curve is for the CSL phase, and the dashed and dash-dotted curves are for the polar phase with $\vartheta = \pi/2$ and $\vartheta = 0$, respectively.

in the factor b in Eq. (165). Physically, this means that, independent of the number of quark flavors which form Cooper pairs, there are always three (massless) quark flavors which screen color charges. The result of extrapolating Eq. (169) to realistic values of μ is shown in Fig. 25 (a) for the various color-superconducting phases considered here.

One observes that the 2SC phase has the largest gap, $\phi_0^{2SC} \simeq 10$ MeV followed by the CFL phase. The spin-one phases have gaps which are about $2 - 3$ orders of magnitude smaller, $\phi_0^{J=1} \sim 10^{-2} - 10^{-1}$ MeV. The gap is approximately zero for chemical potentials below 500 MeV, rapidly rises to assume a maximum around $\mu \simeq 600$ MeV and then decreases. (For larger values of μ it will eventually increase again.) This behavior is due to the dependence of ϕ_0 on g . For large values of g (small values of μ), the power-law behavior g^{-5} from the prefactor b leads to a suppression, while at small values of g (large values of μ), the exponential suppression $\sim \exp(-1/g)$ dominates. This leads to a maximum for intermediate values of μ . (For asymptotically large values of μ , the gap increases again, because the prefactor μ dominates the μ dependence of the remaining factors.)

One can also solve the gap equation at nonzero temperature. One finds that the shape $F(x_r)$ of the gap function hardly changes with T , but that the value of the gap decreases [39]. The gap equation (140) is equivalent to the one obtained in the mean-field approximation [142], and therefore the temperature dependence of the gap follows the predictions from mean-field theory. In particular, the transition to the normal-conducting phase is of second order, irrespective of the symmetries of the order parameter. The critical temperature T_c for this transition can be computed analytically, for details see Refs. [39, 49, 144].

The result is [49]

$$T_c = \frac{e^\gamma}{\pi} \phi_0 (\lambda_1^{a_1} \lambda_2^{a_2})^{1/2} [1 + O(g)] . \quad (170)$$

This result is surprising for two reasons. First, in a phase with a single gapped excitation, like the 2SC phase or the polar phase, where $(\lambda_1^{a_1} \lambda_2^{a_2})^{1/2} \equiv 1$, the critical temperature in QCD, measured in units of the gap, is the *same* as in BCS theory [39], at least to leading order in weak coupling. This is unexpected, since we have seen that the dependence of the gap itself on g is parametrically very different than in BCS theory. Second, in a phase with two different nontrivial excitation branches, like the CFL and CSL phase, the factor $(\lambda_1^{a_1} \lambda_2^{a_2})^{1/2} \neq 1$ *violates* the expectation from BCS theory [48, 49]. In Table 6 I show T_c in units of the critical temperature expected from BCS theory, $T_c^{\text{BCS}} \equiv (e^\gamma/\pi)\phi_0$, to demonstrate this violation. In physical units, say the value of the critical temperature in the 2SC phase, $T_c^{\text{2SC}} = (e^\gamma/\pi)\phi_0^{\text{2SC}}$, the factor $(\lambda_1^{a_1} \lambda_2^{a_2})^{1/2}$ cancels against its inverse in Eq. (169). This leads to the conclusion that, in the mean-field type approach pursued here, the critical temperatures in the 2SC and CFL phases are actually identical. The critical temperatures in the spin-one phases are just a factor e^{-d} smaller than in the 2SC and CFL phases [57].

The critical temperature (170) is shown as a function of μ in Fig. 25 (b). These curves also define the boundaries of the color-superconducting phases in the phase diagram of nuclear matter, cf. Fig. 1. The subleading result (170) for T_c implies that one would have to cool quark matter below temperatures of order 5 MeV, before one enters a color-superconducting quark matter phase (the 2SC or CFL phase). This means that, unless sub-subleading corrections to the gap (169) (and thus to T_c) are large, color-superconductivity is irrelevant in the context of heavy-ion physics, but that it may play a large role for compact stellar objects which have a sufficiently dense core. While spin-zero color-superconducting matter may occur already quite early in the evolution of such a compact stellar object, i.e., while it is still comparatively hot, matter in a spin-one color-superconducting state only occurs after the core of the stellar object has cooled below a temperature of order 10 keV, i.e., in the later stage of its evolution [148].

5.4 Gluon and photon properties

In this section, I take a first step towards a self-consistent solution of the Dyson-Schwinger equations (132) and compute gluon properties in a color superconductor. Within the two-loop approximation to Γ_2 , the gluon self-energy consists of the diagrams shown in Fig. 15. At temperatures of relevance for color superconductivity, $T \leq T_c \sim \phi_0 \sim \mu \exp(-1/g) \ll \mu$, we may neglect the contributions from the gluon (and ghost) loops to the gluon self-energy: they are $\sim g^2 T^2$, while the quark loop is $\sim g^2 \mu^2 \gg g^2 T^2$. Thus, the gluon self-energy in momentum space is

$$\Pi_{ab}^{\mu\nu}(P) = \frac{g^2}{2} \int_K \text{Tr} [\Gamma_a^\mu \mathcal{S}(K) \Gamma_b^\nu \mathcal{S}(K - P)] , \quad (171)$$

where the trace runs over color, flavor, Dirac, and Nambu-Gor'kov space. By introducing the Nambu-Gor'kov basis one has effectively doubled the degrees of freedom by introducing charge-conjugate quarks in addition to quarks [44]. The factor 1/2 in Eq. (171) prevents overcounting these degrees of freedom.

Similarly to the gluon self-energy one can compute the photon self-energy $\Pi_{\gamma\gamma}^{\mu\nu}$ replacing the quark-gluon vertices $\Gamma_a^\mu, \Gamma_b^\nu$ in Eq. (171) by the corresponding ones for the coupling between quarks and photons,

$$\Gamma_\gamma^\mu \equiv \frac{e}{g} \begin{pmatrix} \gamma^\mu Q & 0 \\ 0 & -\gamma^\mu Q \end{pmatrix} , \quad (172)$$

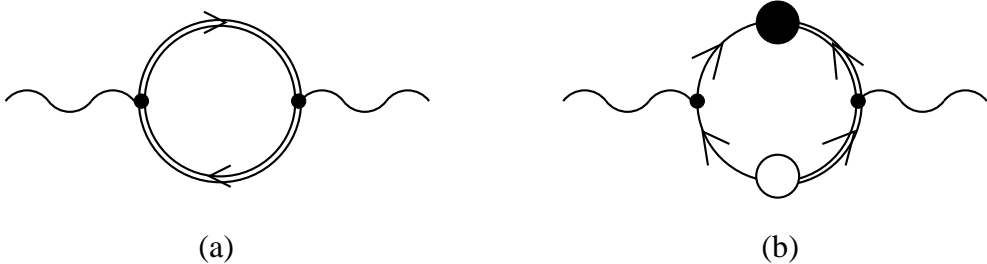


Figure 26: Contributions from (a) normal and (b) anomalous quark propagation to the self-energies of gluons and photons, and the mixed gluon-photon self-energy. The notation follows that of Fig. 23.

where $Q \equiv \text{diag}(2/3, -1/3, -1/3)$ is the quark electric charge matrix. Furthermore, as discussed in Sec. 2.4.2, in a color superconductor gluons can mix with the photon, leading to a “rotated” electromagnetic $[\tilde{U}(1)]$ symmetry in the 2SC and CFL phases. This fact manifests itself in a nonvanishing “mixed” gluon-photon self-energy $\Pi_{a\gamma}^{\mu\nu}$, which follows from Eq. (171) by replacing just one of the quark-gluon vertices with the quark-photon vertex (172). In order to determine the gluon and photon properties in a color superconductor, one has to compute all these different self-energies. For the sake of convenience, in the following let us set the index $\gamma \equiv 9$ and consider Eq. (171) for $a, b = 1, 2, \dots, 9$. I also introduce $T_9 \equiv (e/g)Q$ as the appropriate generator for $[U(1)_{\text{em}}]$.

Taking the trace over Nambu-Gor’kov space in Eq. (171), one realizes that the quark loop consists of four contributions, two “regular” ones with normal propagators G^\pm for quarks and charge-conjugate quarks and two with anomalous propagators Ξ^\pm ,

$$\Pi_{ab}^{\mu\nu}(P) = \frac{g^2}{2} \int_K \text{Tr} \left[\gamma^\mu T_a G^+(K) \gamma^\nu T_b G^+(K - P) + \gamma^\mu T_a^T G^-(K) \gamma^\nu T_b^T G^-(K - P) \right. \\ \left. - \gamma^\mu T_a \Xi^-(K) \gamma^\nu T_b^T \Xi^+(K - P) - \gamma^\mu T_a^T \Xi^+(K) \gamma^\nu T_b \Xi^-(K - P) \right]. \quad (173)$$

The two different topologies corresponding to these contributions are shown in Fig. 26.

To further evaluate the trace one has to specify which color-superconducting phase one would like to consider. The form of the propagators G^\pm, Ξ^\pm can then be determined following the method outlined in Sec. 5.2, see Eqs. (151), (153). After inserting these propagators into Eq. (173), one performs the Matsubara sum. The resulting expressions for the self-energies are rather unwieldy and will not be shown here. For the 2SC phase they were first derived in Ref. [44] and for the CFL phase in Ref. [149]. For the spin-one color-superconducting phases, this was done in Ref. [150]. To further evaluate these expressions, one has to compute the integral over $d^3\mathbf{k}$. For an arbitrary gluon 4-momentum P^μ , this has not yet been done. However, in the static, homogeneous limit, the self-energy $\Pi_{ab}^{\mu\nu}(0)$ was computed in the aforementioned references in order to derive the Debye and Meissner masses in the respective color-superconducting phases. The results will be discussed in more detail in the following. The gluon self-energy in the 2SC phase was also evaluated for nonzero energies and momenta p_0, \mathbf{p} , which are small compared to the quark chemical potential. This calculation is rather technical, and I simply refer to Ref. [115, 151] for the details. The main result was that the modification of the gluon self-energy in a color superconductor does not influence the value for the gap parameter at leading or subleading order in weak coupling. For the other color-superconducting phases, a similar calculation has yet to be done.

In general, in a medium at nonzero temperature and/or density static, long-wavelength (color-) electric fields are screened. The screening length is determined by the (inverse) Debye mass. If the

Table 7: The Debye masses for gluons, photons and from the mixed gluon-photon polarization tensor for various color-superconducting phases. The results are given in units of $N_f \mu^2 / (6\pi^2)$, where $N_f = 2$ in the 2SC phase, $N_f = 3$ in the CFL phase, and $N_f = 1$ in the spin-one color-superconducting phases. The constants are $\zeta \equiv (21 - 8 \ln 2)/54$, $\alpha \equiv (3 + 4 \ln 2)/27$, and $\beta \equiv (6 - 4 \ln 2)/9$.

	gluons								mixed	photon	
a	1	2	3	4	5	6	7	8	1-7	8	9
2SC	0	0	0	$\frac{3}{2}g^2$	$\frac{3}{2}g^2$	$\frac{3}{2}g^2$	$\frac{3}{2}g^2$	$3g^2$	0	0	$2e^2$
CFL	$3\zeta g^2$	$3\zeta g^2$	$3\zeta g^2$	$3\zeta g^2$	$3\zeta g^2$	$3\zeta g^2$	$3\zeta g^2$	$3\zeta g^2$	0	$-\sqrt{12}\zeta eg$	$4\zeta e^2$
CSL	$3\beta g^2$	$3\alpha g^2$	$3\beta g^2$	$3\beta g^2$	$3\alpha g^2$	$3\beta g^2$	$3\alpha g^2$	$3\beta g^2$	0	0	$18q^2e^2$
polar	0	0	0	$\frac{3}{2}g^2$	$\frac{3}{2}g^2$	$\frac{3}{2}g^2$	$\frac{3}{2}g^2$	$3g^2$	0	0	$18q^2e^2$

medium is normal-conducting, static, long-wavelength (color-) magnetic fields are not screened. This changes in a superconductor, where the Meissner effect expels (color-) magnetic fields. They can only penetrate a certain distance into the superconducting medium. For static, long-wavelength (color-) magnetic fields, the (inverse) penetration length is determined by the so-called Meissner mass. The acquisition of a Meissner mass by a gauge boson indicates that the corresponding gauge symmetry is broken via the Anderson-Higgs mechanism. The Debye and Meissner masses are defined as

$$m_{D,ab}^2 \equiv -\lim_{p \rightarrow 0} \Pi_{ab}^{00}(0, \mathbf{p}), \quad m_{M,ab}^2 \equiv \lim_{p \rightarrow 0} \Pi_{ab}^{ii}(0, \mathbf{p}). \quad (174)$$

I present the values for the Debye masses in Table 7 and for the Meissner masses in Table 8 for various color-superconducting phases.

In the 2SC and polar phases, the Meissner mass of the first three gluons vanishes. These gluons correspond to the unbroken $[SU(2)]_c$ subgroup, cf. Table 1. What is interesting is that they also have a vanishing Debye mass, indicating that the corresponding color-electric fields are unscreened. Implications of this result were discussed in Ref. [152]. The other five gluons acquire both a Debye as well as a Meissner mass. Electric and magnetic fields are always screened in these color-superconducting phases. Only the eighth gluon mixes with the photon. Another interesting aspect is, however, that this mixing only occurs in the magnetic sector, electric and color-electric fields remain unmixed. In order to obtain the eigenmodes of the gauge bosons, one has to diagonalize the mass matrices for electric and magnetic gluons. A zero eigenvalue in this mass matrix indicates the presence of an unbroken “rotated” $[\tilde{U}(1)]$ gauge symmetry.

In the CFL phase, all gluons acquire a Debye as well as a Meissner mass, indicating that the $[SU(3)]_c$ color symmetry is completely broken. Photons are Debye- as well as Meissner-screened, and there is again mixing between the eighth gluon and the photon. In contrast to the 2SC and polar phases, however, this mixing extends also to the electric sector. In the CSL phase, all gluons and the photon

Table 8: The Meissner mass for gluons, photons and from the mixed gluon-photon polarization tensor for various color-superconducting phases. The results are given in units of $N_f \mu^2 / (6\pi^2)$, where $N_f = 2$ in the 2SC phase, $N_f = 3$ in the CFL phase, and $N_f = 1$ in the spin-one color-superconducting phases. The constants are $\zeta \equiv (21 - 8 \ln 2)/54$, $\alpha \equiv (3 + 4 \ln 2)/27$, and $\beta \equiv (6 - 4 \ln 2)/9$.

	gluons								mixed	photon	
a	1	2	3	4	5	6	7	8	1-7	8	9
2SC	0	0	0	$\frac{1}{2}g^2$	$\frac{1}{2}g^2$	$\frac{1}{2}g^2$	$\frac{1}{2}g^2$	$\frac{1}{3}g^2$	0	$\frac{1}{\sqrt{27}}eg$	$\frac{1}{9}e^2$
CFL	ζg^2	ζg^2	ζg^2	ζg^2	ζg^2	ζg^2	ζg^2	ζg^2	0	$-\frac{2}{\sqrt{3}}\zeta eg$	$\frac{4}{3}\zeta e^2$
CSL	βg^2	αg^2	βg^2	βg^2	αg^2	βg^2	αg^2	βg^2	0	0	$6q^2e^2$
polar	0	0	0	$\frac{1}{2}g^2$	$\frac{1}{2}g^2$	$\frac{1}{2}g^2$	$\frac{1}{2}g^2$	$\frac{1}{3}g^2$	0	$\frac{2}{\sqrt{3}}qeg$	$4q^2e^2$

obtain Debye and Meissner masses. There is no mixing between the gluons and the photon. This means that the mass matrix of the (former gauge) bosons is already diagonal, and it has no zero eigenvalue. Consequently, there is no unbroken residual symmetry, and no room for a rotation that could generate one. This is in agreement with the general arguments presented in Sec. 2.4.2 and summarized in Table 1. The particular pattern of gluon masses reflects the residual $SO(3)_{c+J}$ symmetry in the CSL phase, cf. Table 1: the gluons corresponding to the three antisymmetric generators of $[SU(3)_c]$ (which are simultaneously generators of $SO(3)$) assume a different mass than the ones corresponding to the symmetric generators.

The final step is to diagonalize the mass matrices $m_{D,ab}^2$, $m_{M,ab}^2$ for electric and magnetic gluons. Since only the eighth gluon mixes with the photon, this diagonalization is achieved by a simple orthogonal rotation in the 2×2 block corresponding to the indices $a = 8, 9$. The resulting diagonal (squared) Debye masses $\tilde{m}_{D,a}^2$ and (squared) Meissner masses $\tilde{m}_{M,a}^2$, as well as the (square of the) cosinus of the rotation angles θ_D , θ_M are shown in Table 9. In the case of an unbroken $[\tilde{U}(1)]$ symmetry, cf. Table 1, the “rotated” (magnetic) photon is massless. The “rotated” gluon remains massive, but its degeneracy with the other massive gluons is lifted.

The case of the polar phase is special. If there is only one quark flavor, or all quark flavors have the same electric charge, the results shown in Tables 7 – 9 hold. In this case, the rotated photon is massless, and there is indeed an unbroken $[\tilde{U}(1)]$ symmetry. However, in the case of two or more quark flavors with different electric charges, the results change [50]. Let us assume that the chemical potentials of all quark flavors are identical. Then the (squared) gluon masses are the same, but in the mixed masses, the factor q has to be replaced by $\sum_f q_f$, while in the photon masses, the factor q^2 is replaced by $\sum_f q_f^2$. In this case, it is not hard to realize that a diagonalization of the Meissner mass matrix does not lead to a massless rotated photon. There is therefore no $[\tilde{U}(1)]$ symmetry. Consequently, spin-one color-superconducting quark matter exhibits a Meissner effect, while color superconductors with spin-zero

Table 9: The diagonal elements of the electric and magnetic gluon-photon mass matrix and the (square of the) cosinus of the rotation angles for Debye and Meissner masses. The results are given in units of $N_f \mu^2 / (6\pi^2)$, where $N_f = 2$ in the 2SC phase, $N_f = 3$ in the CFL phase, and $N_f = 1$ in the spin-one color-superconducting phases. The constants are $\zeta \equiv (21 - 8 \ln 2)/54$ and $\beta \equiv (6 - 4 \ln 2)/9$.

phase	$\tilde{m}_{D,8}^2$	$\tilde{m}_{D,\gamma}^2$	$\cos^2 \theta_D$	$\tilde{m}_{M,8}^2$	$\tilde{m}_{M,\gamma}^2$	$\cos^2 \theta_M$
2SC	$3g^2$	$2e^2$	1	$\frac{1}{3}g^2 + \frac{1}{9}e^2$	0	$3g^2/(3g^2 + e^2)$
CFL	$(3g^2 + 4e^2)\zeta$	0	$3g^2/(3g^2 + 4e^2)$	$(g^2 + 4e^2/3)\zeta$	0	$3g^2/(3g^2 + 4e^2)$
CSL	$3\beta g^2$	$18q^2 e^2$	1	βg^2	$6q^2 e^2$	1
polar	$3g^2$	$18q^2 e^2$	1	$\frac{1}{3}g^2 + 4q^2 e^2$	0	$g^2/(g^2 + 12q^2 e^2)$

Cooper pairs do not. Due to the smallness of the ratio ϕ_0/m_g for spin-one color superconductors, these are very likely of type I, i.e., the magnetic field is completely expelled. This is in contrast to the standard model of a neutron star, where the core is assumed to be a type-II superconductor and thus threaded by magnetic flux tubes. It was recently argued in Ref. [153] that the short precession period of some pulsars contradicts this assumption and requires the core of the pulsar to be a type-I superconductor. The question then is whether the core could be made of spin-one color-superconducting quark matter [50].

6 Conclusions and Outlook

In this review, I have presented the current knowledge of the equilibrium properties of strongly interacting matter at large temperatures and/or densities. In particular, I have qualitatively discussed the phase diagram. I have presented calculations of thermodynamic properties of strongly interacting matter, both via lattice QCD, as well as within analytic approaches. Finally, I have given an overview of color superconductivity in weak coupling.

Our knowledge of the QCD phase transition and the QGP at zero quark chemical potential is fairly complete. Lattice QCD calculations are well under control for the pure $[SU(3)_c]$ gauge theory, and the quality of the data is such that an extrapolation to the continuum limit as well as to the thermodynamic limit has become possible. Lattice calculations with dynamical fermions are more challenging and, consequently, the data are not of the same quality as for the pure gauge theory. The main problem is that, with present methods of putting fermions on the lattice, the pion comes out too heavy. Since pions dominate the equation of state in the hadronic phase, calculations of the pressure below the chiral restoration temperature do not yet reflect the correct physics. The challenge for the future is to improve the methods such that the pion mass on the lattice is close to the value in nature. Besides a reliable computation of the equation of state, this will also allow to decide the question about the order of the QCD phase transition in nature.

Another important development in lattice QCD is to extend the investigation of thermodynamic properties to nonzero quark chemical potentials. For many years, the fermion sign problem has impeded progress in this direction. Recent attempts, like multiparameter reweighting, Taylor expansion around $\mu = 0$, or analytic continuation from imaginary values of μ , have made an attempt to work around this problem. Much work remains to be done to improve these methods in order to correctly determine the location of the critical point in the (T, μ) plane. This is of great phenomenological importance: in order to find a signal for the first-order phase transition to the QGP in nuclear collisions, one has to tune the bombarding energy such that one probes the region of the phase diagram, which is to the right of the critical point. Nuclear collisions at very high energies most likely probe the region to the left, i.e., the crossover region of the quark-hadron transition. By definition, there is no difference between hadronic and QGP phase in this region, and a clear signal for the QGP will be hard to identify.

Although the question about the location of the critical point is important and can be investigated with the above mentioned lattice methods, these methods circumvent the fermion sign problem rather than solving it. Moreover, they are only applicable for $\mu \sim T$. Therefore, one will ultimately have to find a true solution which also works at small temperatures and large chemical potential, so that the color-superconducting quark matter phase can be explored.

Analytic approaches to compute the equation of state of strongly interacting matter at high temperature have advanced rapidly in recent years. The equation of state is now known to all orders which are perturbatively computable. Work is in progress to determine the remaining nonperturbative contribution of order $O(g^6)$. Resummation techniques have been applied to compute the thermodynamic properties of strongly interacting matter. They provide a picture of the QGP as a gas of weakly interacting quasiparticles. It remains to extend these investigations to nonzero quark chemical potential. In contrast to lattice QCD, this is fairly straightforward from a technical point of view.

Color superconductivity is a rapidly evolving field. It is fairly likely that color-superconducting quark matter can be found in the core of compact stellar objects. It remains to explore how this phase influences the properties of the star. Much work has still to be done, for instance to compute the transport properties of color-superconducting matter and the phase diagram under the conditions of electric and color neutrality. Although NJL-type models may give a qualitative picture of possible scenarios, they are unreliable when one wants to draw quantitative conclusions. The task is to improve existing weak-coupling calculations or apply nonperturbative techniques to obtain further knowledge about this interesting, exotic phase of strongly interacting matter.

Acknowledgment

I would like to thank A. Dumitru, Z. Fodor, S. Hands, O. Kaczmarek, F. Karsch, E. Laermann, P. Levai, R. Pisarski, A. Rebhan, T. Schäfer, C. Schmidt, A. Schmitt, Y. Schröder, and A. Steidl for valuable discussions and for help in preparing the figures. I greatly appreciate the hospitality of the INT Seattle, where part of this work was done.

References

- [1] D.J. Gross and F. Wilczek, *Phys. Rev. Lett.* 30 (1973) 1343 ; H.D. Politzer, *Phys. Rev. Lett.* 30 (1973) 1346
- [2] J.C. Collins and M.J. Perry, *Phys. Rev. Lett.* 34 (1975) 1353

- [3] see, for instance: Proc. of the 15th Int. Conf. on Ultra-relativistic Nucleus-Nucleus Collisions, *Quark Matter 2001* (eds. T.J. Hallman, D.E. Kharzeev, J.T. Mitchell, and T.S. Ullrich), *Nucl. Phys. A* 698 (2002) 1
- [4] L. van Hove, *Z. Phys. C* 21 (1983) 93 ; S. Pratt, *Phys. Rev. D* 33 (1986) 1314 ; M. Kataja, V. Ruuskanen, L.D. McLerran, and H. von Gersdorff, *Phys. Rev. D* 34 (1986) 2755 ; C.M. Hung and E.V. Shuryak, *Phys. Rev. Lett.* 75 (1995) 4003 ; D.H. Rischke and M. Gyulassy, *Nucl. Phys. A* 597 (1996) 701 , *Nucl. Phys. A* 608 (1996) 479
- [5] for a review, see for instance: A. Kovner and U.A. Wiedemann, hep-ph/0304151, to appear in: *Quark-Gluon Plasma 3*, eds. R.C Hwa and X.N. Wang (World Scientific, Singapore, 2003)
- [6] L.D. McLerran ad T. Toimela, *Phys. Rev. D* 31 (1985) 545
- [7] P. Arnold, G.D. Moore and L.G. Yaffe, *JHEP* 0111 (2001) 057 , *JHEP* 0112 (2001) 009 , *JHEP* 0206 (2002) 030 ,
- [8] J. Kapusta, P. Lichard, and D. Seibert, *Phys. Rev. D* 44 (1991) 2774 , Erratum *Phys. Rev. D* 47 (1993) 4171
- [9] see, for instance: EOS collaboration, *Phys. Rev. Lett.* 85 (2000) 1194 , *Phys. Rev. C* 64 (2001) 054602 , *Phys. Rev. C* 65 (2002) 054617 ; INDRA Collaboration (J.D. Frankland et al.), *Nucl. Phys. A* 689 (2001) 905, 940 ; S. Das Gupta, A.Z. Mekjian, and M.B. Tsang, nucl-th/0009033 (submitted to *Adv. Nucl. Phys.*)
- [10] J.I. Kapusta, *Finite Temperature Field Theory* (Cambridge University Press, Cambridge, 1983)
- [11] A.D. Linde, *Phys. Lett. B* 96 (1980) 289
- [12] D.J. Gross, R.D. Pisarski, and L.G. Yaffe, *Rev. Mod. Phys.* 53 (1981) 42
- [13] M. Le Bellac, *Thermal Field Theory* (Cambridge University Press, Cambridge, 1996)
- [14] B. Müller, *The Physics of the Quark-Gluon Plasma*, (Lecture Notes in Physics Vol. 225, Springer, Berlin, 1985); L.D. McLerran, *Rev. Mod. Phys.* 58 (1986) 1021 ; H. Stöcker and W. Greiner, *Phys. Rep.* 137 (1986) 277
- [15] F. Karsch, *Lect. Notes Phys.* 583 (2002) 209
- [16] E. Laermann and O. Philipsen, hep-ph/0303042
- [17] J.-P. Blaizot, E. Iancu, and A. Rebhan, hep-ph/0303185, to appear in: *Quark-Gluon Plasma 3*, eds. R.C Hwa and X.N. Wang (World Scientific, Singapore, 2003)
- [18] K. Rajagopal and F. Wilczek, hep-ph/0011333; M. Alford, *Ann. Rev. Nucl. Part. Sci.* 51 (2001) 131
- [19] T. Schäfer and E.V. Shuryak, *Rev. Mod. Phys.* 70 (1998) 323
- [20] J.W. Harris and B. Müller, *Ann. Rev. Nucl. Part. Sci.* 46 (1996) 71 ; S.A. Bass, M. Gyulassy, H. Stöcker, and W. Greiner, *J. Phys. G* 25 (1999) R1
- [21] T. Schäfer, hep-ph/0304281
- [22] B.D. Serot and J.D. Walecka, *Adv. Nucl. Phys.* 16 (1986) 1
- [23] L.D. McLerran and B. Svetitsky, *Phys. Lett. B* 98 (1981) 195 , *Phys. Rev. D* 24 (1981) 450
- [24] L.G. Yaffe and B. Svetitsky, *Phys. Rev. D* 26 (1982) 963
- [25] see, for instance: S.J. Knak Jensen and O.G. Mouritsen, *Phys. Rev. Lett.* 43 (1979) 1736
- [26] G. 't Hooft, *Phys. Rep.* 142 (1986) 357
- [27] A.J. Paterson, *Nucl. Phys. B* 190[FS3] (1981) 188 ; R.D. Pisarski and D.L. Stein, *J. Phys. A* 14 (1981) 3341

- [28] R.D. Pisarski and F. Wilczek, *Phys. Rev. D* 29 (1984) 338
- [29] S. Gavin, A. Gocksch, R.D. Pisarski, *Phys. Rev. D* 49 (1994) R3079
- [30] S.D.H. Hsu and M. Schwetz, *Phys. Lett. B* 432 (1998) 203
- [31] Z. Fodor and S.D. Katz, *Phys. Lett. B* 534 (2002) 87, *JHEP* 0203 (2002) 014
- [32] O. Scavenius, A. Mocsy, I.N. Mishustin, and D.H. Rischke, *Phys. Rev. C* 64 (2001) 045202
- [33] Y. Nambu and G. Jona-Lasinio, *Phys. Rev.* 122 (1961) 345
- [34] M.A. Stephanov, K. Rajagopal, and E.V. Shuryak, *Phys. Rev. Lett.* 81 (1998) 4816, *Phys. Rev. D* 60 (1999) 114028
- [35] Review of Particle Physics by Particle Data Group, *Phys. Rev. D* 66 (2002) 010001
- [36] B.C. Barrois, *Nucl. Phys. B* 129 (1977) 390
- [37] D. Bailin and A. Love, *Phys. Rep.* 107 (1984) 325
- [38] M.G. Alford, K. Rajagopal, and F. Wilczek, *Phys. Lett. B* 422 (1998) 247 ; R. Rapp, T. Schäfer, E. Shuryak, and M. Velkovsky, *Phys. Rev. Lett.* 81 (1998) 53
- [39] R.D. Pisarski and D.H. Rischke, *Phys. Rev. D* 61 (2000) 051501, 074017
- [40] R.D. Pisarski and D.H. Rischke, *Phys. Rev. Lett.* 83 (1999) 37
- [41] S. Elitzur, *Phys. Rev. D* 12 (1975) 3978
- [42] T. Schäfer and F. Wilczek, *Phys. Rev. D* 60 (1999) 074014
- [43] G.W. Carter and D. Diakonov, *Nucl. Phys. B* 582 (2000) 571
- [44] D.H. Rischke, *Phys. Rev. D* 62 (2000) 034007
- [45] D. Vollhardt and P. Wölfle, *The Superfluid Phases of Helium 3* (Taylor & Francis, London, 1990)
- [46] M.G. Alford, K. Rajagopal, and F. Wilczek, *Nucl. Phys. B* 537 (1999) 443
- [47] T. Schäfer and F. Wilczek, *Phys. Rev. Lett.* 82 (1999) 3956
- [48] T. Schäfer, *Phys. Rev. D* 62 (2000) 094007
- [49] A. Schmitt, Q. Wang, and D.H. Rischke, *Phys. Rev. D* 66 (2002) 114010
- [50] A. Schmitt, Q. Wang, and D.H. Rischke, nucl-th/0301090
- [51] M.G. Alford, J. Berges, and K. Rajagopal, *Nucl. Phys. B* 558 (1999) 219
- [52] P. Bedaque, *Nucl. Phys. A* 697 (2002) 569
- [53] I. Shovkovy and M. Huang, hep-ph/0302142; E. Goubankova, W.V. Liu, and F. Wilczek, hep-ph/0304016
- [54] M.G. Alford, J.A. Bowers, and K. Rajagopal, *Phys. Rev. D* 63 (2001) 074016
- [55] H. Müther and A. Sedrakian, hep-ph/0212317
- [56] W.V. Liu and F. Wilczek, *Phys. Rev. Lett.* 90 (2003) 047002
- [57] W.E. Brown, J.T. Liu, and H.-c. Ren, *Phys. Rev. D* 61 (2000) 114012, *Phys. Rev. D* 62 (2000) 054013, 054016
- [58] see, for instance: M. Creutz, *Quarks, gluons and lattices* (Cambridge University Press, Cambridge, 1983)
- [59] K. Wilson, *Phys. Rev. D* 10 (1974) 2445
- [60] K. Symanzik, *Nucl. Phys. B* 226 (1983) 187, 205 ; B. Beinlich, F. Karsch, and E. Laermann, *Nucl. Phys. B* 462 (1996) 415
- [61] P. Hasenfratz and F. Niedermayer, *Nucl. Phys. B* 414 (1994) 785

- [62] J. Kogut and L. Susskind, *Phys. Rev. D* 11 (1975) 395
- [63] R. Narayanan and H. Neuberger, *Phys. Lett. B* 302 (1993) 62 , *Nucl. Phys. B* 443 (1995) 305
- [64] D.B. Kaplan, *Phys. Lett. B* 288 (1992) 342
- [65] P. Hasenfratz, S. Hauswirth, K. Holland, T. Jorg, F. Niedermayer, and U. Wenger, *Int. J. Mod. Phys. C* 12 (2001) 691
- [66] C. Gattringer, *Phys. Rev. D* 63 (2001) 114501
- [67] F. Karsch and P. Hasenfratz, *Phys. Lett. B* 125 (1983) 308
- [68] R.D. Pisarski, *Phys. Rev. D* 62 (2000) 111501 ; A. Dumitru and R.D. Pisarski, *Phys. Lett. B* 504 (2001) 282 , *Phys. Lett. B* 525 (2002) 95 , *Phys. Rev. D* 66 (2002) 096003
- [69] C. Schmidt, C.R. Allton, S. Ejiri, S.J. Hands, O. Kaczmarek, F. Karsch, and E. Laermann, hep-lat/0209009
- [70] F. Karsch, E. Laermann, and A. Peikert, *Nucl. Phys. B* 605 (2001) 579
- [71] F.R. Brown, F.P. Butler, H. Chen, N.H. Christ, Z. Dong, W. Schaffer, L.I. Unger, and A. Vaccarino, *Phys. Rev. Lett.* 65 (1990) 2491
- [72] JLQCD collaboration (S. Aoki et al.), *Nucl. Phys. Proc. Suppl.* B 73 (1999) 459
- [73] F. Karsch, E. Laermann, and C. Schmidt, *Phys. Lett. B* 520 (2001) 41
- [74] F. Karsch and C. Schmidt, private communication
- [75] F. Karsch, E. Laermann and A. Peikert, *Phys. Lett. B* 478 (2000) 447
- [76] G. Boyd, J. Engels, F. Karsch, E. Laermann, C. Legeland, M. Lütgemeier, and B. Petersson, *Phys. Rev. Lett.* 75 (1995) 4169 , *Nucl. Phys. B* 469 (1996) 419
- [77] O. Kaczmarek, F. Karsch, E. Laermann, and M. Lütgemeier, *Phys. Rev. D* 62 (2000) 034021
- [78] O. Kaczmarek, F. Karsch, and P. Petreczky, and F. Zantow, *Phys. Lett. B* 543 (2002) 41 , hep-lat/0301015
- [79] F. Karsch, P. Petreczky, S. Stickan, and I. Wetzorke, *Phys. Lett. B* 530 (2002) 147
- [80] CERES collaboration, *Nucl. Phys. A* 661 (1999) 23c ; nucl-ex/0212015
- [81] M. Asakawa, T. Hatsuda, and Y. Nakahara, *Phys. Rev. D* 60 (1999) 091503 , *Prog. Part. Nucl. Phys.* 46 (2001) 459
- [82] G. Aarts and J.M. Martinez Resco, *JHEP* 0204 (2002) 053 , *JHEP* 0211 (2002) 022
- [83] C.R. Allton, S. Ejiri, S.J. Hands, O. Kaczmarek, F. Karsch, E. Laermann, C. Schmidt, and L. Scorzato, *Phys. Rev. D* 66 (2002) 075407
- [84] P. de Forcrand and O. Philipsen, *Nucl. Phys. B* 642 (2002) 290 ; M. D'Elia, M.-P. Lombardo, *Phys. Rev. D* 67 (2003) 014505
- [85] I.M. Barbour, S.E. Morrison, E.G. Klepfish, J.B. Kogut, and M.-P. Lombardo, *Nucl. Phys. Proc. Suppl.* A 60 (1998) 220
- [86] C.N. Yang and T.D. Lee, *Phys. Rev.* 87 (1952) 404
- [87] F. Csikor, G.I. Egri, Z. Fodor, S.D. Katz, K.K. Szabo, A.I. Toth, hep-lat/0301027
- [88] S. Chandrasekharan and U.J. Wiese, *Phys. Rev. Lett.* 83 (1999) 3116 ; M.G. Alford, S. Chandrasekharan, J. Cox, and U.J. Wiese, *Nucl. Phys. B* 602 (2001) 61
- [89] S.J. Hands and D.N. Walters, *Phys. Lett. B* 548 (2002) 196
- [90] B. Freedman and L. McLerran, *Phys. Rev. D* 16 (1977) 1169
- [91] E. Shuryak, *J.E.T.P.* 47 (1978) 212

- [92] J. Kapusta, *Nucl. Phys.* B 148 (1979) 461
- [93] T. Toimela, *Phys. Lett.* B 124 (1983) 407
- [94] P. Arnold and C. Zhai, *Phys. Rev.* D 50 (1994) 7603 , *Phys. Rev.* D 51 (1995) 1906
- [95] C. Zhai and B. Kastening, *Phys. Rev.* D 52 (1995) 7232
- [96] E. Braaten and A. Nieto, *Phys. Rev. Lett.* 76 (1996) 1417
- [97] K. Kajantie, M. Laine, K. Rummukainen, and Y. Schröder, *Phys. Rev. Lett.* 86 (2001) 10 , *Phys. Rev.* D 65 (2002) 045008 , hep-ph/0211321, hep-ph/0304048
- [98] B. Kastening, *Phys. Rev.* D 56 (1997) 8107 ; T. Hatsuda, *Phys. Rev.* D 56 (1997) 8111
- [99] R.R. Parwani, *Phys. Rev.* D 63 (2001) 054014 , *Phys. Rev.* D 64 (2001) 025002
- [100] P. Ginsparg, *Nucl. Phys.* B 170 (1980) 388 ; T. Appelquist and R.D. Pisarski, *Phys. Rev.* D 23 (1981) 2305 ; S. Nadkarni, *Phys. Rev.* D 27 (1983) 917 , *Phys. Rev.* D 38 (1988) 3287
- [101] E. Braaten and A. Nieto, *Phys. Rev.* D 51 (1995) 6990 , *Phys. Rev.* D 53 (1996) 3421
- [102] see, for instance: P. Arnold and L.G. Yaffe, *Phys. Rev.* D 57 (1998) 1178 , *Phys. Rev.* D 62 (2000) 125014 ; D. Bödeker, *Nucl. Phys.* B 559 (1999) 502 , *Nucl. Phys.* B 647 (2002) 512 ; P. Arnold, G.D. Moore, and L.G. Yaffe, *JHEP* 0011 (2000) 011 , *JHEP* 0301 (2003) 030
- [103] D.H. Rischke, M.I. Gorenstein, A. Schäfer, H. Stöcker, and W. Greiner, *Phys. Lett.* B 278 (1992) 19
- [104] D.H. Rischke, J. Schaffner, M.I. Gorenstein, A. Schäfer, H. Stöcker, and W. Greiner, *Z. Phys.* C 56 (1992) 325
- [105] A. Chodos, R.L. Jaffe, K. Johnson, C.B. Thorn, and V.F. Weisskopf, *Phys. Rev.* D 9 (1974) 3471
- [106] A.L. Fetter and J.D. Walecka, *Quantum Theory of Many Particle Systems* (McGraw-Hill, New York, 1971)
- [107] V. Goloviznin and H. Satz, *Z. Phys.* C 57 (1993) 671
- [108] W. Greiner and D.H. Rischke, *Phys. Rep.* 264 (1996) 183
- [109] A. Peshier, B. Kämpfer, O.P. Pavlenko, and G. Soff, *Phys. Rev.* D 54 (1996) 2399
- [110] P. Levai and U.W. Heinz, *Phys. Rev.* C 57 (1998) 1879
- [111] A. Peshier, B. Kämpfer, and G. Soff, *Phys. Rev.* C 61 (2000) 045203
- [112] J. Fingberg, U.M. Heller, and F. Karsch, *Nucl. Phys.* B 392 (1993) 493
- [113] E. Braaten and R.D. Pisarski, *Nucl. Phys.* B 337 (1990) 569 , *Nucl. Phys.* B 339 (1990) 310 ; J. Frenkel and J.C. Taylor, *Nucl. Phys.* B 334 (1990) 199 , *Nucl. Phys.* B 374 (1992) 156
- [114] J.-P. Blaizot and J.-Y. Ollitrault, *Phys. Rev.* D 48 (1993) 1390 ; H. Vija and M.H. Thoma, *Phys. Lett.* B 342 (1995) 212 ; C. Manuel, *Phys. Rev.* D 53 (1996) 5866 .
- [115] D.H. Rischke and I.A. Shovkovy, *Phys. Rev.* D 66 (2002) 054019
- [116] H.A. Weldon, *Phys. Rev.* D 26 (1982) 1394
- [117] R.D. Pisarski, *Physica* A 158 (1989) 146, 246
- [118] H.A. Weldon, *Phys. Rev.* D 26 (1982) 2789 , *Phys. Rev.* D 40 (1989) 2410 ; G. Baym, J.-P. Blaizot, and B. Svetitsky, *Phys. Rev.* D 46 (1992) 4043
- [119] E. Braaten and R.D. Pisarski, *Phys. Rev.* D 42 (1990) 2156
- [120] J.M. Cornwall, R. Jackiw, and E. Tomboulis, *Phys. Rev.* D 10 (1974) 2428
- [121] G. Baym, *Phys. Rev.* 127 (1962) 1391
- [122] B. Vanderheyden and G. Baym, *J. Stat. Phys.* 93 (1998) 843

- [123] A. Arrizabalaga and J. Smit, *Phys. Rev. D* 66 (2002) 065014
- [124] R.E. Norton and J.M. Cornwall, *Ann. Phys.* 91 (1975) 106
- [125] H. van Hees and J. Knoll, *Phys. Rev. D* 65 (2002) 025010, 105005 , *Phys. Rev. D* 66 (2002) 025028
- [126] J.-P. Blaizot, E. Iancu, and A. Rebhan, *Phys. Rev. Lett.* 83 (1999) 2906 , *Phys. Lett. B* 470 (1999) 181 , *Phys. Rev. D* 63 (2001) 065003
- [127] A. Peshier, *Phys. Rev. D* 63 (2001) 105004
- [128] J.O. Andersen, E. Braaten, and M. Strickland, *Phys. Rev. Lett.* 83 (1999) 2139 , *Phys. Rev. D* 61 (2000) 014017,074016 ; J.O. Andersen, E. Braaten, E. Petitgirard, and M. Strickland, *Phys. Rev. D* 66 (2002) 085016
- [129] CP-PACS collaboration (M. Okamoto et al.), *Phys. Rev. D* 60 (1999) 094510
- [130] P.M. Stevenson, *Phys. Rev. D* 23 (1981) 2916 ; A. Okopińska, *Phys. Rev. D* 36 (1987) 2415 ; F. Karsch, A. Patkós, and P. Petreczky, *Phys. Lett. B* 401 (1997) 69 ; S. Chiku and Hatsuda, *Phys. Rev. D* 58 (1998) 076001
- [131] R. Baier and K. Redlich, *Phys. Rev. Lett.* 84 (2000) 2100
- [132] N. Petropoulos, *J. Phys. G* 25 (1999) 2225
- [133] J.T. Lenaghan and D.H. Rischke, *J. Phys. G* 26 (2000) 431
- [134] J.T. Lenaghan, J. Schaffner-Bielich, and D.H. Rischke, *Phys. Rev. D* 62 (2000) 085008
- [135] D. Röder, J. Ruppert, and D.H. Rischke, nucl-th/0301085 (to appear in *Phys. Rev. D*)
- [136] B. Alles, M. D'Elia, and A. Di Giacomo, *Nucl. Phys. B* 494 (1997) 281
- [137] J.T. Lenaghan, *Phys. Rev. D* 63 (2001) 037901
- [138] J. Baacke and S. Michalski, *Phys. Rev. D* 67 (2003) 085006
- [139] J. Ruppert and D.H. Rischke, (work in progress)
- [140] C. Manuel, *Phys. Rev. D* 62 (2000) 114008
- [141] T. Fugleberg, *Phys. Rev. D* 67 (2003) 034013
- [142] R.D. Pisarski and D.H. Rischke, *Phys. Rev. D* 60 (1999) 094013
- [143] C. Manuel, *Phys. Rev. D* 62 (2000) 076009
- [144] Q. Wang and D.H. Rischke, *Phys. Rev. D* 65 (2002) 054005
- [145] D. Boyanovsky and H.J. de Vega, *Phys. Rev. D* 63 (2001) 034016, 114028 ,
- [146] D.H. Rischke, *Phys. Rev. D* 64 (2001) 094003
- [147] D.T. Son, *Phys. Rev. D* 59 (1999) 094019 ; T. Schäfer and F. Wilczek, *Phys. Rev. D* 60 (1999) 114033 ; D.K. Hong, V.A. Miransky, I.A. Shovkovy, and L.C.R. Wijewardhana, *Phys. Rev. D* 61 (2000) 056001 .
- [148] M. Prakash, J.M. Lattimer, J.A. Pons, A.W. Steiner, and S. Reddy, *Lect. Notes Phys.* 578 (2001) 364
- [149] D.H. Rischke, *Phys. Rev. D* 62 (2000) 054017
- [150] A. Schmitt, Q. Wang, and D.H. Rischke, (in preparation)
- [151] D.H. Rischke, *Phys. Rev. D* 64 (2001) 094003
- [152] D.H. Rischke, D.T. Son, and M.A. Stephanov, *Phys. Rev. Lett.* 87 (2001) 062001
- [153] B. Link, astro-ph/0302441